The Institute of Paper Chemistry

Appleton, Wisconsin

Doctor's Dissertation

Transition Metal Ion Catalyzed Oxidation of a Residual Lignin-Related Compound by Alkaline Hydrogen Peroxide

Philip K. Smith

June, 1984

TRANSITION METAL ION CATALYZED OXIDATION OF A RESIDUAL LIGNIN-RELATED COMPOUND BY ALKALINE HYDROGEN PEROXIDE

A thesis submitted by

Philip K. Smith

B.S. 1978, Miami University

M.S. 1980, Lawrence University

in partial fulfillment of the requirements
of The Institute of Paper Chemistry
for the degree of Doctor of Philosophy
from Lawrence University,
Appleton, Wisconsin

June, 1984

TABLE OF CONTENTS

ABSTRACT

This thesis deals with the mechanisms of reactions believed to occur during the delignification of kraft pulp by alkaline hydrogen peroxide or oxygen. The kinetics and mechanistic pathways of the reaction between 1,1'-methylenebis-(2-hydroxy-3-methoxy-5(2-carboxyethyl)benzene) (MBB) and alkaline H_2O_2 was investigated with and without the addition of transition metal ions. The substrate was chosen to represent the condensed phenolic structural units which may be present in the residual lignin of unbleached softwood kraft pulps.

All reactions were conducted at 45°C and pH 11.0-11.4 in a Teflon-lined reactor. Precautions were taken to ensure that the system was free of contamination by catalytic impurities. The consumption of MBB and H_2O_2, and the formation of MBB degradation products were followed over the course of the reaction. Peroxide decomposition was monitored by continuously measuring the volume of oxygen evolved.

The addition of a catalytic amount of Cu (12 $\mu\underline{M}$ $CuSO_4$), Mn (21 $\mu\underline{M}$ $MnSO_4$), Fe (300 $\mu\underline{M}$ $FeSO_4$), or ferricyanide (300 $\mu\underline{M}$ $K_3Fe(CN)_6$) ion changed the rate and the order with respect to hydrogen peroxide concentration for both MBB oxidation and H_2O_2 decomposition. The metal ions differed from one another in these respects. In the presence of added Cu, MBB oxidation was zero order in H_2O_2. Fe and Mn catalyzed H_2O_2 decomposition more than MBB oxidation, while ferricyanide was a more effective catalyst for oxidation than for decomposition. Under conditions in which H_2O_2 decomposition was strongly inhibited (by addition of stabilizers), MBB was found to be unreactive.

Addition of metal ions did not induce major changes in the stoichiometry or reaction products. The nature of the observed product mixture is consistent with the intermediacy of cyclohexadienone hydroperoxides which result from

reaction of superoxide ($O_2^{\bullet-}$) or oxygen with the phenoxy radical of MBB. A major primary route of MBB degradation involves direct cleavage of the diphenylmethane bond.

These results indicate that transition metal ions perform two central roles in the alkaline H_2O_2 oxidation of phenolic lignin units: catalysis of H_2O_2 decomposition into reactive intermediates and phenoxy radical formation. Both reactions can be catalyzed to different extents by different metal ion species. The practical significance of these findings is discussed with reference to peroxide delignification of pulp.

INTRODUCTION

PERSPECTIVE

Demands for improved environmental quality have created a need for the pulp and paper industry to develop bleaching processes with substantially reduced effluent BOD, toxicity and color loads. New processes utilizing hydrogen peroxide to partially delignify alkaline chemical pulps prior to conventional bleaching have recently been developed for this purpose. The effluent from the peroxide stage can be sent to the recovery unit, thus decreasing the pollution load emanating from the bleach plant.

The chemistry associated with peroxide delignification is quite complex and not fully understood. Catalytic quantities of transition metal ions present in pulp (e.g., iron, manganese, copper) strongly influence peroxide delignification. A review of the literature indicates that transition metal ions play two roles. First, these metals catalyze the decomposition of hydrogen peroxide into radical intermediates which can react with lignin. Second, they can catalyze phenoxy radical formation which is believed to be the first step in the oxidation of phenolic lignin units.

This investigation was directed at obtaining a better understanding of the effects of these catalysts on the reaction rates and pathways of peroxide delignification. Improved knowledge in this area should aid in finding ways to more efficiently utilize hydrogen peroxide in the delignification of chemical pulps. In addition, this study is relevant to oxygen bleaching, since the chemistry associated with both processes is closely related.

BACKGROUND

Since peroxide delignification is relatively new technology, certain general aspects of the process will first be reviewed. Following this, the mechanisms of alkaline hydrogen peroxide decomposition and peroxide delignification are examined.

Peroxide Delignification

The technical feasibility of using hydrogen peroxide as a delignifying agent in the first stage of a bleach sequence for alkaline chemical pulps has only recently received attention (1-9). Studies demonstrate that the efficiency and selectivity of lignin removal is comparable with oxygen bleaching (1,4). Whereas oxygen bleaching is a well established commercial process (10), the use of hydrogen peroxide to delignify pulps is a quite new development. Indeed, the first (and so far only) commercial implementation of peroxide delignification was in 1979 in a 600 tpd hardwood kraft mill (9).

Generally, a 30-50% reduction in lignin content can be achieved with reasonably low levels of peroxide addition (1-3% H_2O_2 on ovendry pulp). For example, Lachenal and co-workers (6) report that the optimum conditions for peroxide delignification of softwood kraft pulp (kappa No. 30) are:

- 12-20% consistency
- 2 hour retention time
- 80-100°C temperature
- 2.5% NaOH on ovendry pulp or a starting pH of 12.5
- 1% H_2O_2 on ovendry pulp

Under these typical peroxide delignification conditions, the kappa number was reduced by 40% without affecting the strength properties of the pulp. Comparable results are achieved in commercial oxygen bleaching under these representative conditions: 10-30% consistency, 0.5-1.5 hour retention, 90-130°C, 0.5-5% NaOH (on ovendry pulp), and 5-15 atm oxygen pressure.

The effects of the trace levels of transition metal ions present in pulp on peroxide delignification have not been fully investigated. However, it is apparent that these metals can have both detrimental and beneficial effects on the efficiency of peroxide delignification (3-5,8). Metal catalysis of hydrogen peroxide decomposition is probably responsible for the negative effect. Significant amounts of the applied peroxide charge can be lost through a rapid decomposition to oxygen.

A number of researchers (3-5) have shown that removal of metal ions from pulp (by pretreatment with acid and/or chelating agents) significantly enhances the extent of peroxide delignification. Of the metal ions commonly found in pulp, manganese appears to be the most detrimental (3,4). Results of experiments (Table 1) by Lachenal, et al. (4) illustrate the negative impact that transition metal ions (particularly manganese) have on peroxide delignification.

Table 1. Effect of increasing the metal ion content of kraft pulp on peroxide delignification (P) in alkaline medium (4).

	Pulp Washed with 0.01N H_2SO_4						
	--	+ Mn	+ Mn	+ Cu	+ Cu	+ Fe	+ Fe
	--	20 ppm	100 ppm	10 ppm	50 ppm	20 ppm	50 ppm
	Concentration, ppm						
Fe	31	31	31	31	31	51	81
Cu	4	4	4	14	54	4	4
Mn	10	30	110	10	10	10	10
Kappa No. after P Stage	17.4	20.0	21.0	18.0	18.8	18.4	18.7

Note: P stage conditions - consistency 12%; NaOH 3%; H_2O_2 1.5%; 90°C; 120 min. Initial kappa No. = 30.

Acid washing conditions - consistency 3%; 20°C; 30 min.

Metal ion content before washing: Fe-53, Cu-9, Mn-103 ppm.

Model compound studies (discussed later) show that peroxide decomposition is necessary for phenolic lignin units to be attacked by hydrogen peroxide. In agreement with this, experiments with pulp have shown that addition of peroxide stabilizers can inhibit peroxide delignification (8). Thus, it is believed that peroxide delignification should be most efficient when hydrogen peroxide decomposition is controlled at a suitable (low) rate (3,8).

Alkaline Hydrogen Peroxide Decomposition

A substantial body of literature concerning the decomposition of hydrogen peroxide exists. It is well known that hydrogen peroxide decomposes at a greater rate in alkaline solution than in either neutral or acidic media. Noting that hydrogen peroxide is a weak acid [pK_a = 11.8 (11)], some researchers have ascribed this alkali-induced decomposition to the hydrogen peroxide species (H_2O_2, HO_2^-) acting as oxidant and reductant in either an ionic (12,13) or radical (14,15) bimolecular mechanism (Fig. 1). In support of this mechanism, Duke and Haas (13) and others (12,16,17) have reported finding a maximum in the decomposition rate at a pH equal to the pK_a of H_2O_2.

$$H_2O_2 + HO^- \rightleftharpoons HO_2^- + H_2O$$

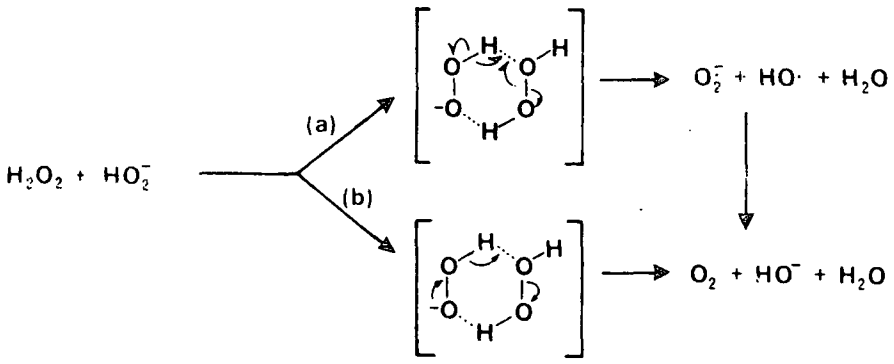

Figure 1. Proposed (a) radical (15), and (b) ionic (13) bimolecular mechanisms for the decomposition of hydrogen peroxide in aqueous alkali.

However, several researchers have shown that this rate maximum is due to the catalytic effect of trace contaminants (18,19). In purified alkaline solutions, the rate is generally observed to remain constant or gradually increase with an increase in pH (18-21). The preponderance of evidence in the literature indicates that the major (and perhaps only) mechanism operating is a free radical redox chain mechanism involving catalytic quantities of transition metal ions (18-22).

The fact that silicates, magnesium salts, or chelating agents stabilize alkaline solutions of hydrogen peroxide (18,19,21), strongly supports this view. The first two additives are thought to remove transition metal ions from alkaline solutions through coprecipitation with magnesium hydroxide or adsorption onto the colloidal surfaces of silicates (23-25). Chelating agents form complexes with the metal ions which are usually inactive as catalysts (21,26).

In addition, ESR spectroscopy has been used to detect the presence of radical species formed during peroxide decomposition (14,19,27,28). Galbacs and Csanyi (19) found that the radical concentration (and decomposition rate) of an alkaline hydrogen peroxide solution increased considerably upon addition of iron salts.

Figure 2 presents a reaction scheme which I believe describes the important steps occurring during alkaline hydrogen peroxide decomposition after having reviewed the pertinent literature. In this scheme, M and M+ represent the reduced and oxidized states of the transition metal ion with its associated ligands.

Reactions (1) and (3) define the catalytic cycle involving oxidation/reduction of metal ions and formation of hydroxyl and hydroperoxy radicals. This cycle is analogous to the chain mechanism proposed by Barb et al. (29) for the ferrous ion catalyzed decomposition of hydrogen peroxide in acid solution

(i.e., Fenton's reagent). Considerable insight into the properties and reactions of these radical species can be gleaned from the field of radiation chemistry (30-31).

$$H_2O_2 + M \longrightarrow HO\cdot + HO^- + M^+ \quad (1)$$

$$H_2O_2 + HO^- \rightleftharpoons HO_2^- + H_2O \quad (2)$$

$$HO_2^- + M^+ \longrightarrow HO_2\cdot + M \quad (3)$$

$$HO_2\cdot + HO^- \rightleftharpoons O_2^{\cdot-} + H_2O \quad (4)$$

$$O_2^{\cdot-} + M^+ \rightleftharpoons O_2 + M \quad (5)$$

$$O_2^{\cdot-} + HO\cdot \longrightarrow O_2 + HO^- \quad (6)$$

$$2\,O_2^{\cdot-} + H_2O \longrightarrow O_2 + HO_2^- + HO^- \quad (7)$$

$$HO\cdot + HO_2^- \longrightarrow H_2O + O_2^{\cdot-} \quad (8)$$

$$HO\cdot + M \longrightarrow HO^- + M^+ \quad (9)$$

$$HO\cdot + HO\cdot \longrightarrow H_2O_2 \quad (10)$$

Figure 2. Proposed metal-catalyzed radical chain mechanism for decomposition of hydrogen peroxide in aqueous alkali.

Under alkaline conditions, essentially all of the hydroperoxy radicals formed from the metal ion oxidation of hydrogen peroxide [Reaction (3)] exist as superoxide radical anions [pK_a = 4.8 (32)]. Superoxide can undergo further reactions which result in the formation of oxygen [Reactions (5)-(7)]. A large number of metal ions and metal complexes have been shown to be efficient single-electron oxidants of superoxide (33,34). In addition, hydroxyl radicals oxidize superoxide at diffusion controlled rates [k_6 = 1 x 10^{10} M^{-1} s^{-1} (35)].

The rate of superoxide disproportionation [Reaction (7)] is highly dependent on pH and the presence of transition metal ions (36,37). In very pure aqueous

solutions the rate of this reaction decreases rapidly with increasing pH [e.g., at pH 7 $k_7 = 5 \times 10^5 \underline{M}^{-1}\ s^{-1}$ and at pH 12 $k_7 = 5 \underline{M}^{-1}\ s^{-1}$ (36)]. However, trace levels of transition metal ion species can effectively catalyze Reaction (7) (36,38).

A number of researchers have presented experimental evidence which indicates that a portion of the oxygen produced from superoxide disproportionation (39-41) or alkali-induced peroxide decomposition (42,42) is in the singlet state, $^1O_2(^1\Delta_g)$. However, to the contrary, results of other studies indicate that little or no $^1O_2$ is formed in these reactions (44-46). This is still a matter of considerable debate, and whether $^1O_2$ is a product of hydrogen peroxide decomposition in aqueous alkali is purely speculative.

Superoxide reduction of hydrogen peroxide by the so-called Haber-Weiss reaction (47) [Reaction (11) below] is not a likely step in the chain mechanism (48). This reaction has been reported to occur at rates which are too slow to compete with more favorable reactions [$k_{11} = 0.13 \underline{M}^{-1}\ s^{-1}$ (49)]. The insignificant rate of Reaction (11) indicates that the decomposition chain cannot be propagated by this reaction. This provides additional support for the role of metal ions in the chain mechanism (Fig. 2).

$$H_2O_2 + O_2^{\cdot-} \longrightarrow HO\cdot + HO^- + O_2 \qquad (11)$$

The highly reactive hydroxyl radical can undergo other reactions in the system like those illustrated by Reactions (8)-(10) of Fig. 2. Since these reactions are very rapid [e.g., $k_8 = 7.5 \times 10^9 \underline{M}^{-1}\ s^{-1}$ (50) and $k_{10} = 5 \times 10^{10} \underline{M}^{-1}\ s^{-1}$ (35)], the steady state concentration of hydroxyl radicals is extremely low [$1 \times 10^{-17} \underline{M}$ in purified alkaline H_2O_2 (19)]. Reaction of HO· with H_2O_2 occurs at a much lower rate [$k = 2.7 \times 10^7 \underline{M}^{-1}\ s^{-1}$ (50) than with HO_2^- [Reaction (8)].

At higher alkalinities (pH > 12) the weakly acidic hydroxyl radical [pK_a = 11.9 (30)] exists mainly as the oxide radical ion, $O^{\bullet -}$. Like the hydroxyl radical, $O^{\bullet -}$ can rapidly react with HO_2^- (and H_2O_2) to form superoxide [$k_{12} = 4 \times 10^8 M^{-1} s^{-1}$ (50)].

$$O^{\bullet -} + HO_2^- \ (H_2O_2) \longrightarrow HO^- + O_2^{\bullet -} \ (HO_2^{\bullet}) \qquad (12)$$

The oxide radical ion, unlike HO•, reacts readily with dissolved oxygen to form the ozonide ion, O_3^- [$k_{13} = 2.9 \times 10^9 M^{-1} s^{-1}$ (31)]. The reactions of O_3^- are characterized by a rate determining step of dissociation of O_3^- to $O^{\bullet -}$ (51,52).

$$O^{\bullet -} + O_2 \rightleftharpoons O_3^- \qquad (13)$$

Several forms of the transition metal ions (M or M+) may catalyze hydrogen peroxide decomposition. In alkali these metal ions form hydroxides and oxyhydroxides of limited solubility which function as heterogeneous catalysts (18,20,53). Soluble forms of transition metal ions (e.g., hydrated, chelated, and complexed) serve as homogeneous catalysts (53). For example, ammonia and citrate complexes of cobalt (54), and the iron chelates - Fe(III)-EDTA (55) and Fe(III)-DTPA (26) - are catalytic. The transition metal ions in pulp are probably present in both forms. Insoluble sulfides and/or hydroxides likely form during the pulping process. Also, metal ions complexed by certain pulp constituents [e.g., hydroxy acids and polyols (23,56,57)] are probably present.

Hydrogen Peroxide Oxidation of Lignin-related Compounds

In a comprehensive review of the reactions of lignins and model compounds with hydrogen peroxide and oxygen in alkali, Gierer and Imsgard (58) pointed out that phenolic and enolic structures in lignin constitute the main sites of initial

oxidative attack. During oxygen and peroxide delignification both oxidants (O_2 and H_2O_2) are involved in each process, but to greatly varying extents. In oxygen bleaching small quantities of hydrogen peroxide are generated by autoxidation reactions with both the carbohydrates and lignin. On the other hand, low levels of oxygen are present during peroxide delignification as the result of partial decomposition of the bleaching reagent (58).

In alkaline hydrogen peroxide, phenolic model compounds (and lignin units) are extensively degraded via side chain displacement and/or ring fragmentation reactions (58-63). Such reactions are important in delignification, since they break up the lignin macromolecule and make the fragments more hydrophilic (58).

Examples of these types of reactions are illustrated by the work of Bailey and Dence (59). They investigated the alkaline hydrogen peroxide oxidation of creosol and α-methylvanillyl alcohol. The reaction pathways depicted in Fig. 3 were proposed by them to account for the identified products from these two lignin-related compounds.

Until recently, these reactions were presumed to result mainly from the action of the hydroperoxy anion (HO_2^-) on the phenolic substrate (64). Studies have now demonstrated that simple phenolic compounds are not attacked by the hydroperoxy anion (16,65). Agnemo and Gellerstedt (16,65) showed that in the presence of a peroxide decomposition stabilizer (sodium silicate), and under a nitrogen atmosphere, creosol, and α-methylsyringyl alcohol are unreactive in alkaline hydrogen peroxide. In the absence of stabilizers, or when peroxide decomposition is catalyzed by addition of transition metal ions, these model compounds are rapidly degraded (16,61,62,65). These results indicate that hydrogen peroxide decomposition products (viz. O_2, $O_2^{\cdot-}$, $HO^{\cdot}$) are the species which attack phenolic lignin units during peroxide delignification.

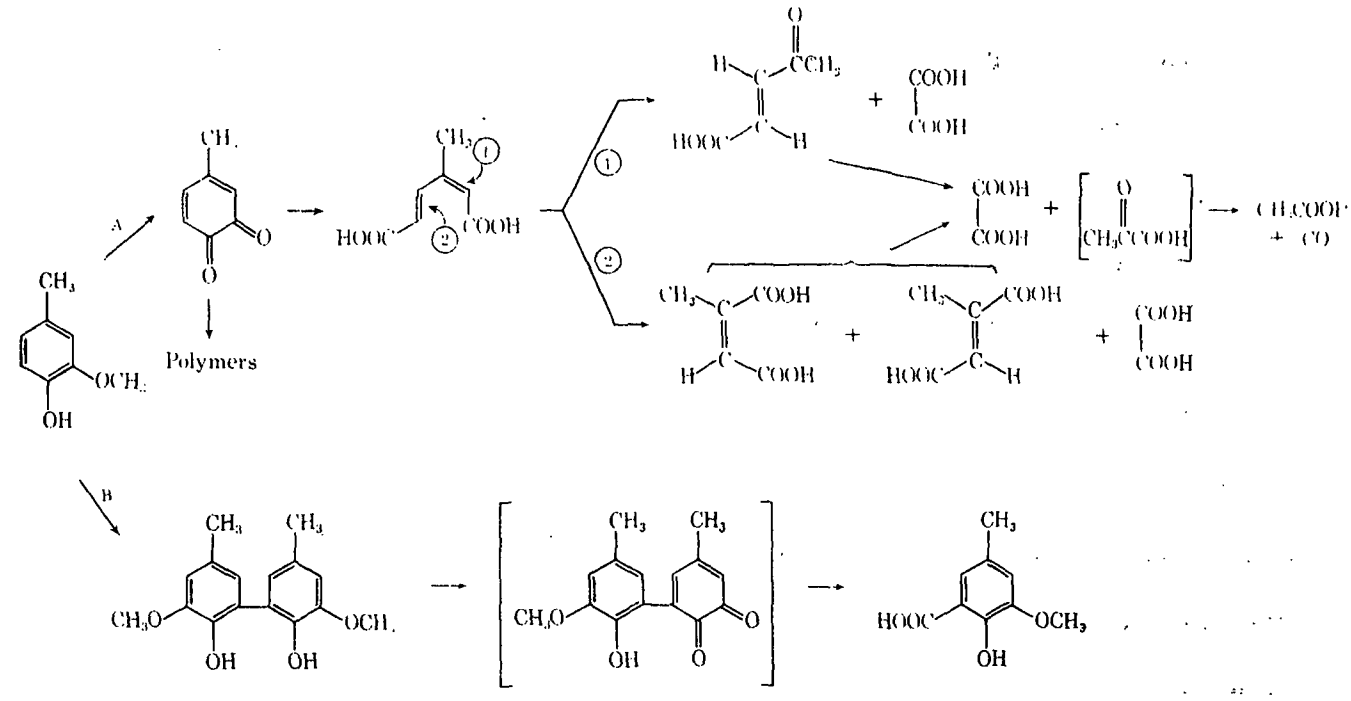

(a) Reaction pathways for creosol: A - major, B - minor.

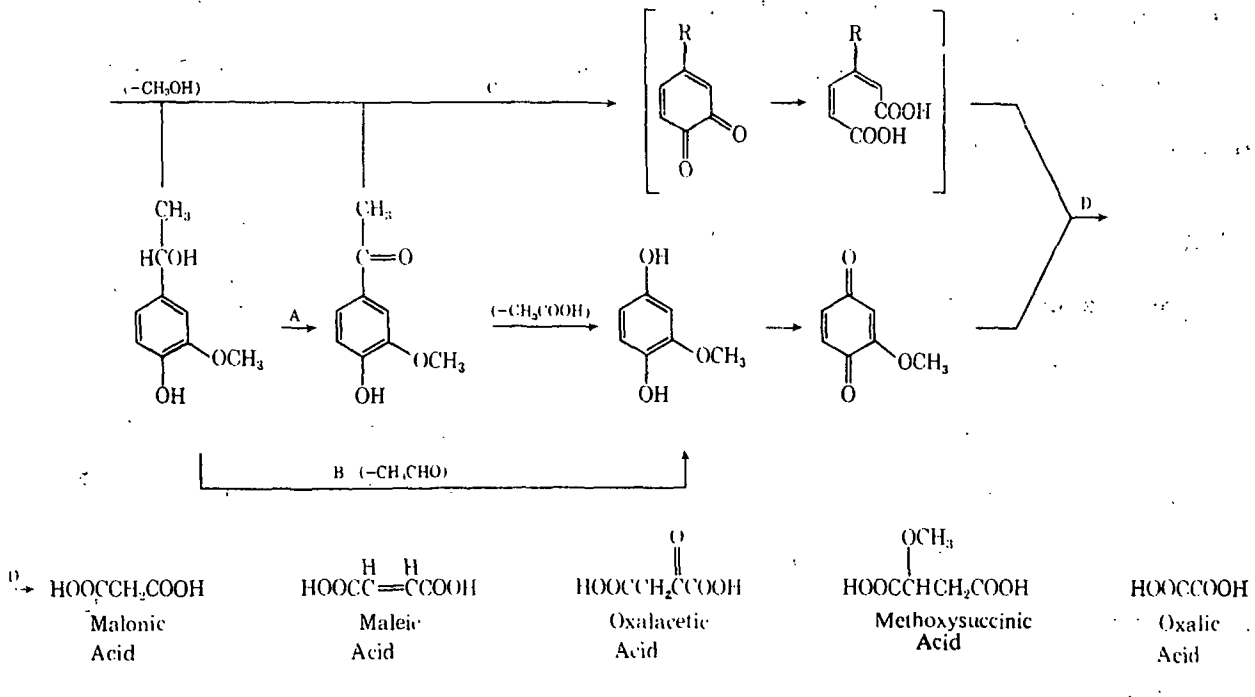

(b) Reaction pathways for α-methylvanillyl alcohol: A - major, B - minor.

Figure 3. Sequences for the reactions of (a) creosol, and (b) α-methylvanillyl alcohol with alkaline hydrogen peroxide (59).

Kratzl, et al. (62,63,66) have studied the reactions of creosol under alkaline oxygen and hydrogen peroxide conditions in great depth. They conclude from their studies that the degradation of phenols by both oxidants proceeds by the same reaction pathways. Thus the chemistry associated with both oxygen and peroxide delignification is closely related.

In oxygen-alkali, it has been well documented that the reaction of phenolic substrates proceeds through initial formation of a cyclohexadienone hydroperoxide (58). The generally recognized mechanism (67-72) for the formation of these intermediates is presented in Fig. 4 and discussed below.

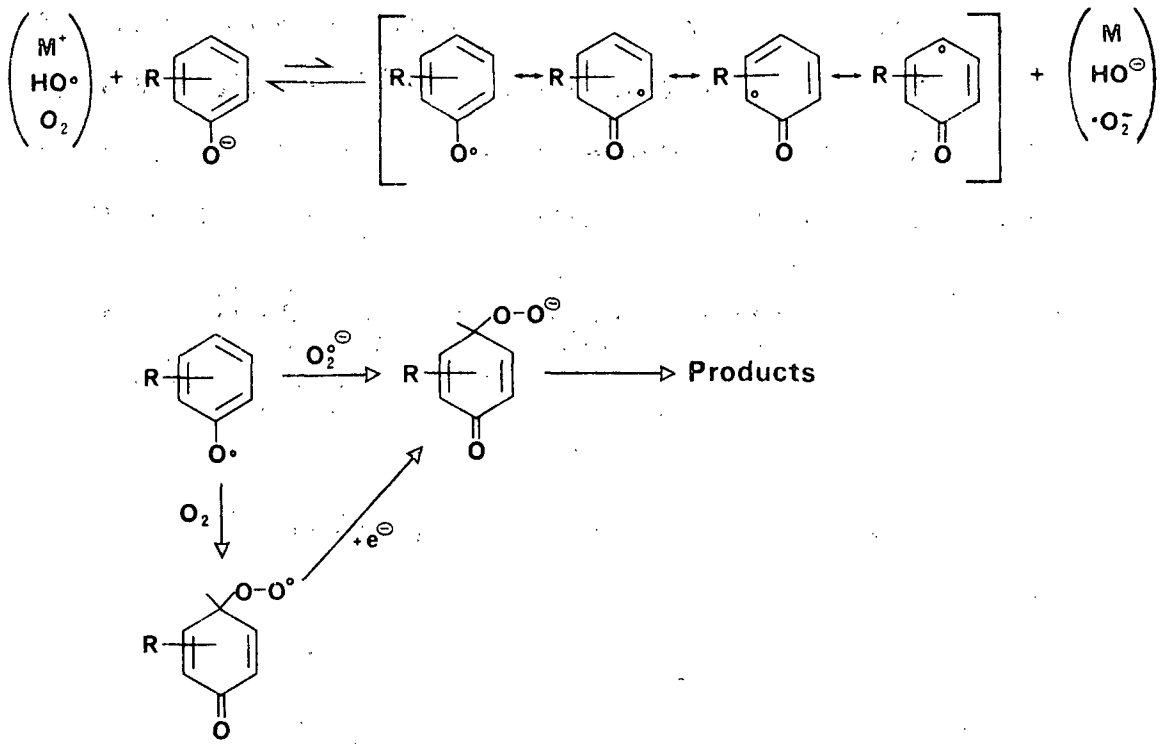

Figure 4. Oxidation scheme for substituted phenols under alkaline oxygen and/or hydrogen peroxide conditions (16,67-72).

Formation of a resonance-stabilized phenoxy radical (Fig. 4) represents the rate-determining step in the reaction scheme (67-71). Phenoxy radicals arise

from the single-electron oxidation of phenolate anions (73,74). Their existence has been verified by ESR spectroscopy (73,75). In addition, the formation of dimers (from phenoxy radical coupling) under alkaline oxidative conditions is well known (76).

Many transition metal ion species are quite effective single-electron oxidants for phenoxy radical generation (69,72,75). Landucci (69) has shown that the dimerization of 2-t-butyl-4-methylphenol is catalyzed by various trace metal ions under alkaline conditions in the presence of oxygen. His results (Table 2) show that copper and manganese (hydroxides/oxides) are more effective catalysts for phenoxy radical formation than iron (hydroxides/oxides) (69,72). The results also suggest that oxygen itself is a relatively poor oxidant for phenoxy radical formation. As a possible explanation for these findings, Landucci (69) proposed that the oxidized state of the catalyst (M+) acts as an electron transfer agent between the phenolate anion and oxygen (Fig. 5).

Table 2. Influence of transition metals on the oxidative coupling of 2-t-butyl-4-methylphenol. Reaction conditions: 80°C, 3 hr, 50 psig oxygen, pH 9 buffer system, 1:30 metal to phenol molar ratio (69,72).

Additive	Dimer Content, %[a]
Control	23
$CuSO_4$	67
$MnSO_4$	54
$Fe_2(SO_4)_3$	15
Purified control[b]	7
Purified control plus $Fe_2(SO_4)_3$	7

[a]Weight percent based on mixture of monomer and dimer.
[b]Treated with chelating resin.

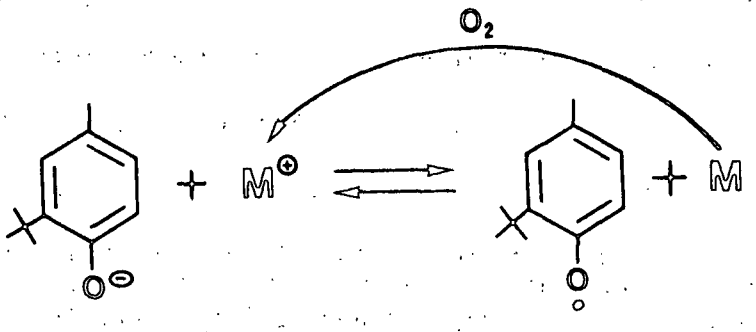

Figure 5. Catalytic formation of phenoxy radicals by transition metal ion species (M+) under alkaline oxidative conditions (69).

Both hydroxyl radicals and oxide radical ions (from peroxide decomposition) are also capable of forming phenoxy radicals from phenols (77,78). Hydroxyl radicals react by an addition mechanism (followed by elimination of H_2O or HO^-) (77), while $O^{\cdot-}$ reacts by a direct electron transfer (78).

Superoxide is likely formed at a rate which is proportional to the rate of peroxide decomposition (19). Once a resonance-stabilized phenoxy radical is created it can rapidly couple with available superoxide (16,79,80) to form a (para or ortho) cyclohexadienone hydroperoxide intermediate (Fig. 4). This intermediate may also arise from the addition of oxygen (from peroxide decomposition) to a phenoxy radical followed by reduction of the resulting hydroperoxide radical (Fig. 4) (70,81).

The reactions of cyclohexadienone hydroperoxides under alkaline conditions in the presence (and absence) of oxygen have been extensively studied (58,66,68, 72,82). Under alkaline hydrogen peroxide conditions the reaction pathways are probably quite similar (62,63), but more extensive degradations occur due to the much higher concentration of hydroperoxy anions in this system.

In their studies on the autoxidation of t-butyl-substituted phenols in alkaline media, Gierer and Imsgard (67) classified the primary reactions of cyclohexadienone hydroperoxides as follows: (a) conversion to quinols, (b) rearrangement to epoxidated quinols, (c) dehydration to quinones, and (d) rearrangement with cleavage of the ring to muconic acid derivatives. Examples of each of these reactions (for hydroperoxides of 4-t-butylguaiacol) are given in Fig. 6.

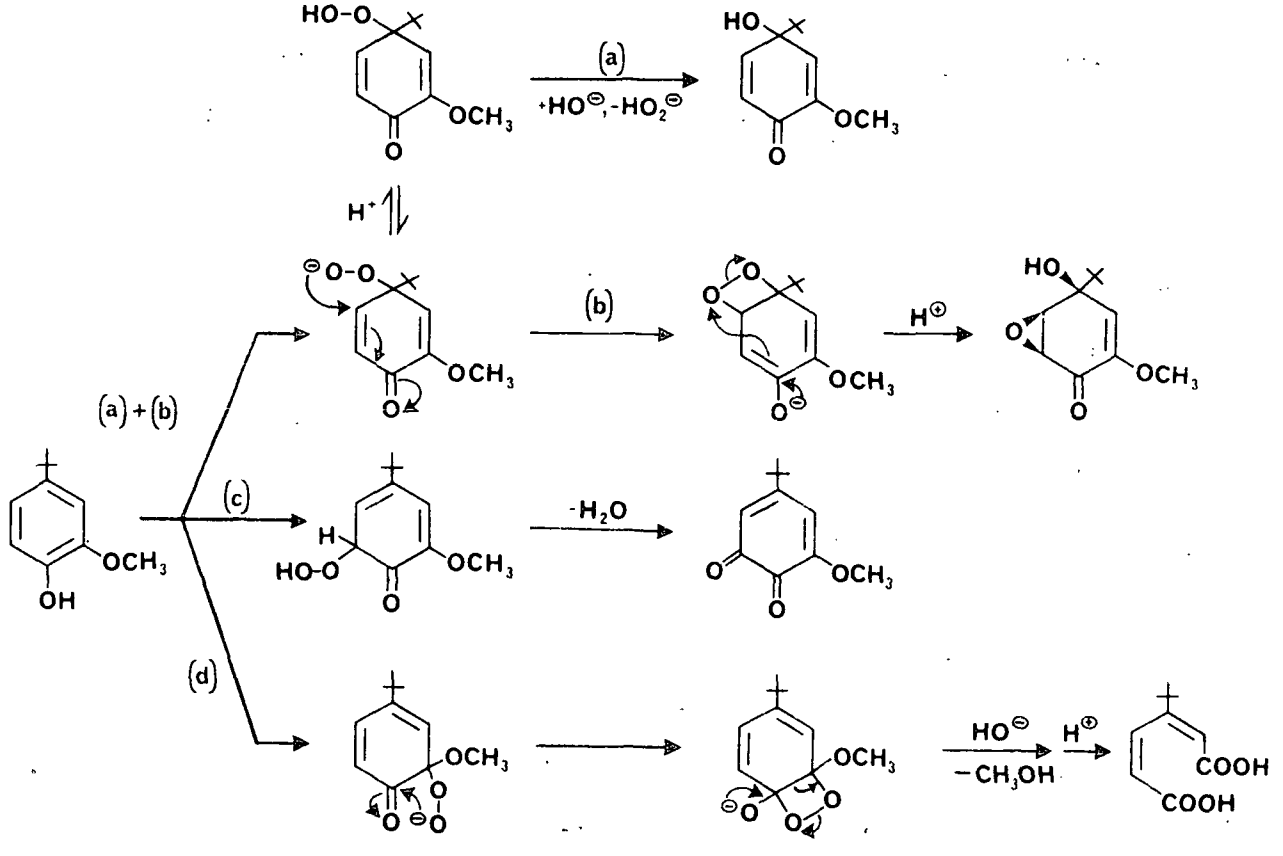

Figure 6. Examples of primary reactions of cyclohexadienone hydroperoxides from the autoxidation of 4-t-butylguaiacol in alkaline media (67): (a) conversion to quinols, (b) rearrangement to epoxidated quinols, (c) dehydration to quinones, and (d) rearrangement with cleavage to muconic acid derivatives.

The products of these primary reactions (viz. quinols, quionones, epoxy quinols, and muconic acid structures) are rapidly degraded under alkaline hydrogen peroxide conditions by a number of possible reaction pathways (62). These reactions involve nucleophilic additions of HO^-/HO_2^- followed by alkaline and oxidative conversions and degradations to lower molecular weight acidic products (59,62,67,76,82). Examples will be shown in the MBB Oxidation Products section.

THESIS OBJECTIVE

The broad goal of this study was to increase our understanding of the chemisty associated with peroxide delignification of alkaline chemical pulps. Based on the literature, it is evident that hydrogen peroxide decomposition is a necessary condition for extensive lignin degrading reactions to occur (16). The presence of transition metal ions should play a central role in these reactions. These ions not only catalyze hydrogen peroxide decomposition, but can also participate in the oxidation of phenolic lignin units via phenoxy radical formation (69). Thus, the specific goal of this study was to investigate the effects that individual transition metal ions have on lignin degrading reactions.

EXPERIMENTAL APPROACH

In order to study the effects of transition metal ions on peroxide delignification of pulp at a fundamental level, a model system was employed. Briefly, a model compound related to residual lignin in pulp was reacted in alkaline hydrogen peroxide solutions containing added transition metal ions. The reaction pathways for this model, and the effects of the metals on these pathways were determined by examination of the reaction products. Further effects were assessed through a study of the reaction kinetics.

A diphenylmethane structure was chosen for the model substrate under the assumption that residual lignin is a high molecular weight, highly condensed structure formed during the pulping process (83,84). Diphenylmethane structures (Fig. 7) are formed by condensation of phenols with quinone methides or formaldehye (85-87). Formaldehyde is present during pulping as a result of a retrograde aldol condensation reaction of γ-carbinol groups in lignin (88,89). Direct ^{13}C-NMR spectroscopic evidence for the presence of these structures in kraft lignin has recently been presented (90,91).

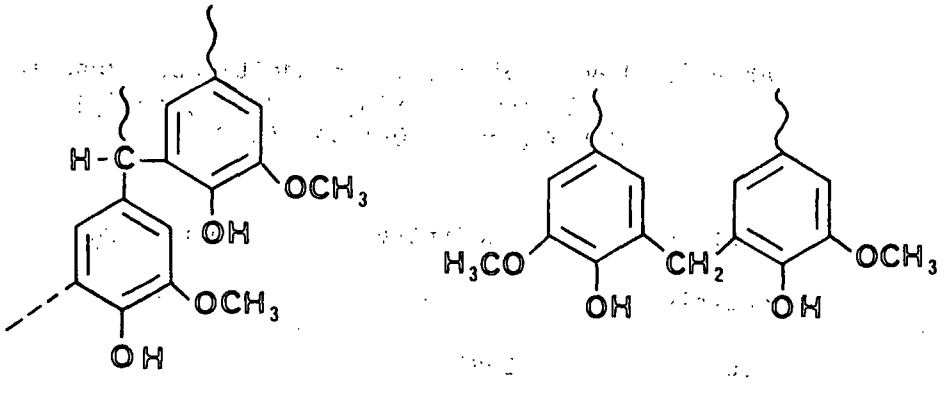

(a) (b)

Figure 7. Diphenylmethane lignin structures resulting from (a) α-5', and (b) phenol-formaldehyde condensation reactions during pulping.

The model selected - 1,1'-methylenebis(2-hydroxy-3-methoxy-5(2-carboxyethyl)-benzene) or MBB - is shown in Fig. 8. In addition to having a relatively straightforward synthesis, MBB is very soluble in aqueous alkali. This made the need for an organic cosolvent unnecessary. The presence of a cosolvent in the reaction system would have caused several interferences.

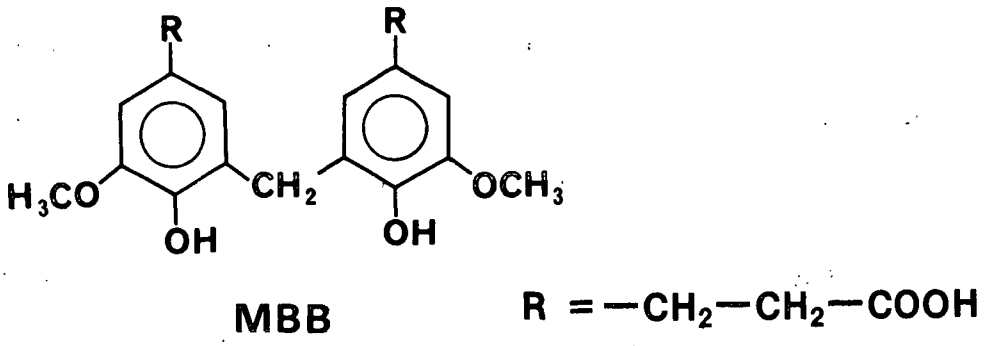

Figure 8. Structures of the model compound: 1,1'-methylenebis(2-hydroxy-3-methoxy-5(2-carboxyethyl)benzene), or MBB.

Three common transition metal ions found in alkaline chemical pulps (iron, copper, and manganese) were chosen as additives. In separate reactions, the effects of each metal ion on the peroxide oxidation of MBB was studied. Each metal was added at a level (Table 3) which gave approximately the same increase in hydrogen peroxide decomposition in the absence of MBB (see Kinetics section).

Table 3. Levels of metal ion additives. Reaction conditions: $[MBB]_o$ = 20 mM, $[H_2O_2]_o$ = 100 mM, pH 11.0-11.4, 45°C.

Reaction	Additive	Conc., μM
Controls	--	--
Cu	$CuSO_4$	12
Mn	$MnSO_4$	21
Fe	$FeSO_4$	300
FC	$K_3Fe(CN)_6$	300

In the presence of H_2O_2 and dilute alkali, these metal ions probably exist as hydrated metal oxides in high oxidation states (viz. Fe_2O_3, CuO, MnO_2) (92). At pH 11 (and 25°C) the solubilities of these oxides are reported to be: Fe_2O_3 - 1.7×10^{-10} M, CuO - 2×10^{-9} M, MnO_2 - insoluble (93). Therefore, the levels in Table 3 are not true solution concentrations.

Ferricyanide ion (Table 3) was included in the study because it is a well known single electron oxidant of phenols under alkaline conditions (72). Also, it is totally soluble in alkali; thus a homogeneous system was obtained. It was added at the same level as $FeSO_4$.

Standard reaction conditions for all MBB oxidations were: pH 11.0-11.4, 45°C, $[MBB]_o$ = 20 mM, $[H_2O_2]_o$ = 100 mM. These conditions were selected in order to provide sufficient degradation of MBB at reasonable reaction rates. In addition, the state of ionization of MBB is essentially constant over this pH range. MBB predominantly exists with only a single phenolic hydroxyl group (and both carboxylic acid groups) ionized around pH 11 (Appendix X).

Reactions were conducted in a magnetically-stirred Teflon-lined batch reactor. The reactions were initiated by injecting a concentrated H_2O_2 solution into the reactor containing the MBB solution and metal additive at 45°C. The solution pH was rapidly adjusted to 11.0 within the first minute. Reaction samples were periodically removed and analyzed for remaining reactants (MBB and H_2O_2) and selected MBB oxidation products.

The extent of hydrogen peroxide decomposition was monitored independently of its consumption by the substrate by continuously measuring the volume of oxygen evolved during the reaction. Separate experiments in the absence of MBB

demonstrated that this technique provides a good estimation of peroxide decomposition (Appendix I: Tables 14, 17).

Experimental procedures are detailed in the Experimental section, and reaction data are tabulated in Appendixes I and II.

RESULTS AND DISCUSSION

This section of the thesis is divided into three major parts. General aspects of the reaction of MBB in alkaline hydrogen peroxide are considered in the first part. In particular, the stability of MBB to hydroperoxy anions and the catalytic effects of added metal ions on the consumption of the reactants (H_2O_2 and MBB) are demonstrated.

A kinetic analysis of the reaction data is presented in the second part of this section. This analysis shows that added metal ions strongly influence the reaction kinetics.

Finally, in the third part, the formation of MBB degradation products are examined. The results indicate that metal ions have little influence on the types or distribution of products formed during MBB oxidation. Possible reaction pathways to account for the observed products are also presented.

H_2O_2/MBB Oxidation Reactions

Control Reaction

Initial H_2O_2 decomposition and MBB oxidation reactions without additives were conducted to establish baseline data for comparisons and to check the reproducibility of the reactions. As indicated in the Background section, peroxide decomposition is extremely sensitive to the presence of trace contaminants. In this study high purity reagents and careful experimental techniques were employed to obtain reproducible results. As illustrated in Fig. 9. these efforts were successful, since triplicate H_2O_2 decomposition runs (in the absence of MBB) showed very good reproducibility.

Duplicate MBB/H_2O_2 oxidations (designated Control and Control-A reactions) were performed under the standard reaction conditions. The procedure for the

Control-A reaction differed from the standard procedure used for the Control and all subsequent reaction runs. In the Control-A run the order of reactant addition was reversed, i.e., the reaction was initiated by addition of a concentrated MBB solution to the reactor containing the alkaline H_2O_2 solution (see Experimental section).

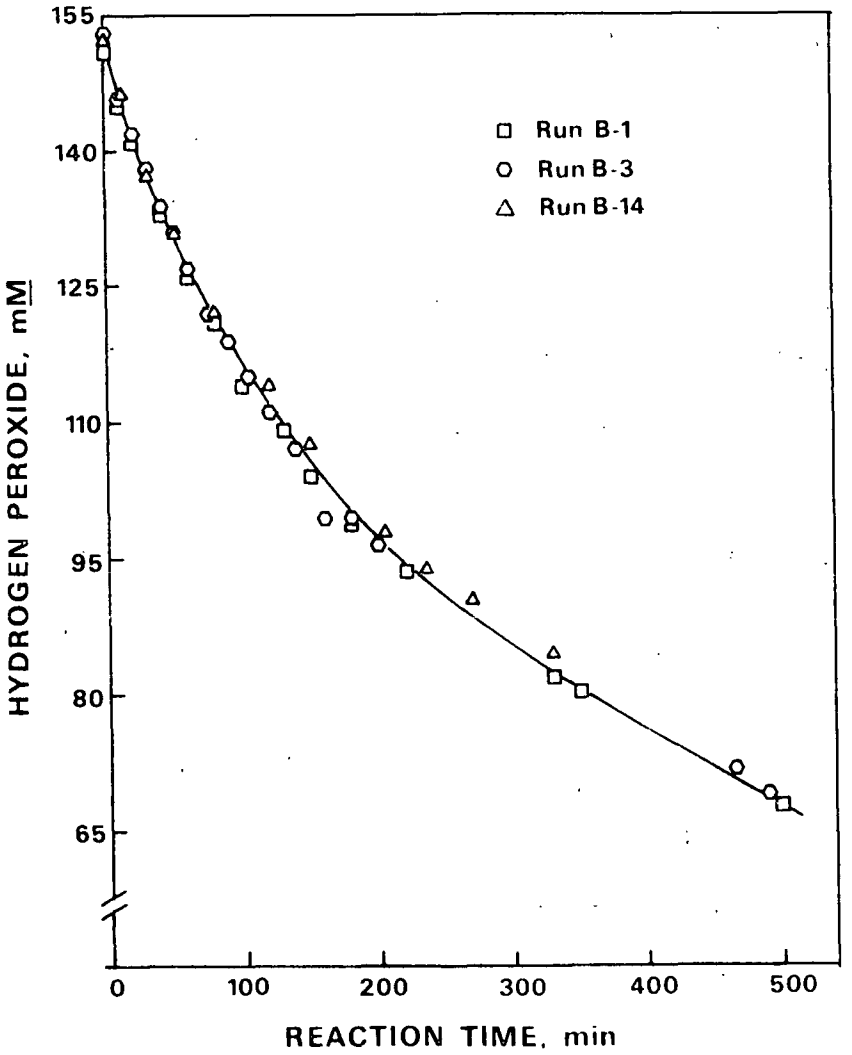

Figure 9. Hydrogen peroxide decomposition in the absence of MBB (45°C, initial pH 11.0). The runs were performed on the following dates: B-1, 9/14/1981; B-3, 9/29/1981; B-14, 5/11/1983.

Both procedures gave similar rates of reactant consumption and product formation (Fig. 10-12). This demonstrates that the Control reaction was reproducible

and not influenced by the order of addition of the two reactants. Over the course of the reaction (300 min), 85% of the initial hydrogen peroxide charge was consumed (Fig. 10). Of this amount, ca. 42% had decomposed to oxygen (Fig. 10), and 58% (by difference) was consumed in reactions with ca. 30% of the MBB (Fig. 11).

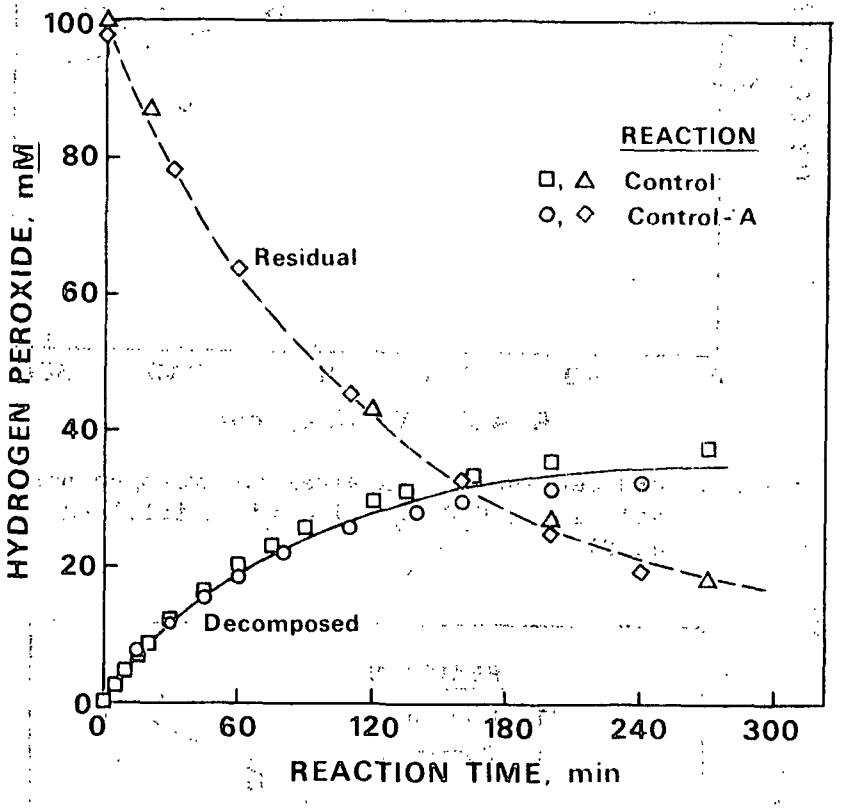

Figure 10. Residual and decomposed hydrogen peroxide levels as a function of time for the Control MBB reactions (initial pH 11.0, $[MBB]_o$ = 20 mM, 45°C).

The two Control reactions also gave the same rate of formation of methanol (Fig. 12). Methanol results from demethoxylation of MBB and its reaction products. The yield of methanol (at 300 min) represents ca. 68% of the theoretical amount based on MBB consumed (two methoxyls per MBB). The formation of methanol and other products is examined in further detail in the MBB Oxidation Products section.

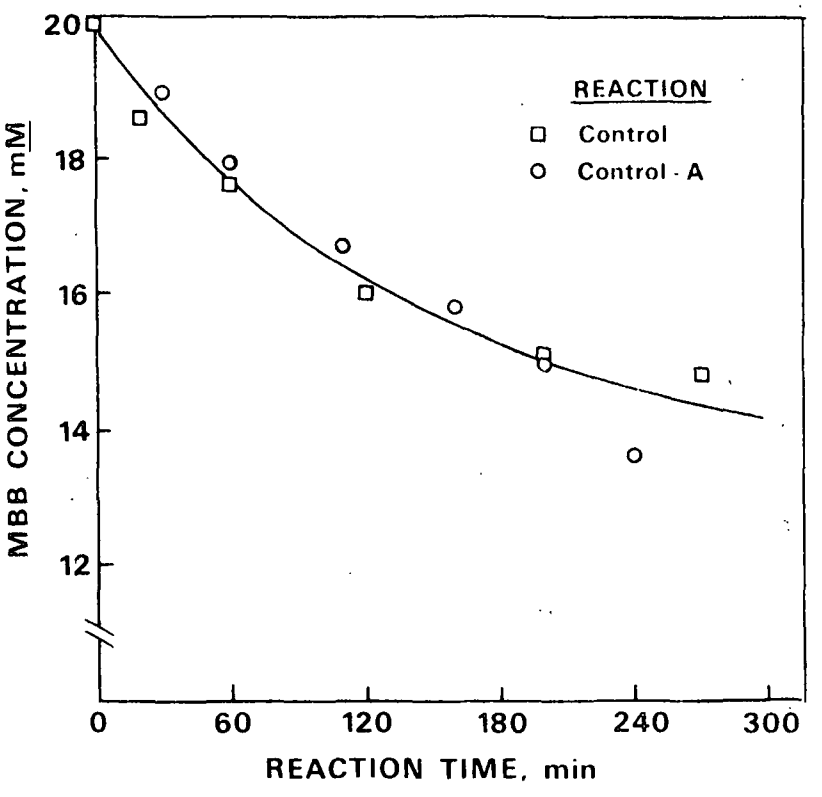

Figure 11. MBB degradation in alkaline hydrogen peroxide solution ($[H_2O_2]_o$ = 100 mM, initial pH 11.0, 45°C).

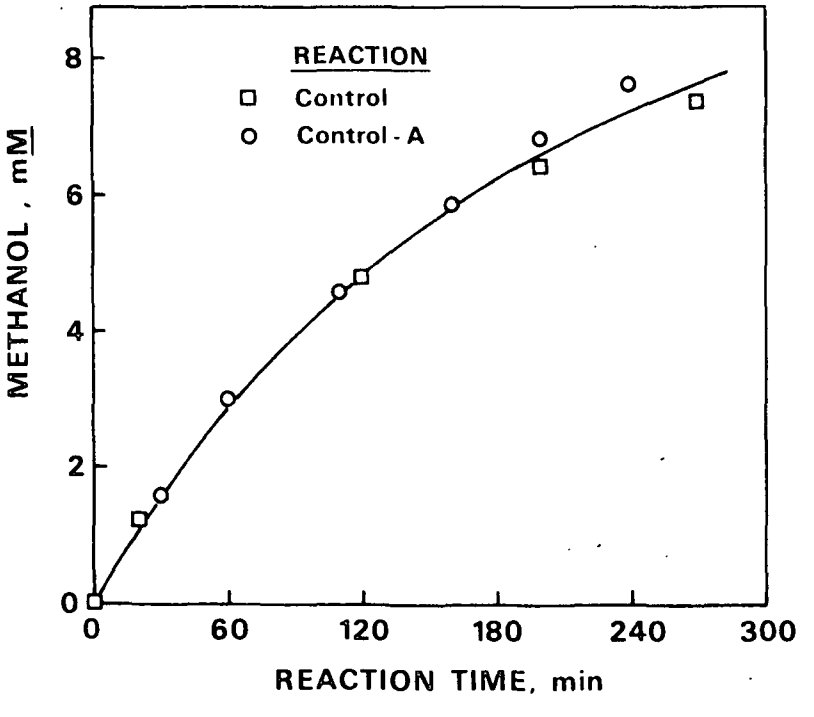

Figure 12. Methanol formation from H_2O_2 oxidation of MBB ($[H_2O_2]_o$ = 100 mM, $[MBB]_o$ = 20 mM, initial pH 11.0, 45°C).

Stabilized Reaction Run

The stability of MBB to hydroxyl and hydroperoxy anions was demonstrated by adding MBB to an alkaline solution of hydrogen peroxide containing decomposition inhibitors (sodium silicate and magnesium sulfate). The results (Table 4) show that these additives effectively inhibited peroxide decomposition, and, in accord with the results of previous studies of the reactions of H_2O_2 with other lignin compounds (63,64), inhibited MBB oxidation.

Table 4. Stabilized reaction run.

Reaction time, min	$[H_2O_2]$, mM	[MBB], mM	[Methanol], mM
0	101.3	20.4	0.0
20	101.3	20.4	0.0
100	98.8	ND	ND
200	96.5	20.1	1.1
275	95.9	20.3	ND

ND - Not determined.

Note: The reaction solution contained 10 mM $MgSO_4$/5 mM Na_2SiO_3 and was continuously purged with N_2 (pH 11.0, 45°C).

The results of the Control and Stabilized reaction runs indicate that simple phenolic units are not subject to initial attack by hydroperoxy anions. Thus hydrogen peroxide decomposition is a necessary condition for these groups to be degraded in lignin.

Catalyzed Reaction Runs

The addition of trace amounts of the transition metal ions (Table 3) had marked catalytic effects on the rates of reactant consumption and product formation. The effects on reactant consumption, total acidic products formation, and reaction stoichiometry are examined in this section, while the effects on

the formation of individual products are considered in the MBB Oxidation Products section. Data for the reaction runs are tabulated in Appendix II.

H_2O_2 Consumption

During each reaction run hydrogen peroxide was consumed through (1) decomposition to oxygen, and (2) reaction with MBB (and its products). Therefore, the plot of residual peroxide concentration as a function of reaction time (Fig. 13)* represents the net effect of the catalysts on the rates of these two reactions. The effects on the rate of peroxide decomposition were separately determined by measuring the volume of evolved oxygen during each run (Fig. 14).

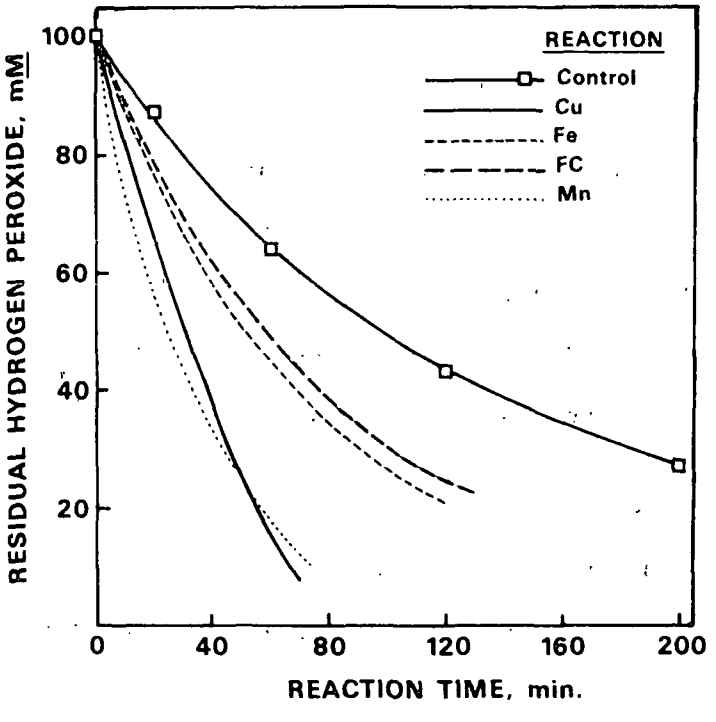

Figure 13. Effects of added metal ions on the residual level of H_2O_2 during the MBB reactions (initial pH 11.0, $[MBB]_o$ = 20 mM, 45°C, added metal ion levels given in Table 3).

*The curves in Fig. 13-15(a) showed a very close fit to the data in all cases. Thus, for the sake of clarity, only the data points for the Control reaction were included in the plots.

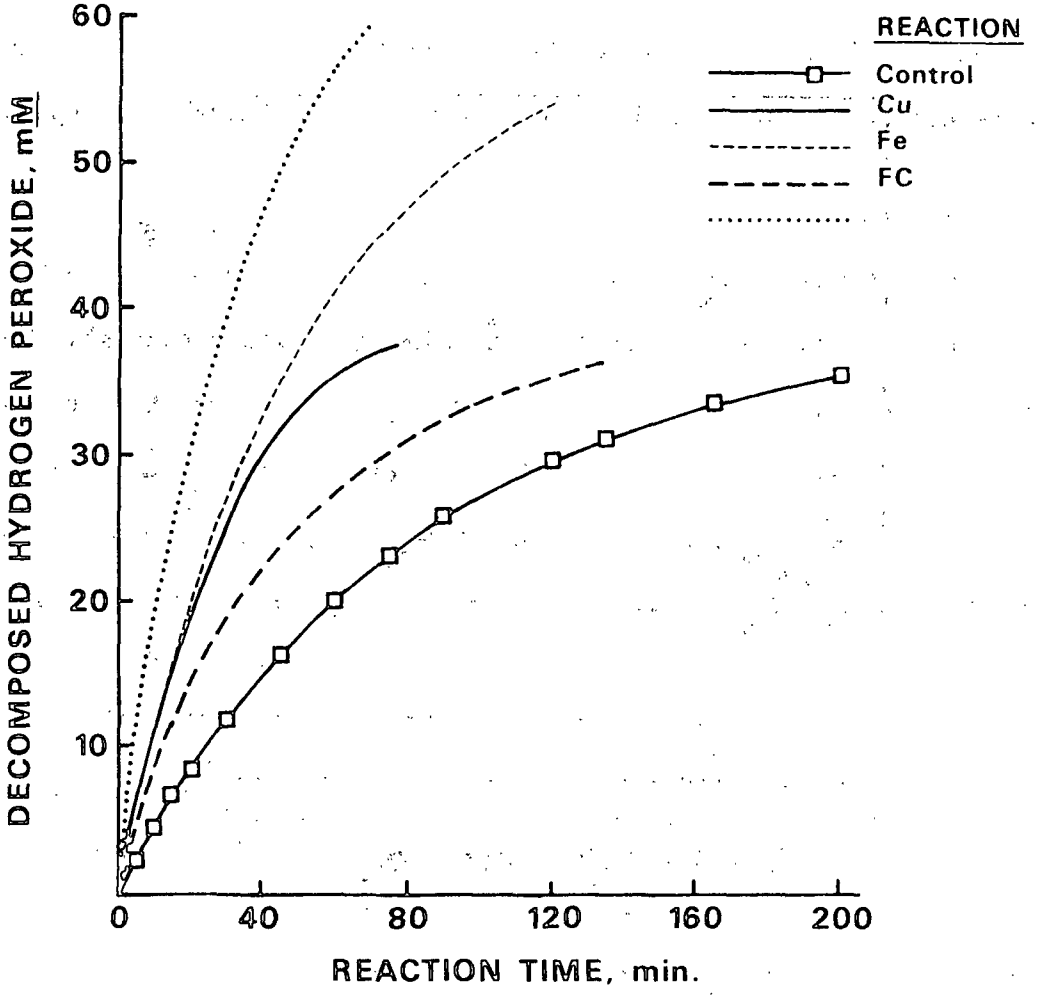

Figure 14. Effects of added metal ions on the decomposition of H_2O_2 during the MBB reactions (initial pH 11.0, [MBB] = 20 mM, $[H_2O_2]$ = 100 mM, 45°C, added metal ion levels given in Table 3).

The amount of hydrogen peroxide consumed in oxidation reactions with MBB is equal to the difference between the initial peroxide concentration and the sum of the residual and decomposed peroxide concentrations [Eq. (14)]. Figure 15(a) illustrates the effect of the catalysts on the rate of hydrogen peroxide consumption by MBB.

$$[H_2O_2]_c = [H_2O_2]_o - ([H_2O_2]_r + [H_2O_2]_d) \qquad (14)$$

Comparisons of Fig. 14 and 15(a) show that the metals catalyzed peroxide decomposition and its reaction with MBB to different extents. The plot of

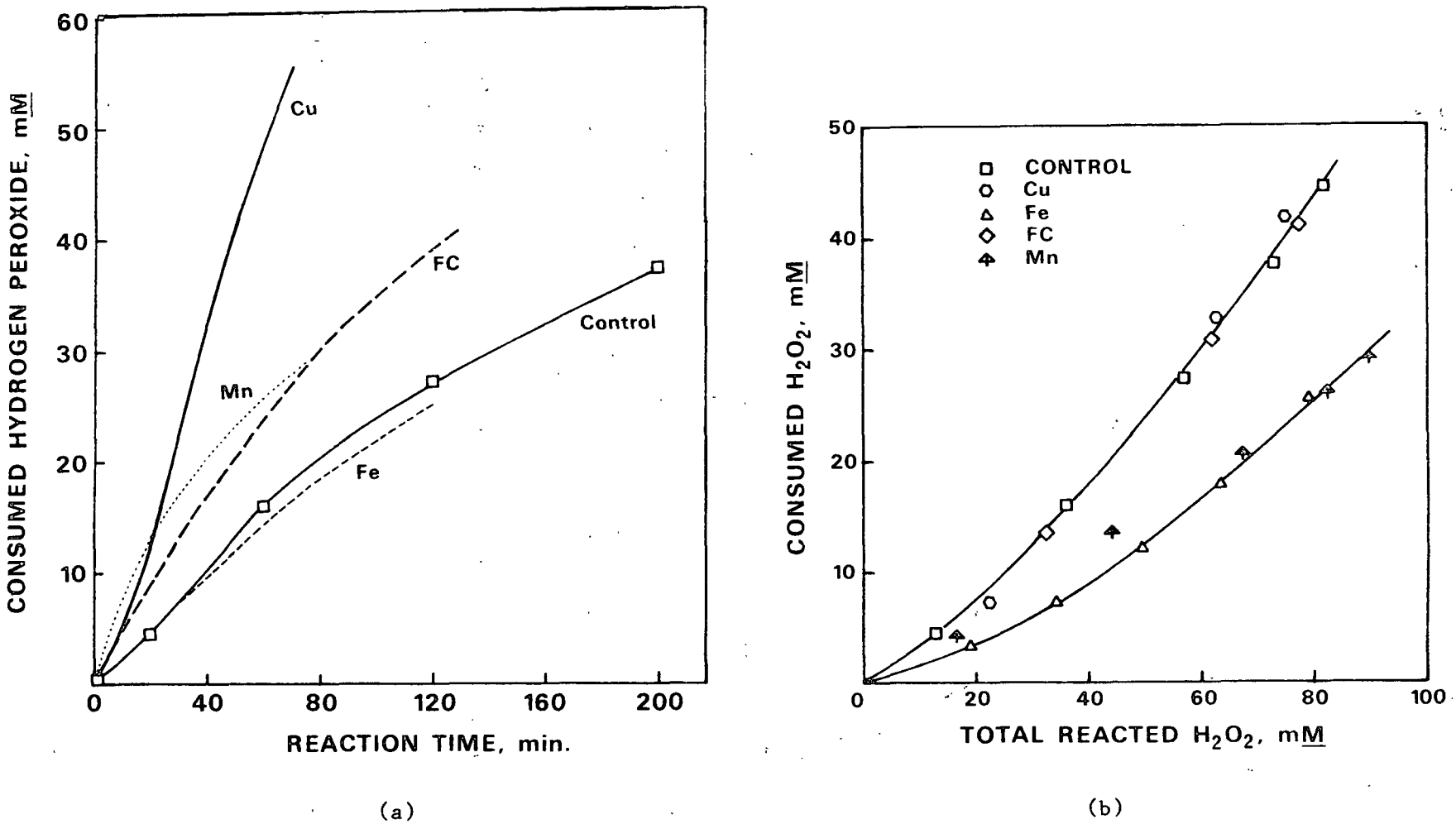

Figure 15. Effects of added metal ions on the (a) rate, and (b) utilization of H_2O_2 consumed in the oxidation of MBB (initial pH 11.0, $[MBB]_o$ = 20 mM, $[H_2O_2]_o$ = 100 mM, 45°C, added metal ion levels given in Table 3).

consumed H_2O_2 as a function of residual peroxide concentration [Fig. 15(b)] demonstrates that in the FC and Cu reactions, the limiting reactant (H_2O_2) was utilized in MBB degradation reactions to about the same extent as in the Control. However, in the Mn and Fe reactions significantly less peroxide was consumed in this manner. Thus the added Mn and Fe catalysts caused greater amounts of the peroxide to decompose to oxygen. This matter is discussed further in the Kinetics section where it is treated in a more quantitative manner.

MBB Degradation

The Cu, Mn, and FC additives clearly catalyzed MBB degradation with Cu exerting the strongest effect (Fig. 16). The Fe additive apparently had no effect, since it followed the degradation curve for the Control. However, since the peroxide concentration in each run varies to different extents with time (Fig. 13), the MBB degradation curves cannot be directly compared. In other words, Fig. 16 represents the net effect of catalysis of H_2O_2 decomposition and oxidation of MBB. These effects were separated through an analysis of the reaction kinetics for each system (results discussed in the Kinetics sections).

Total Acidic Products Formation

During each of the reaction runs the solution pH was observed to increase by 0.2-0.4 unit (Appendix II). A similar result was noted during the peroxide delignification of pulp (3). This observation appeared to contradict the fact that acidic reaction products were shown to be formed during the reactions (see MBB Oxidation Products section).

A closer examination of the data, however, revealed the explanation. Hydrogen peroxide decomposition to oxygen represents the loss of an acid (H_2O_2 pK_a = 11.3

at 45°C) from the reaction solution; thus the pH should rise due to this effect. However, based only on this effect, calculations showed that the pH of the reaction solutions should have increased by a greater amount than observed. This difference can be ascribed to alkali consuming reactions due to the formation of acidic products.

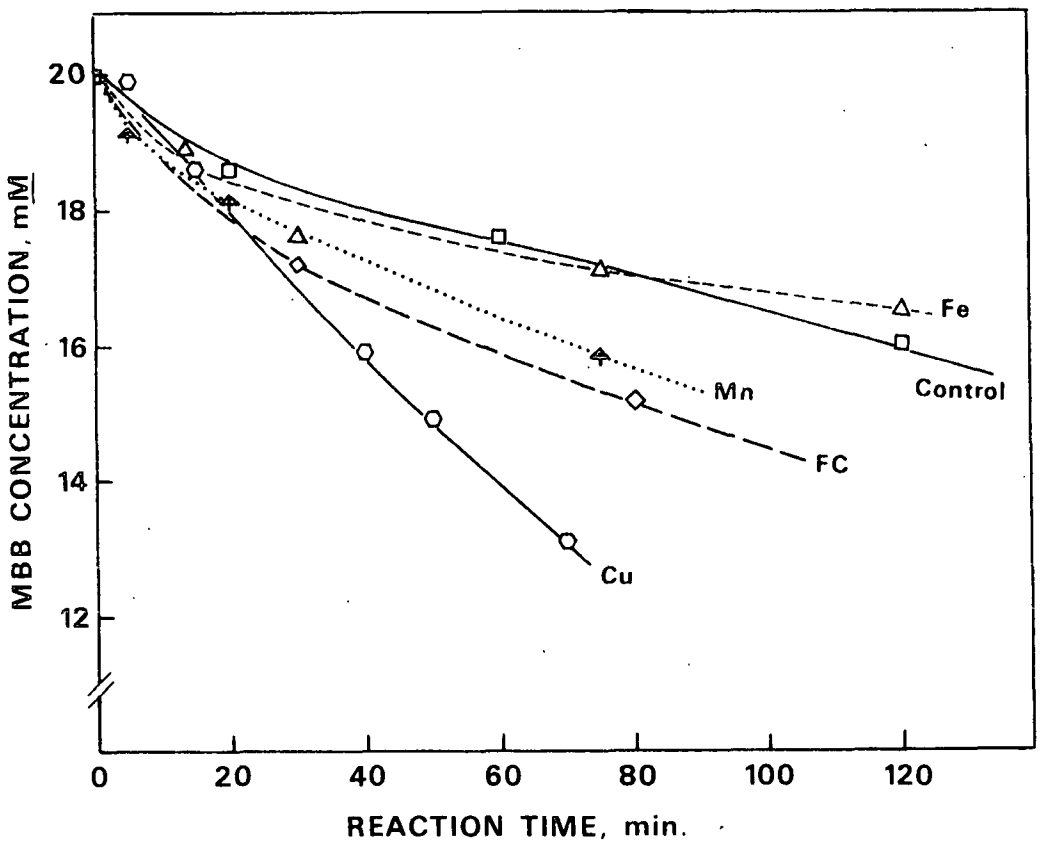

Figure 16. Effects of added metal ions on the degradation of MBB in alkaline hydrogen peroxide (initial pH 11.0, $[H_2O_2]_o$ = 100 mM, 45°C, added metal ion levels are given in Table 3).

The total equivalents of base consumed during each reaction run was calculated by the procedure in Appendix III and the results are plotted in Fig. 17. The added metals affected the rate of formation of acidic products in a manner similar to the consumption of H_2O_2 [Fig. 15(a)]. This result is considered further in the following section on reaction stoichiometry.

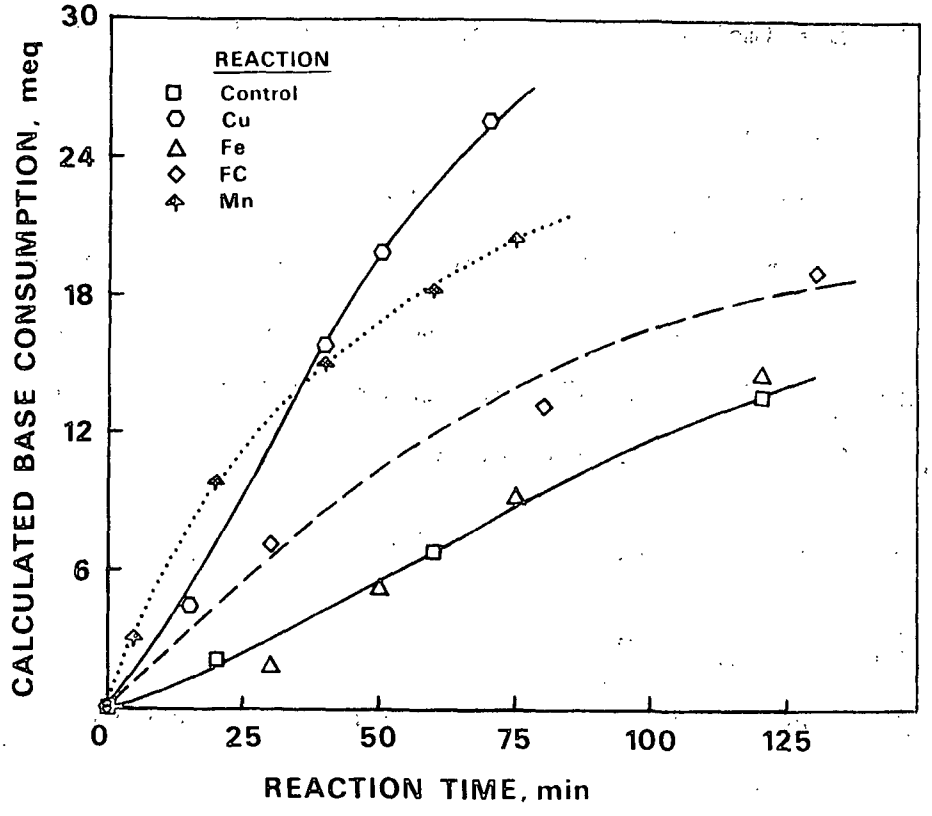

Figure 17. Effects of added metal ions on the formation of total acidic groups during peroxide oxidation of MBB (initial pH 11.0, $[H_2O_2]_o$ = 100 mM, $[MBB]_o$ = 20 mM, 45°C, added metal ion levels given in Table 3).

The pH could have been controlled to a constant value by addition of an acid during the reaction runs. However, separate experiments (in the absence of MBB) showed that H_2O_2 decomposition increased if small amounts of acids were added to the system. (Reagent grade glacial acetic acid, and ultrapure grades of H_2SO_4 and HCl were tested.) This result implies that the system was very sensitive to trace contaminants or anions introduced by the acids. For this reason, and the fact that the pH rise was very small, it was decided not to control the pH during the reaction runs.

Reaction Stoichiometry

The formation of acidic groups during the reactions is related to the consumption of H_2O_2 by the stoichiometric relationship:

$$S_1 = (\text{moles of } H_2O_2 \text{ consumed})/(\text{mole of acid formed}) \quad (15)$$

Generally the reaction runs gave a value of approximately two for this ratio (Table 5). However, in the Mn reaction the ratio was slightly lower (ca. 1.4). This lower ratio implies that a greater percentage of the acids formed in the Mn reaction resulted from oxidation of carbon atoms (of MBB) having higher oxidation numbers. An explanation for this apparent selectivity of peroxide attack in the Mn reaction is not readily evident.

Table 5. Stoichiometric ratios for the reaction runs.

Residual $[H_2O_2]$, mM		80	60	40	20
Reaction	Stoich.	Stoichiometric Ratio[a]			
Control	S_1	2.4	2.2	2.0	2.0
	S_2	4.7	6.3	6.6	8.2
Fe	S_1	3.5	2.7	2.0	1.8
	S_2	2.4	4.1	6.0	7.1
FC	S_1	1.9	2.0	2.2	2.2
	S_2	3.8	5.1	6.3	7.4
Mn	S_1	1.4	1.3	1.4	1.4
	S_2	5.7	6.6	6.8	7.0
Cu	S_1	1.6	1.8	2.1	2.2
	S_2	5.9	6.7	8.1	8.3

[a]Stoichiometric relationship: S_1 = (consumed peroxide)/(acid), S_2 = (consumed peroxide)/(MBB).

A second stoichiometric relationship can be calculated using the data for the consumed H_2O_2 and reacted MBB [Eq. (16)].

$$S_2 = (\text{moles of } H_2O_2 \text{ consumed})/(\text{mole of MBB reacted}) \quad (16)$$

As each reaction progressed, this ratio increased (Table 5). Complex reactions are characterized by stoichiometric coefficients which vary with the extent

of reaction. The variation means that the reactants (H_2O_2, MBB) are involved in more than one reaction (exclusive of H_2O_2 decomposition in this analysis) in such a way that their rate of disappearance is the sum or difference of the rates of the separate reactions (94).

For example, hydrogen peroxide is consumed not only by MBB, but also by many of the degradation products formed during the reactions. The observation that the ratio (S_2) increases with reaction time implies that some of these products are oxidized at rates slower than or equal to the rate of MBB oxidation. It is apparent that a large amount of peroxide is consumed in these secondary reactions; this point will be discussed further in the MBB Oxidation Products section.

These results indicate that the additives do not have a great effect on the way in which hydrogen peroxide degrades MBB. This is in agreement with the results of the product analyses presented in the MBB Oxidation Products section.

KINETICS

Further insights into the effects of the metal ion catalysts on the peroxide oxidation of MBB can be gained through an examination of the reaction kinetics of these systems. This section presents a kinetic analysis of the reaction data.

After a brief review of the treatment of kinetic data, the effects of the catalysts on hydrogen peroxide decomposition in both the absence and presence of MBB are examined. Next, the kinetics of the MBB oxidation reaction are analyzed. Finally, this information is brought together in a kinetic model of each system with respect to the two reactants.

Introduction

The two most common methods for treating kinetic data are the method of integration and the differential method (94,95). In the integration method, a differential rate equation is chosen which is thought to apply to the reaction under study. Acceptance of this rate equation is based on how well the data from a given reaction run fit the integrated form of the equation. If the fit is good, then the assumed rate law is accepted and the rate constant can be obtained from the slope of the line.

In the differential method, the actual rates of reaction (determined by measuring the slopes of tangents on the concentration-time curves) are used with the differential rate equation. The method can be applied in two ways. The first procedure involves measuring initial rates at various initial reactant concentrations. The slope of the line from a log-log plot of this data gives the reactant order with respect to concentration, or true order (95). In the second procedure, reaction rates are determined at various times in a single reaction run. A log-log plot of this data gives a line with a slope equal to the apparent order.

The apparent order is not always equal to the true order in complex reactions (e.g., autocatalyzed and autoinhibited reactions) (95). In addition, reactions occurring by complex mechanisms (such as those in this study) often have complicated rate expressions in which the reactant concentrations appear in the denominator of the expression. Such reaction orders are strictly empirical quantities that relate reaction rate to concentrations. However, these empirical reaction orders were found useful for comparing the kinetics of the various catalyzed systems in this study.

Hydrogen Peroxide Decomposition

The kinetics of hydrogen peroxide decomposition in both the absence and presence of MBB and metal ions are examined here.

With No Additives

Hydrogen peroxide decomposes to oxygen according to the following overall reaction:

$$2H_2O_2 \longrightarrow O_2 + 2H_2O \qquad (18)$$

In the absence of a reactive substrate the rate equation for this reaction is assumed to be:

$$-d[H_2O_2]/dt = k_1[H_2O_2]^{n_1} \qquad (19)$$

where

k_1 = rate constant

n_1 = reaction order

$[H_2O_2]$ = molar concentration of H_2O_2

Note that all of the rate constants discussed in this kinetic analysis will be for constant $[OH^-]$ and temperature. All reactions were initiated at pH 11.0 and progressed over a small pH range (pH 11.0-11.4) at 45°C.

The reaction order (n_1) for peroxide decomposition in the absence of any additives was evaluated by using data obtained by both procedures of the differential method (Appendix IV: Table 26). The results (Fig. 18) indicate that the reaction order changes from 2.5 to 2.0 at peroxide concentrations below about 60 mM.

Such a change in reaction order is an indication that the reaction may be proceeding by two or more parallel paths (96). This is a plausible explanation

considering the complex scheme by which this reaction is thought to proceed (see Background section).

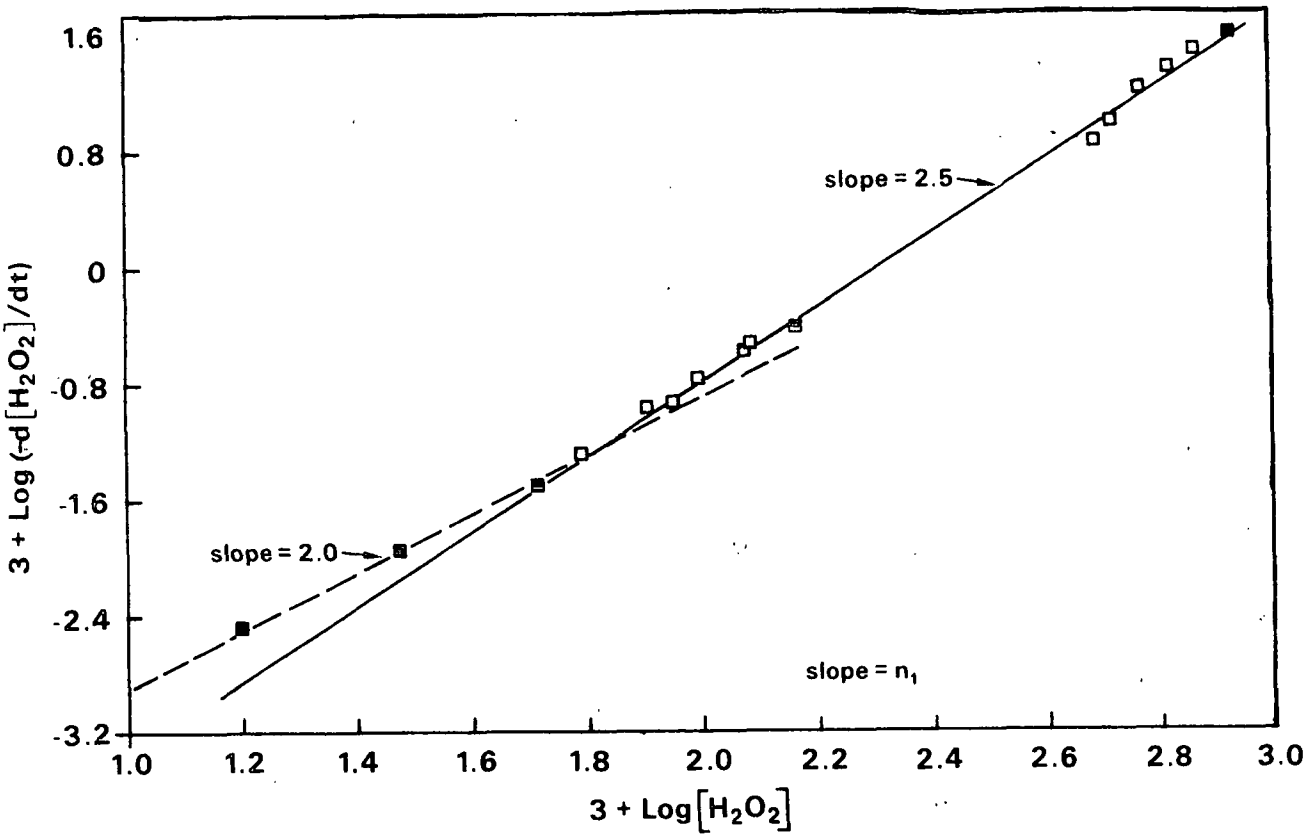

Figure 18. Kinetic plot of hydrogen peroxide decomposition data without additives (pH 11.0-11.4, 45°C). Data plotted according to the differential method using initial rates (■), and rates at various reaction times (□).

One of the most thorough studies of hydrogen peroxide decomposition kinetics in very pure alkaline solutions has recently been published (19). Using the initial rate method ($[H_2O_2]$ from 100 to 1000 mM), Galbacs and Csanyi (19) found a second order dependence on $[H_2O_2]$ at pH 12.5 and 11.2. However, in agreement with the above statement of the complexity of this reaction, they found the order decreased to 1.8 at pH 10.0.

With Metal Ions Added

The integration method was used to evaluate the effects of added Cu, Mn, and Fe ions on the decomposition kinetics. Hydrogen peroxide decomposition over the range of about 150 to 90 mM was studied at different levels of added catalyst. [Decomposition over this concentration range was studied in case the alternate reaction procedure (see Experimental) was to be employed.] The data tabulated in Appendix I were plotted in accordance with the integrated rate equation having an assumed reaction order of 1.0 or 2.5. These kinetic plots are contained in Appendix IV (Fig. 45, 46) and the resulting rate constants are tabulated in Table 6.

Table 6. Hydrogen peroxide decomposition kinetics in the absence of MBB. Metal ions added as the salts: $MnSO_4$, $CuSO_4$, $FeSO_4$. Conditions: pH 11.0-11.4, Temperature 45°C.

Metal Ion Additive	Additive Level, μM	$[H_2O_2]$ Range, mM	Reaction Order, n_1	Rate Constant,[a] k_1	ppt.[b]
Control	--	< 60	2.0	1.36 ± 0.51	0
Control	--	> 60	2.5	1.69 ± 0.34	0
Mn	1.8	90-150	2.5	2.10 ± 0.10	0
Fe	1.8	90-150	2.5	2.88 ± 0.07	0
Fe	18.2	90-150	1.0	3.50 ± 0.09	2
Fe	285	90-150	1.0	5.80 ± 0.33	3
Cu	1.8	90-150	1.0	8.45 ± 0.07	1
Cu	9.1	90-150	1.0	8.72 ± 0.26	2
Cu	18.2	90-150	1.0	8.83 ± 0.49	2
Cu	285	90-150	1.0	26.4 ± 3.1	3
Mn	9.1	90-150	1.0	4.85 ± 0.06	1
Mn	18.2	90-150	1.0	7.33 ± 0.14	1
Mn	285	90-150	1.0	202 ± 58	3

[a]Units (order): $min^{-1} \cdot 10^{-3}$ (1.0), $mM^{-1} \cdot min^{-1} \cdot 10^{-5}$ (2.0), $mM^{-1.5} \cdot min^{-1} \cdot 10^{-6}$ (2.5). ± 95% Confidence limits based on triplicate runs for the controls and single runs for the rest.

[b]Qualitative measure of metal hydroxide precipitate: 0 = none, 1 = barely noticeable, 2 = noticeable, 3 = very noticeable.

The effects of ferricyanide ions (FC) on peroxide decomposition were not examined in detail. However, preliminary experiments showed that the rate of H_2O_2 decomposition in the presence of 300 μM FC was about the same as in the presence of 18.2 μM Fe ions.

These results, in agreement with several other studies, show that addition of trace amounts of metal ions have observable effects on the decomposition reaction. Very low levels of added Mn and Fe ions (1.8 μM) did not change the reaction order (2.5) but did increase the rate (Table 6). Higher levels of added Mn and Fe ions, and all levels of added Cu ions studied, shifted the reaction to a first order dependence on $[H_2O_2]$. Galbacs and Csanyi (19) also found that the order did not change upon addition of very low levels of metal ions (Cu, 0.05 μM and Fe, 1.0 μM), but did change to first order at higher levels (Mn, 10 μM).

Precipitated metal hydroxides and oxyhydroxides were observed at the levels of added metal ion in which the decomposition was first order (Table 6). Under these conditions, the decomposition reaction probably proceeds by a heterogeneous mechanism which other studies (20,28) have shown to be first order with respect to $[H_2O_2]$.

With MBB Present

Hydrogen peroxide decomposition in the reaction runs with MBB was monitored by measuring oxygen evolution during the reaction. The rate law for the decomposition reaction was assumed to be:

$$d[Ox]/dt = k_2[H_2O_2]^{n2} \qquad (20)$$

where

$[Ox] = O_2$ as $[H_2O_2]$

The differential method was applied to the [Ox] - time curves (Fig. 14) from each reaction run (rates tabulated in Appendix IV: Table 27). In each case, the log-log plot (Fig. 19) shows a very good fit to the data over most of the reaction. The Cu, Fe, and Mn reactions did show unpredictably high initial rates. At the start of the reaction, these catalysts might be in a different physical form or oxidation state which is more active than that which is quickly reached after addition of the H_2O_2.

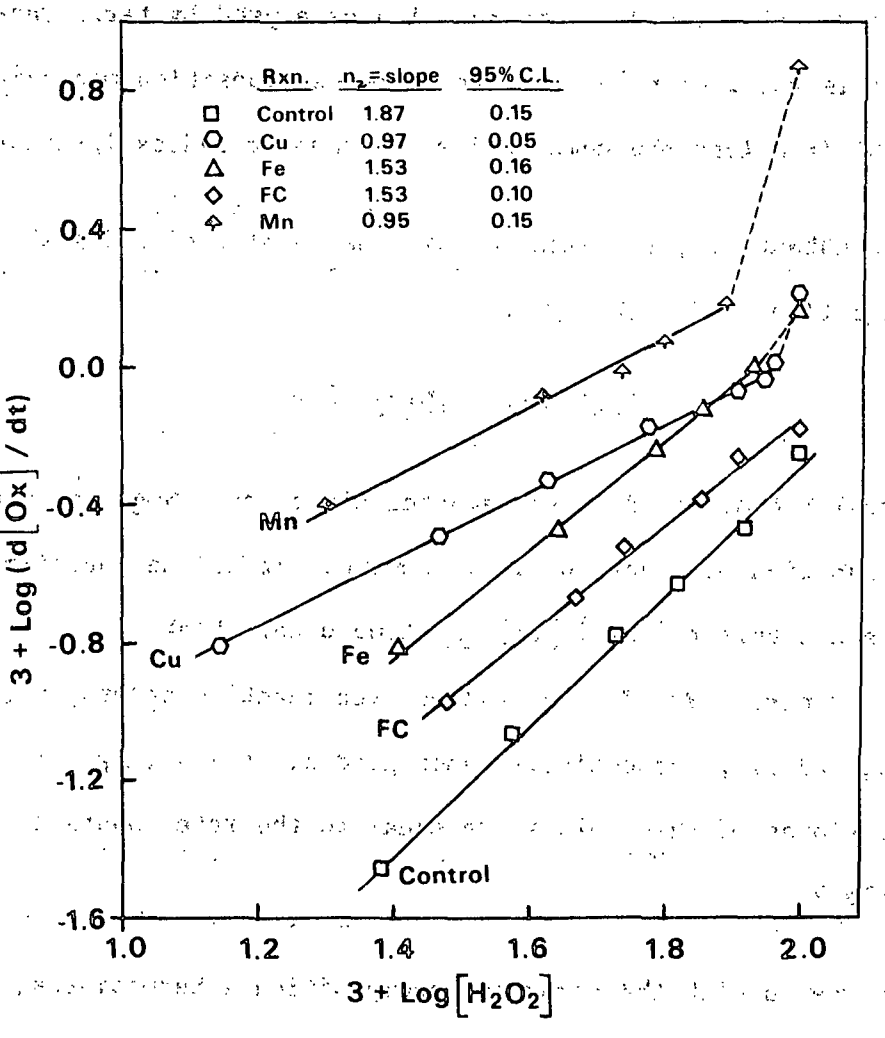

Figure 19. Kinetic plot of hydrogen peroxide decomposition data for the Control, Cu, FC, Fe, and Mn reaction runs. Data plotted according to the differential method. Reaction, additive concentration: Control, none; Cu, 12 μM; FC, 300 μM; Fe, 300 μM; Mn, 21 μM.

The slope of each line in Fig. 19 is equal to the reaction order (n_2) with respect to $[H_2O_2]$. For the Control, Cu, and Mn reactions, the reaction orders (n_2) were very close to the orders (n_1) found in the absence of MBB (2, 1, and 1, respectively). This suggests that the same decomposition pathway is followed in both the absence and presence of MBB in these systems.

The presence of MBB in the Fe reaction apparently affected the decomposition mechanism, since the order increased from 1.0 (n_1) to 1.5 (n_2). Interestingly, a 1.5 order (n_2) was also found in the reaction catalyzed by ferricyanide ions (reaction FC). This result implies that the same decomposition mechanism is operating whether the iron ions are complexed with cyano or hydroxyl/oxyhydroxyl ligands.

The rate constant, k_2, for each reaction was evaluated using the integration method. Integration of Eq. (20) gives:

$$[Ox] = k_2 \int_o^t [H_2O_2]^{n2}\, dt \qquad (21)$$

The integral cannot be exactly evaluated since the $[H_2O_2]$ is an unknown mathematical function of reaction time. However, it can be approximated by applying Simpson's Rule to the $[H_2O_2]$ vs. time data. Plots of Eq. (21) for the reaction runs (Control, FC, Fe, Cu, and Mn with reaction orders, n_2, of 2.0, 1.5, 1.5, 1.0, and 1.0, respectively) show good linearity (Appendix IV: Fig. 46, 47). The slopes of these plots are equal to the rate constants, k_2, and are listed in Table 7.

Since MBB reacts with the peroxide decomposition intermediates, its presence might be expected to inhibit peroxide decomposition. However, comparison of the rate constants, k_1 and k_2 (Table 6 and 7), shows that peroxide decomposition in the Control, Mn, and Cu reactions was accelerated with MBB present. The two rate constants for the Fe reaction cannot be compared since the reaction orders,

n_1 and n_2, are different. This acceleration effect was also observed in studies in which methyl β-D-glycopyranoside (97,98) or glucose (99) was added to alkaline H_2O_2. The effect might be due to the organic substrate acting as a chain transfer agent in the radical decomposition reaction (98). For example, the single electron oxidation of MBB by M+ (Fig. 4) provides an additional route for M to be formed. As shown in Fig. 2 (step 1), M is involved in the chain mechanism for peroxide decomposition.

Table 7. Hydrogen peroxide decomposition kinetics in the presence of MBB. Metal ions added as the salts: $MnSO_4$, $CuSO_4$, $FeSO_4$ (pH 11.0-11.4, 45°C).

Reaction	Additive Conc., μM	Reaction Order, n_2	Rate[a] Constant, k_2
Control	--	2.0	5.42 ± 0.20
Fe	300	1.5	11.6 ± 1.1
FC	300	1.5	7.28 ± 0.57
Mn	21	1.0	19.5 ± 0.6
Cu	12	1.0	10.8 ± 0.3

[a]Units (order): $mM^{-1} \cdot min^{-1} \cdot 10^{-5}$ (2.0), $mM^{-0.5} \cdot min^{-1} \cdot 10^{-4}$ (1.5), $min^{-1} \cdot 10^{-3}$ (1.0). ± 95% Confidence limits.

This catalytic effect might also be due to the introduction of trace contaminants to the reaction solutions from the MBB. The identical source of triply-distilled water and ultrapure NaOH (see Experimental) used in this study was also used in a previous study by Graves (100). He obtained complete trace metal analyses of several of his reaction solutions which contained ca. twice the concentration of NaOH as the reaction solutions in the present study. Results of those analyses showed that Mn, Co, Cr, and Cu were present below detectable limits (< 0.05 ppm) while Fe was present at 0.26 ppm [Appendix I of Ref. (100)].

In the present study a small, but detectable level of Cu (0.08 ppm, Table 8) was found in the Control reaction solution. This trace level of Cu might explain the accelerated decomposition rate in the Control reaction. However, since H_2O_2 decomposition is relatively insensitive to Cu concentration over the range 1.8-18 μM (Table 6), it is unlikely that this Cu contaminant also caused the decomposition rate to increase in the Cu reaction. Thus, (by the mechanism discussed above) the presence of MBB is probably the primary cause of the accelerated decomposition rate.

Table 8. Trace metals in Control reaction solution.

Metal	Concentration[a]	
	μM	ppm
Copper	1.3	0.08
Iron	2.2	0.12
Manganese	<0.4	<0.02
Cobalt	<0.8	<0.05
Chromium	<0.8	<0.04

[a]Analysis conducted by Badger Laboratories using atomic absorption.

MBB OXIDATION

The following rate expression was used to describe the peroxide oxidation of MBB for each of the reaction systems:

$$-d[MBB]/dt = k_3[MBB]\ [H_2O_2]^{n3} \qquad (22)$$

A first order dependence on [MBB] was assumed based on a similar kinetic study by Agnemo and Gellerstedt (16). The differential method was applied to each reaction run (rate data in Appendix IV: Table 28) to determine n_3, and the integration method was employed to evaluate the rate constant, k_3.

Effect of Ferricyanide

The rate data for the Control and FC reactions show good linearity over the course of the reaction (Fig. 20) with an order, n_3, of ca. 1.3 for both reactions.

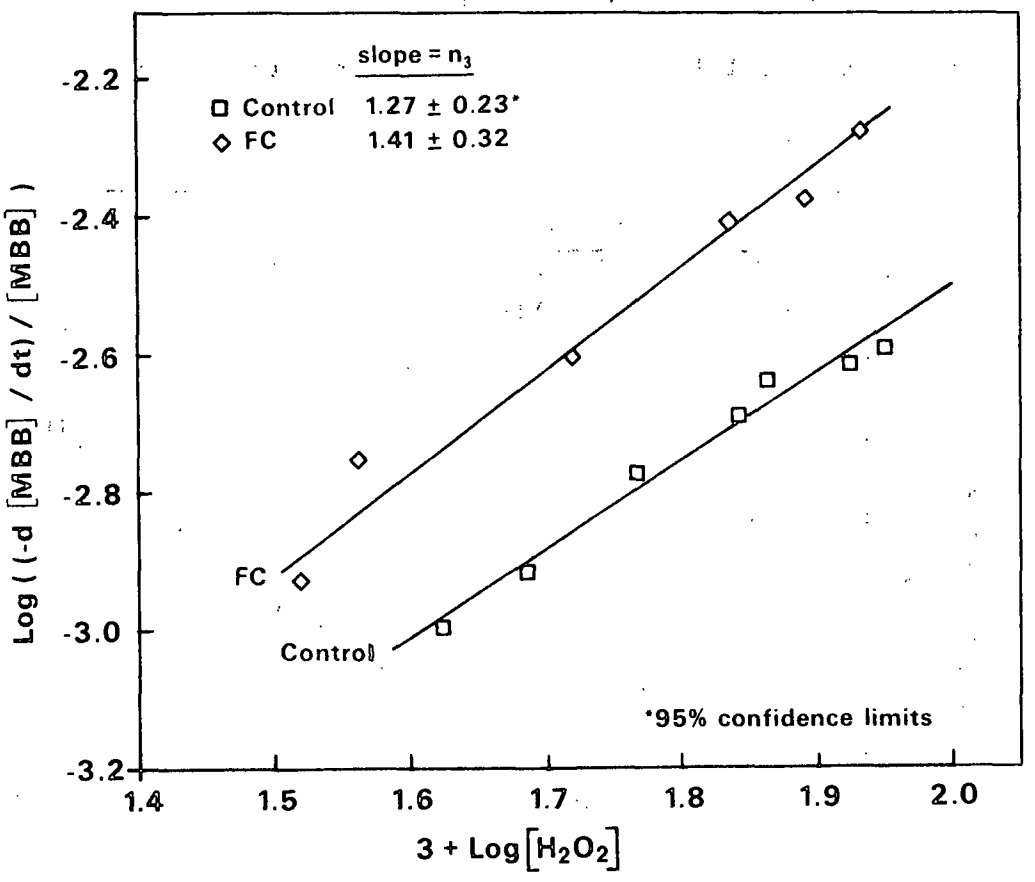

Figure 20. Kinetic plot of MBB data for the Control and FC reactions according to the differential method (n_3 = 1.3).

The integration method was used to provide a cross-check for the reactant order found above and to evaluate the rate constant, k_3, for the Control and FC reactions. Integration of Eq. (22) gives:

$$\log ([MBB]_o/[MBB]) = (2.303)\, k_3 \int_o^t [H_2O_2]^{n_3}\, dt \qquad (23)$$

where

$[MBB]_o$ = initial [MBB]

2.303 = log to ln conversion factor

The integral was evaluated using Simpson's Rule and $n_3 = 1.3$. The data from the Control and FC reactions show a good fit (Fig. 21) to Eq. (23). The measured rate constants indicate that catalytic amounts of ferricyanide ions doubled the rate of MBB oxidation.

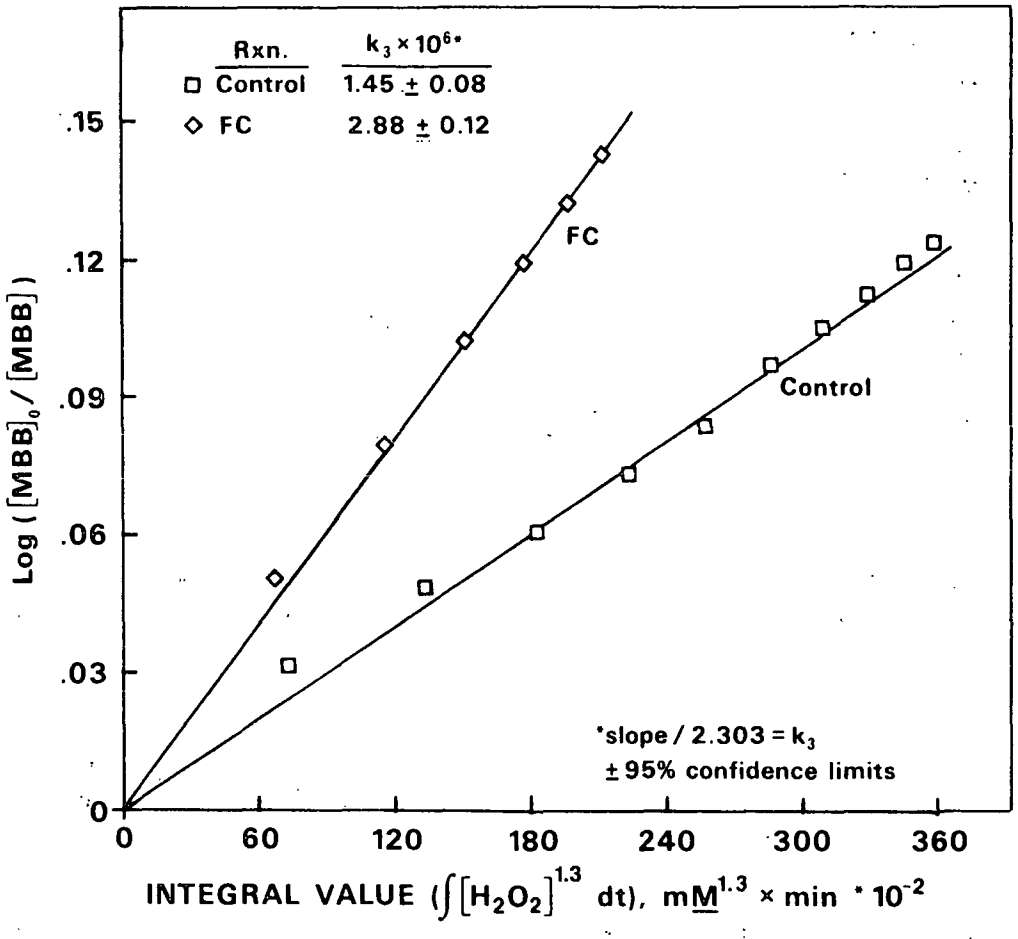

Figure 21. Kinetic plot of MBB data for the Control and FC reactions according to the integral method.

Effect of Fe and Mn

Quite different results were obtained for the Fe and Mn reactions. Figure 22 shows the log-log plots for the Fe and Mn reaction rate data. In these two

reactions, it appears that the reactant order (n_3) abruptly decreases from a higher initial value to about one-half order over the course of the reaction. A possible explanation for this observation is that the nature of the Fe and Mn catalysts change as reaction products form.

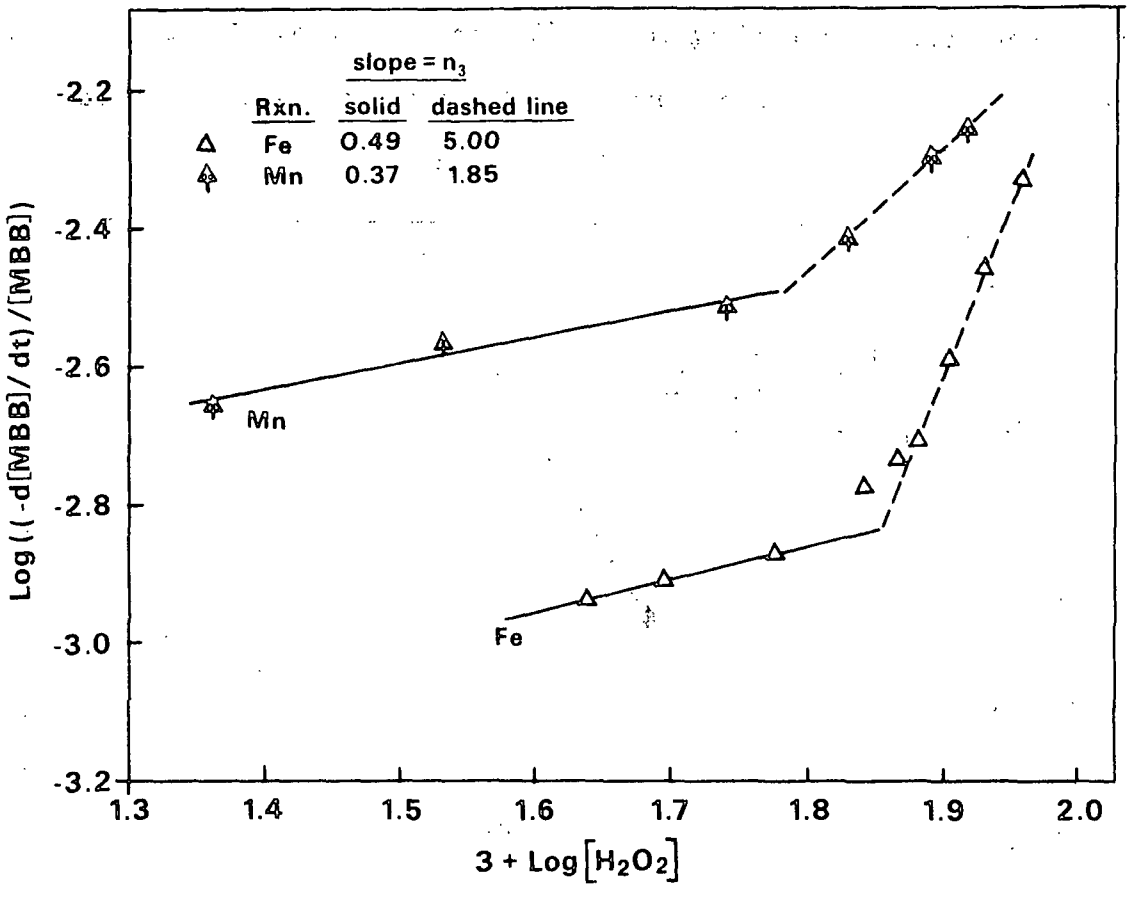

Figure 22. Kinetic plot of MBB data for the Fe and Mn reactions according to the differential method.

At the start of the reaction most of the added metal ions are present as insoluble hydroxides and/or oxyhydroxides. As the reaction progresses, MBB oxidation products likely form complexes or chelates with the metal ions. These chelates apparently exert a catalytic effect on the reaction which lowers the dependence of the rate on $[H_2O_2]$.

The integration method was applied to evaluate the rate constant, k_3, for the region in the Mn and Fe reactions where $n_3 \cong 0.5$. This region was chosen under the assumption that the catalysts had reached some equilibrium form. For both reactions this was reached after the $[H_2O_2]$ had decreased below ca. 60 mM. Thus, the data from the Mn reaction after 20 minutes and the Fe reaction after 40 minutes were plotted according to Eq. (23) for $n_3 = 0.5$. The plots (Fig. 23) show excellent linearity, and comparison of the rate constants shows that the Mn reaction is 2.5 times faster than the Fe reaction.

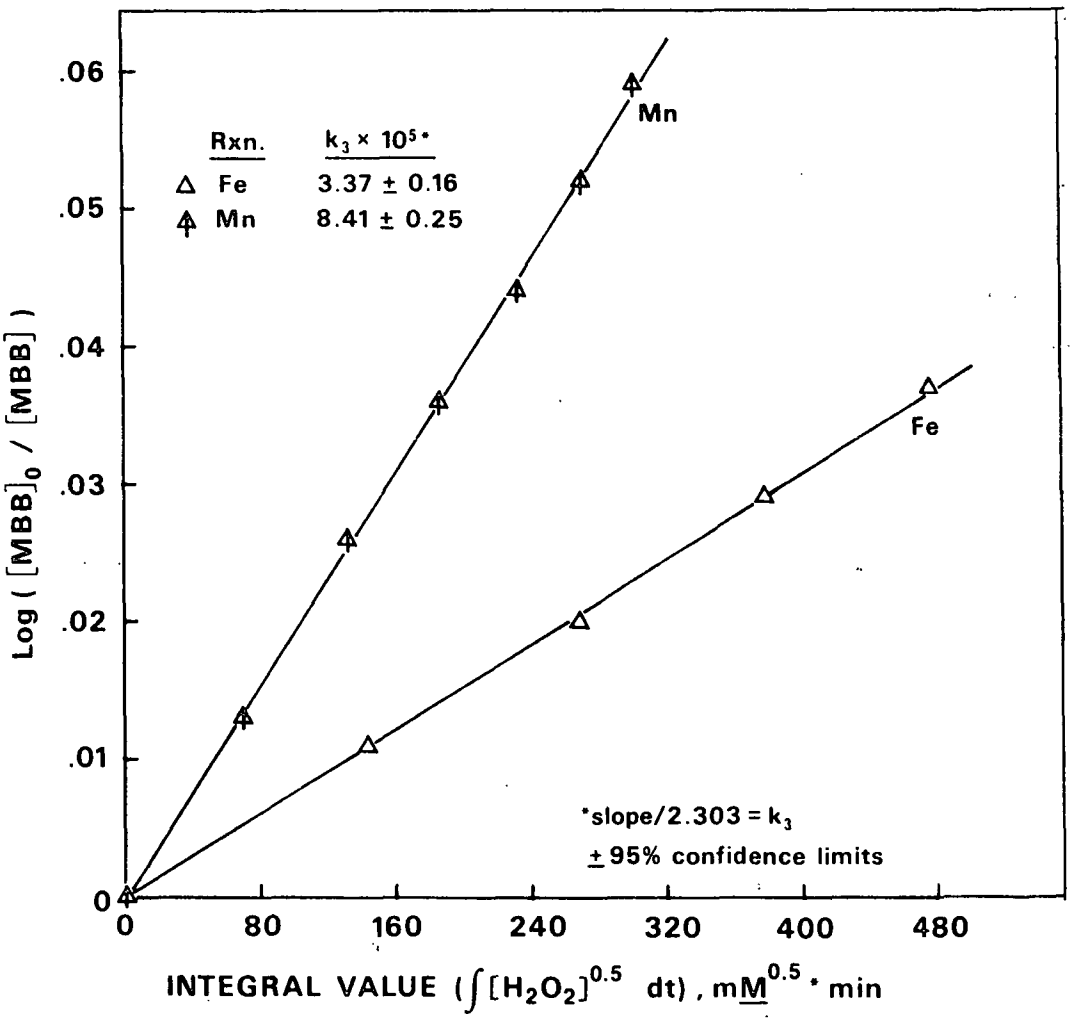

Figure 23. Kinetic plot of MBB data for the Fe and Mn reactions. Data plotted according to the integral method over the reaction region for which $n_3 = 0.5$.

Effect of Cu

A log-log plot of the rate data from the Cu reaction showed a very poor fit to Eq. (22). However, if the order, n_3, is set to zero, then the rate data fit the resulting equation [Eq. (24)] quite well (Fig. 24).

$$-d[MBB]/dt = k_4 [MBB] \qquad (24)$$

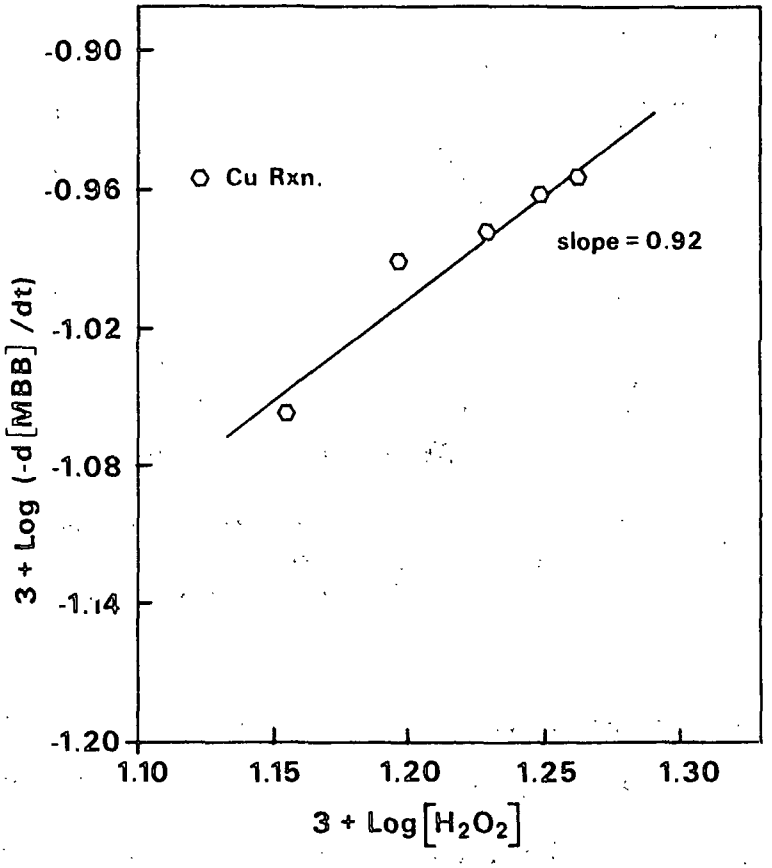

Figure 24. Kinetic plot of MBB data for the Cu reaction according to the differential method.

Equation (25) results from integration of Eq. (24).

$$\log ([MBB]_o/[MBB]) = (2.303)\ k_4\ t \qquad (25)$$

A plot of Eq. (25) using the [MBB] vs. time data for the Cu reaction also shows good linearity (Fig. 25). This further supports the overall first order rate expression given in Eq. (24).

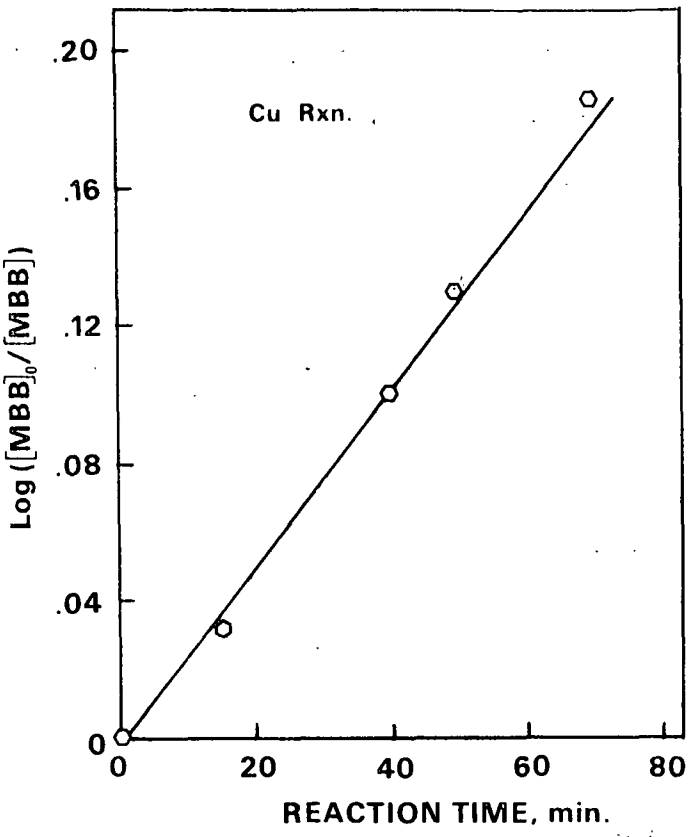

Figure 25. Kinetic plot of MBB data for the Cu reaction according to the integral method (from the slope, k_4 = 6.10 ± 0.44 • 10^{-3} min^{-1}).

Results in the MBB Oxidation Products section show that the types and distribution of products were not greatly influenced by the Cu catalyst. In addition, the stoichiometric coefficients (Table 5) were not affected by the presence of the added Cu. These observations indicate that in each system the reaction proceeds through a common intermediate, viz. cyclohexadienone hydroperoxides (see Background section).

The observed independence of the rate of MBB degradation on [H_2O_2] suggests that Cu only shifted the reaction pathway that leads to the formation of these intermediates. The likely mechanism for H_2O_2 oxidation of phenols under alkaline

conditions was presented in Fig. 4 (Background section). In that scheme, cyclohexadienone hydroperoxide intermediates are shown to result from the reaction of phenoxy radicals with (1) superoxide (an intermediate in peroxide decomposition), or (2) oxygen (a product of peroxide decomposition).

The observed kinetics can be explained by postulating that the Cu catalyst favored a reaction of oxygen with MBB (or the phenoxy radical of MBB). Since the decomposing hydrogen peroxide maintains a saturated solution of oxygen (i.e., constant concentration), the reaction rate depends only on [MBB]. Thus, k_4 would be termed a pseudo first-order rate constant at constant oxygen concentration.

It is postulated here that the Cu catalyst effectively competes with the phenoxy radical for superoxide ions. Thus reaction of phenoxy radicals with oxygen (followed by reduction of the resulting hydroperoxy radical, Fig. 26) becomes the favored pathway to the formation of cyclohexadienone hydroperoxides.

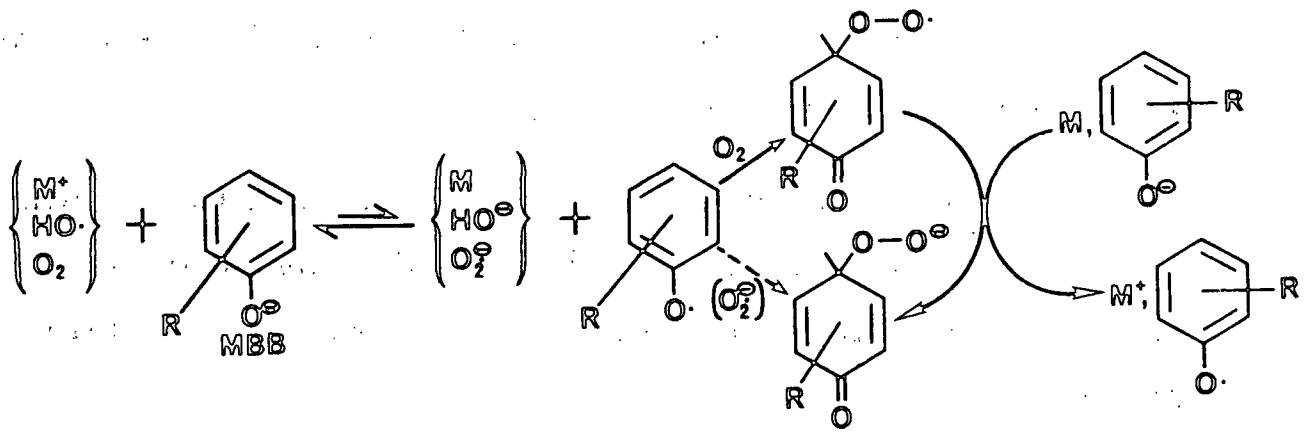

Figure 26. Proposed mechanism for the Cu catalyzed alkaline/H_2O_2 oxidation of MBB.

The same mechanism may have operated to some degree in the Mn and Fe catalyzed reactions. These two systems exhibited a one-half order with respect to $[H_2O_2]$ (over most of the reaction); this is between the 1.3 order for the Control reaction and the zero order for the Cu reaction.

A large number of metal ions and their complexes are simple one-electron oxidants [Reaction (26)] of superoxide (37). In addition, superoxide dismutation [Reaction (26) and (27) combined] is known to be catalyzed by various complexes of Cu, Mn, and Fe (34).

$$O_2^{\cdot-} + M^{+} \longrightarrow O_2 + M \qquad (26)$$

$$M + O_2^{\cdot-} + H_2O \longrightarrow HO_2^{-} + HO^{-} + M^{+} \qquad (27)$$

The nature of the metal catalysts in the Mn, Fe, and Cu reaction systems in the present study is not known. However, studies of superoxide dismutation and oxidation by well defined metal complexes tend to support the mechanism postulated above. For example, the oxidation of superoxide by hydrated Cu(II) ions has been shown to occur at very high rates [$k = 8 \times 10^9 \underline{M}^{-1}\ s^{-1}$ (101)]. Also, reaction of hydrated Cu(I) ions with superoxide [Reaction (27)] occurs near diffusion controlled rates [$k \simeq 10^{10} \underline{M}^{-1}\ s^{-1}$ (101)].

However, superoxide dismutation in the presence of ferricyanide/ferrocyanide ions occurs at much lower rates [$k \simeq 10^3 \underline{M}^{-1}\ s^{-1}$ (102)]. This probably explains why the reaction order with respect to $[H_2O_2]$ was the same in both the Control and FC reactions.

Kinetic Models

Because the reactant order, n_3, for the Control was different from that found for the Mn and Fe reactions, a direct and exact comparison of the respective

rate constants, k_3, cannot be made. However, it was possible to make a qualitative comparison of the rates of MBB oxidation in these reaction systems. This was accomplished by applying the same general kinetic model to the experimental data from each reaction.

The kinetic model employed [Eq. (28) and (29)] was evaluated by a computer using a multiresponse parameter estimation program (Appendix V). For each reaction the program found values for k_5 and k_6 which produced the best fit of the experimental data to the calculated values. Plots of the experimental data with the calculated $[H_2O_2]$-time and [MBB]-time curves are shown in Fig. 48-51 of Appendix V.

$$-d[MBB]/dt = k_5 [MBB] [H_2O_2] \quad (28)$$

$$-d[H_2O_2]/dt = k_2 [H_2O_2]^{n2} + k_6 [MBB] [H_2O_2] \quad (29)$$

The above kinetic model represents a simplification of the actual reaction systems. For instance, the observed increase in reaction stoichiometry with time (Table 5) is not predicted by the model. Also, as shown in the previous section, the order with respect to $[H_2O_2]$, n_3, in Reaction (22) is only approximately equal to one. Nevertheless, Fig. 48-51 of Appendix V demonstrate that this simplified model does predict reactant concentrations as a function of time with reasonable accuracy. Thus this procedure provides a convenient, qualitative means of comparing the MBB oxidation rates (k_5's) in the Control, Mn, Fe, and FC reactions.

Table 9 summarizes the rate constants, k_5 (relative to the Control), found by this analysis. These results are in qualitative agreement with the findings from the preceding section. For instance, MBB oxidation rate for the FC reaction is double the rate for the Control. Also, the rate for the Mn reaction is ca. 2.5 times the rate of the Fe reaction.

Table 9. Relative rate constants obtained through the kinetic model analysis.

Reaction	Relative,[a] k_5
Control	1.00
Fe	1.34
FC	2.00
Mn	3.20

[a]Ratio of k_5 for the given reaction to k_5 for the Control.

Since this analysis gives results comparable to those found in the preceding section, k_5 for the FC, Mn, and Fe reactions can be compared to the Control. Such a comparison shows that Fe ions gave the least increase in the MBB oxidation rate. Since the rate determining step in the oxidation of MBB is assumed to be phenoxy radical formation, the results found here indicate that Fe ions do not catalyze this step to a great extent. This is consistent with Landucci's observation that Fe(III) does not catalyze 2-t-butyl-4-methylphenol dimerization under mild oxygen/alkaline conditions (69).

These results have further implications. The rate of radical production, from hydrogen peroxide decomposition, should be greater in the Fe reaction than the Control based on the work of Galbacs and Csanyi (19). However, since the MBB oxidation rate increased by a relatively small amount, it follows that the direct attack of these intermediate radical species on MBB, to form a phenoxy radical, is much slower than the reactions leading to oxygen formation or combination with a phenoxy radical.

The increase in MBB oxidation rate for the FC reaction was ca. three times that for the Fe reaction. In both reactions, the catalyst was added at the same

level (300 μM). Under the alkaline reaction conditions most of the Fe ions were present as a precipitate of iron hydroxides/oxyhydroxides, while the ferricyanide was totally soluble. This fact might account for some of the difference observed in the catalytic activities of these two iron species.

However, most of the difference is probably due to the differences in their redox potentials. Using cyclic voltammetry, Landucci (72) showed that the redox potentials of ferricyanide and ferric ions, under alkaline conditions, are quite different. The redox couple for ferricyanide is much more favorable for phenoxy radical formation. Indeed, ferricyanide ion is a well known single electron transfer agent for the oxidative coupling of phenols (75).

Addition of Mn ion catalyzed the MBB oxidation to a greater extent than either Fe or FC. Landucci (69,72) also found that Mn ion was a more effective catalyst for phenoxy radical formation than either Fe(III) or ferricyanide (Table 2).

Since the rate of MBB oxidation in the Cu reaction was independent of $[H_2O_2]$, the kinetic model defined by Eq. (28) and (29) gave a very poor fit to the data. However, the use of Eq. (24) and (30) as the kinetic model produced a very good fit of the experimental data to the calculated $[H_2O_2]$-time and [MBB]-time curves (Appendix V: Fig. 52). This finding further supports Eq. (24) as the rate law for the Cu reaction.

$$-d[H_2O_2]/dt = k_2 [H_2O_2] + k_7 [MBB] \qquad (30)$$

Catalytic Effectiveness

Results of the analysis in this section demonstrate that addition of trace amounts of transition metal ions strongly influenced the reaction kinetics of

both MBB oxidation and H_2O_2 decomposition. The additives increased the rates of both reactions. It is of practical significance to compare the relative increase in the rates of these two reactions for each catalyzed system. An increase in the ratio of the rates of MBB oxidation to H_2O_2 decomposition would be desirable in the context of peroxide delignification.

Unfortunately, the rate constants obtained for the five systems (k_2, k_3, k_4) cannot be directly compared since the added catalysts also caused changes in the reaction orders (n_2, n_3). However, an interesting comparison can be made under the assumption that the rate of H_2O_2 decomposition is proportional to the rate of MBB oxidation, i.e.:

$$d[Ox]/dt = E \cdot (-d[MBB]/dt) \tag{31}$$

where

$[Ox] = O_2$ as $[H_2O_2]$

E = proportionality constant

Integration of Eq. (31) gives:

$$[Ox] = E \cdot ([MBB]_o - [MBB]) \tag{32}$$

The constant, E, is a measure of the "effectiveness" of the additive in catalyzing oxidation over decomposition (the higher the value of E, the less effective it is). Data from the five reaction systems were plotted (Fig. 27) according to Eq. (32).

The results show that the Fe and Mn additives were equally "ineffective" catalysts. In these two reactions ca. 15 moles of H_2O_2 were decomposed to oxygen per mole of MBB consumed (Fig. 27). While the rates of MBB oxidation in the Fe and Mn reactions were greater than in the Control (Table 9), considerably more H_2O_2 was lost through decomposition to oxygen.

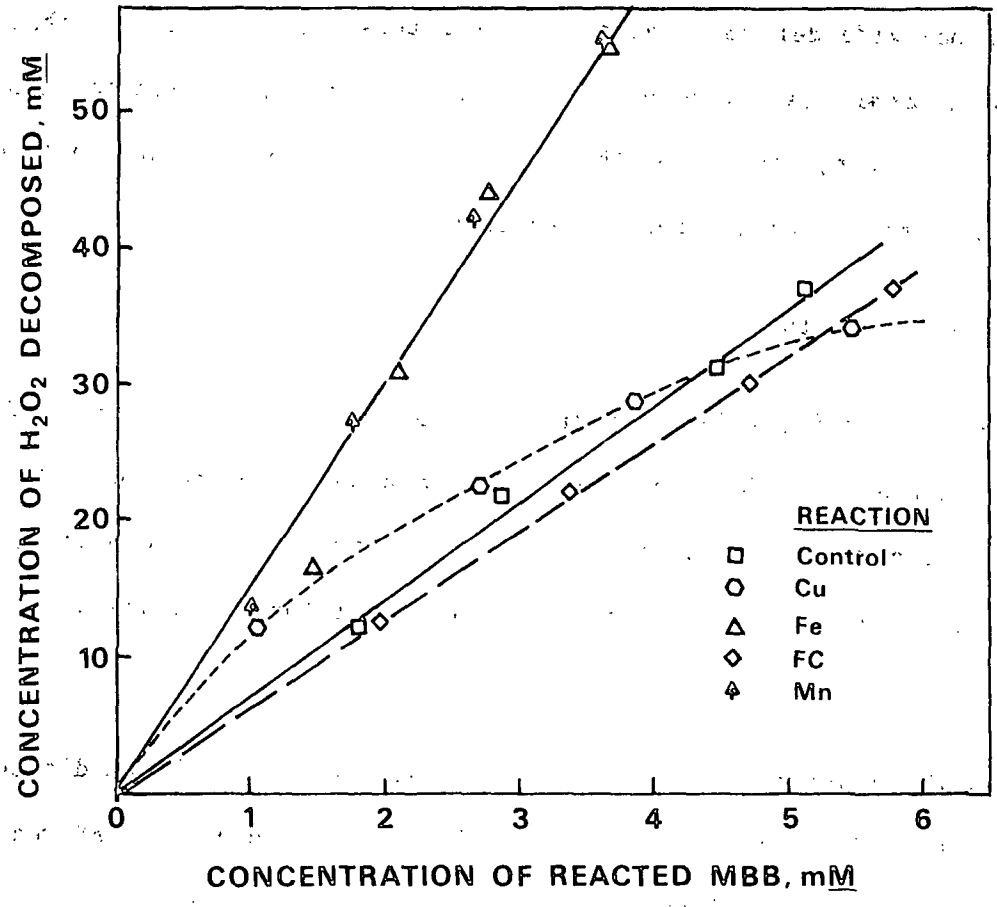

Figure 27. Influence of metal ions on the relationship between peroxide decomposition and MBB oxidation.

In contrast to Mn and Fe, ferricyanide (FC) was found to be an "effective" catalyst (6.7 moles H_2O_2 decomposed per mole MBB consumed) (Fig. 27). As an added benefit, the added ferricyanide ions doubled the rate of MBB oxidation (Table 9).

The Cu reaction gave a nonlinear response (Fig. 27) to Eq. (32). This is due to the independence of the MBB oxidation rate on $[H_2O_2]$ as shown earlier. As a result, the added Cu changed from an "ineffective" to an "effective" catalyst as the reaction progressed. The Cu reaction also exhibited the highest rates of MBB oxidation of the five systems (Appendix IV: Table 28).

These observations graphically demonstrate that the added transition metal ions catalyzed MBB oxidation and H_2O_2 decomposition to varying extents. In the

context of peroxide delignification of pulp, these results suggest that the presence of some metals (e.g., Fe and Mn) waste H_2O_2 through increased decomposition to oxygen. However, results of the Cu and FC reactions indicate that not all metal species may be considered detrimental.

MBB OXIDATION PRODUCTS

Some of the products formed during the MBB oxidations were examined to determine whether the added metal ions caused a shift in the types of products formed or a change in the distribution of products. The major products were identified, and likely reaction pathways for their formation are proposed.

Methanol

During the reactions methanol is liberated through: (1) the direct demethylation of MBB, and (2) oxidation and/or hydrolysis of secondary MBB reaction products (Fig. 6). Methanol liberation was measured by quantitative GLC using ethanol as an internal standard (see Experimental). The results are tabulated in Appendix II. In separate experiments (without MBB present), methanol was shown to be stable under the reaction conditions (100 mM H_2O_2, 45°C, pH 11.0, 6 h) in the absence or presence of added catalyst (12 μM $CuSO_4$).

The added metal ions increased the rate of methanol formation (Fig. 28) in a manner comparable to the increase in the rates of total acid group formation (Fig. 17) and hydrogen peroxide consumption [Fig. 15(a)]. Over the course of the reactions, 50 to 80 percent of the theoretical yield of methanol (based on two moles of methanol formed per mole of MBB consumed) was formed (Fig. 29).

Generally the methanol production increased as the reaction progressed (dashed line in Fig. 29). In accordance with the stoichiometry results (Table

5) some portion of the liberated methanol likely results from slower, secondary reactions of MBB oxidation products. In contrast to the other reaction runs, the theoretical yield of methanol found during the Cu reaction remained fairly constant (Fig. 29) and at a higher value, ca. 80% of theoretical.

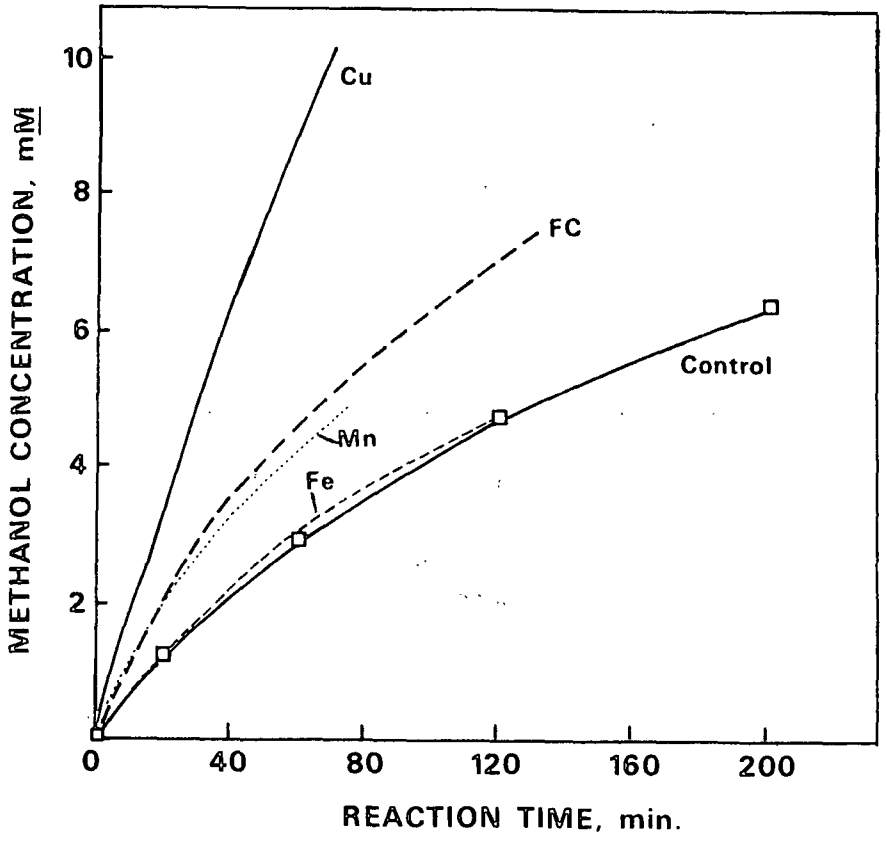

Figure 28. Effects of added metal ions on the rate of methanol formation from the peroxide oxidation of MBB (initial pH 11.0, $[H_2O_2]_o$ = 100 mM, $[MBB]_o$ = 20 mM, added metal ion levels given in Table 3).

The yields of methanol obtained in each reaction were less than 100% of the theoretical because a portion of the total methoxyls were retained in some of the acidic products. These and other MBB degradation products are discussed in the following section.

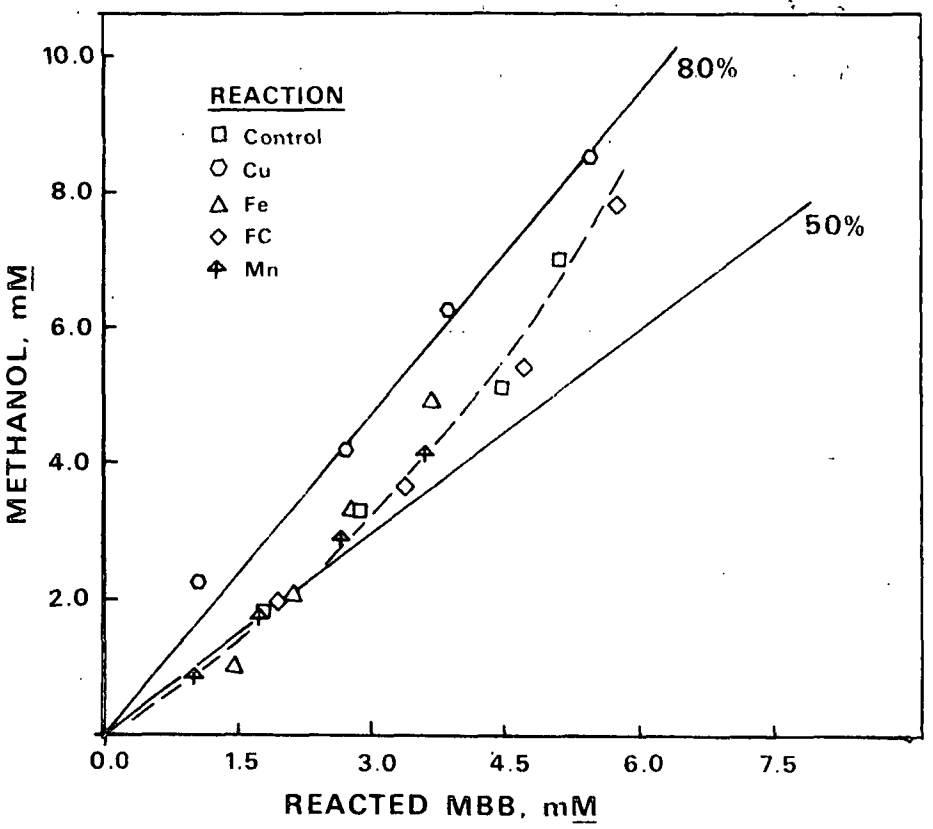

Figure 29. Effects of added metal ions on the theoretical yield of methanol from MBB oxidation in alkaline H_2O_2 (conditions listed in Fig. 28). The straight lines mark the 50 and 80% theoretical yield values defined by: $[MeOH]/(2x([MBB]_o - [MBB])) \times 100\%$.

Acidic Products

General Comments

The distributions of acidic products formed during the Control, Fe, FC, Mn, and Cu reactions were examined. These products were analyzed as their per-O-trimethylsilyl (TMS) derivatives by GLC and GLC/MS. Semiquantitative estimates of acidic product concentrations were made by using estimated and experimentally determined response factors relative to an internal standard (vanillic acid). The sample workup procedure is detailed in the Experimental section. Appendixes II and VII present, respectively, the tabulated acidic product results, and the GLC conditions and response factors.

The acidic products were mainly identified by interpretation of their mass spectra and/or comparison of their relative GLC retention times and mass spectra with authentic compounds (see Appendix VIII: Product Identifications).

A representative GLC chromatogram of the acidic products from MBB degradation is shown in Fig. 30 with the identities of the numbered peaks listed in Table 10 and Fig. 31. Due to the sample workup procedure, the peak labeled MBB in Fig. 30 does not represent all of the unreacted MBB in the sample. During sample workup, most of the unreacted MBB precipitated from solution when the pH was lowered. This white precipitate was removed by filtration before completing the sample workup, and was shown to contain only MBB by GLC and TLC analyses.

Influence of Metal Ions

A comparison of the GLC chromatograms and GLC/MS analyses of reaction samples from each run showed that the added metal ions did not induce major changes in the types of acidic products produced during MBB degradation. In other words, the same products were common to all reaction systems. The results of the semiquantitative GLC analyses of the acidic products did point out some differences though in the product distributions with respect to reacted MBB. Table 11 compares the yields of some major acidic products (on a mole percent of reacted MBB basis) produced during each reaction.

With a few exceptions, the results show that the distributions of acidic products are fairly similar for all five reactions. The main differences are found in the lower molecular weight degradation products. For example, the Fe and Mn reactions produced much lower yields of product III, IV, and V, whereas product I was formed in higher yields in the Fe and FC reactions. An explanation for these differences is not readily apparent.

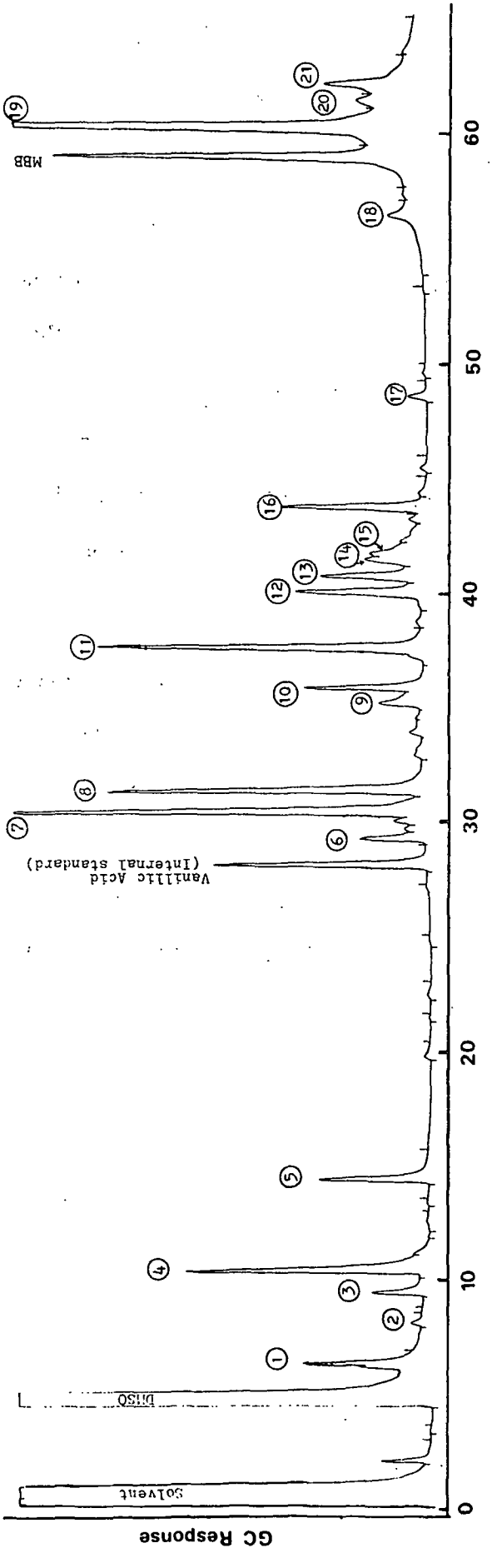

Figure 30. Representative gas-liquid chromatogram of the TMS derivatives of the acidic products from the peroxide oxidation of MBB (sample from the Cu catalyzed reaction, 70 min).

Table 10. Acidic MBB degradation products.

Peak[a]	Product[b] Structure	Identification	Identification[c] Method	Yield[d]
1	I	Glycolic acid	1,2	4.4
2	II	3-Hydroxypropanoic acid	2	1.2
3	III	Oxalic acid	1,2	7.1
4	IV	Levulinic acid	1,2	19.8
5	V	Succinic acid	1,2	16.0
6	VI	3-Carboxy-hexanedioic acid	3,6	8.1
7	VII	Cis-3-carboxy-2-hexenedioic acid	3,6	13.1
8	VIII	4-(2-Carboxyethyl)-2-furoic acid	3,4,5,6	9.6
9	IX	--	--	2.9
10	X	--	--	6.3
11	XI	5-Hydroxymethyl-hydroferulic acid	1,2,5	13.3
12	XII	--	--	3.1
13	XIII	--	--	4.0
14	XIV	5-Carboxymethyl-hydroferulic acid	3	4.6
15	XV	--	--	--
16	XVI	(Impurity from workup)	--	--
17	XVII	(Column artifact)	--	--
18	XVIII	5-(2,6-Dicarboxy-4-oxo-hexane)-hydroferulic acid	3	2.1
19	XIX	A lactonic acid	3,4	12.5
20	XX	A lactonic acid	3,4	0.4
21	XXI	An epoxy quinol	3	0.4

[a]Peak number in the chromatogram shown in Fig. 30.
[b]Structures of minor products IX, X, XII, XIII, and XV were not determined; others are depicted in Fig. 31.
[c]Method of identification (discussed in Appendix VII):
1. Comparison of GLC retention times with known sample
2. Comparison of mass spectrum with known sample
3. Interpretation of mass spectrum of the compound
4. Examination of infrared spectrum of the compound
5. Examination of H-NMR of the compound
6. Chemical evidence
[d]Mole % yield ([product]/($[MBB]_o$ - [MBB]) x 100%) for Control (270 min). Yields determined by GLC (see Experimental).

Examination of Table 23 (Appendix II) shows that low molecular weight acidic products are formed early in the reactions. This is consistent with the mechanism for peroxide oxidation of phenols discussed in the Background section. The initially formed cyclohexadienone hydroperoxide rapidly undergoes alkaline and oxidative conversions and degradations to lower molecular weight products.

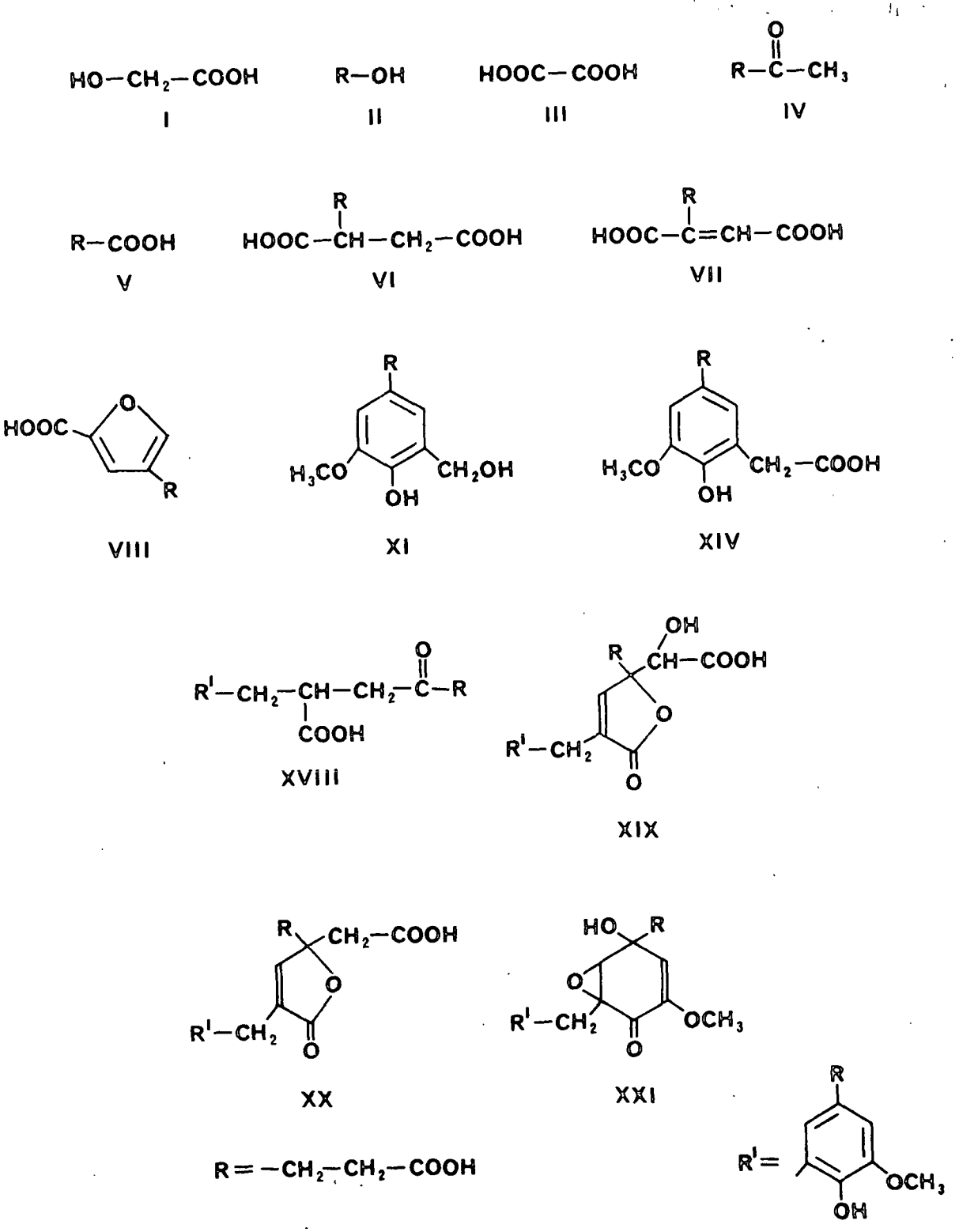

Figure 31. Structures of identified products from the alkaline hydrogen peroxide oxidation of MBB.

Table 11. Acidic products distribution from MBB degradations in the absence and presence of added metal ions. Yields are given in mole percent of reacted MBB.

Reaction	Control		Fe		FC	Mn		Cu	
Reaction[a], %	20.0	26.0	14.3	17.9	28.0	15.0	21.0	20.4	34.8
Product[b]	Mole Percent Yield[c]								
I	7	4	13	14	15	8	3	8	6
III	3	7	0	1	4	0	1	4	4
IV	21	20	9	11	21	10	12	29	24
VI	7	8	5	6	4	4	3	3	3
VII	14	13	7	8	16	16	10	21	17
VIII	9	10	6	7	11	10	11	14	15
XI	16	13	15	13	12	18	14	20	13
XIV	4	5	2	3	4	1	2	3	2
XIX	14	13	10	10	11	17	15	20	15

[a]Based on initial [MBB] = 20.0 mM.
[b]Structures given in Fig. 31.
[c]Product concentrations estimated by GLC analysis of silylated product mixtures using response factors listed in Appendix VI. For a given acidic product, the standard deviation for duplicate silylations was generally in the range of ± 10-20% of the stated concentration. Mole % yield = [product]/($[MBB]_o$ - [MBB]) x 100%.

Reacted MBB Balance

The acidic products and methanol produced during each of the reaction runs account for ca. 40-70% (Table 12) of the reacted MBB (based on carbon). In addition, there are three types of products which if included in the total balance would increase the accountable yield by several percent. First, there are numerous minor acidic fragmentation products present in the reaction mixtures at very low concentrations. These products were detectable by GLC (especially at higher detector attenuations), but were not quantitated due to their low concentrations. Collectively, such products might account for several percent of the reacted MBB.

Table 12. Carbon balance on reacted MBB based on acidic products and methanol produced during the reaction runs. Yields are given in mole percent of reacted MBB on a carbon basis.

Reaction		Control		Fe		FC	Mn		Cu	
Rxn. time, min		120	270	75	120	130	40	75	40	70
Reacted MBB, mM		4.0	5.2	2.9	3.5	5.6	2.9	4.2	4.1	6.9
Product[a]	Carbons[b]	Percent Yield[c]								
I	2	0.7	0.4	1.2	1.4	1.4	0.8	0.3	0.8	0.6
II	3	0.0	0.2	0.0	0.0	0.0	0.0	0.0	0.1	0.1
III	2	0.3	0.7	0.0	0.2	0.4	0.0	0.1	0.4	0.4
IV	5	5.1	4.7	2.2	2.7	4.9	2.3	2.9	7.0	5.7
V	4	1.5	3.0	0.4	0.9	2.1	0.0	0.9	1.6	1.6
VI	7	2.4	2.7	1.7	2.0	1.5	1.4	1.0	1.1	0.9
VII	7	4.6	4.4	2.3	2.8	5.3	5.3	3.5	6.9	5.8
VIII	8	3.5	3.7	2.4	2.8	4.2	3.9	4.2	5.5	5.6
IX	(10)	0.6	1.4	0.0	0.3	0.7	0.0	0.0	0.4	0.4
X	(10)	2.1	3.0	1.3	1.6	2.2	1.7	2.3	1.8	1.8
XI	11	8.5	7.0	7.7	7.0	6.3	9.4	7.5	10.7	6.5
XII	(12)	1.6	1.8	1.0	1.0	1.6	1.1	2.2	4.1	3.8
XIII	(12)	2.3	2.3	1.6	2.1	2.2	2.3	3.1	2.4	3.0
XIV	12	2.3	2.6	1.6	1.4	2.0	0.4	1.4	1.5	1.1
XVIII	20	0.2	2.0	0.0	0.0	0.5	0.0	0.7	0.0	0.4
XIX	20	13.6	11.9	10.0	9.6	10.7	15.9	14.3	19.1	14.1
XX	20	0.2	0.4	0.0	0.0	0.4	0.0	0.2	0.9	0.4
XXI	21	0.3	0.4	0.0	0.0	0.4	1.7	2.6	0.5	1.4
Methanol	1	5.7	6.7	6.0	6.5	6.3	5.2	5.6	7.6	7.0
Total, %		55.5	59.3	39.4	42.3	53.1	51.4	52.8	72.4	60.6

[a]Structures given in Fig. 31.
[b]Number of carbon atoms in individual product = carbons/product, numbers in parentheses are estimated.
[c]Yield = ([product] x carbons/product)/([reacted MBB] x carbons/MBB).

Volatile, low molecular weight degradation products (other than methanol) lost during the sample workup represent a second source of unaccounted for MBB. In a separate experiment, MBB was reacted under base line conditions and the terminal reaction solution was analyzed by ion chromatography. Carbon dioxide (as carbonate) and formic acid (as formate) were found to be present at levels representing, respectively, 7.8 and 5.6 percent of the reacted MBB (based on carbon).

Finally, some of the MBB degradation products might not be volatile enough for detection by GLC under the conditions used to examine the acidic products. Low yields of products in comparable studies (62) have been attributed to formation of high molecular weight condensation products. However, such reactions are probably minimal in the present study.

It is likely that all major degradation products in the MBB/H_2O_2 reaction were detected by the techniques employed in this study. Possible reaction pathways and mechanisms which can account for the formation of the identified products are explored in the following section.

Possible Reaction Pathways

General Comments

Numerous studies have established that the formation of a cyclohexadienone hydroperoxide intermediate is the initial step in the degradation of simple phenolic structures in alkali by hydrogen peroxide or oxygen (see Background). The hydroperoxide group may be oriented *para* or *ortho* to the original phenolic hydroxyl as shown for MBB (Fig. 32). These structures are susceptible to nucleophilic additions of hydroperoxy and hydroxyl anions followed by alkaline and oxidative conversions and degradations to acidic reaction products (59,67).

Based upon the understanding of the mechanisms involved, some of the possible reaction pathways which might account for the products of MBB degradation are examined in this section.

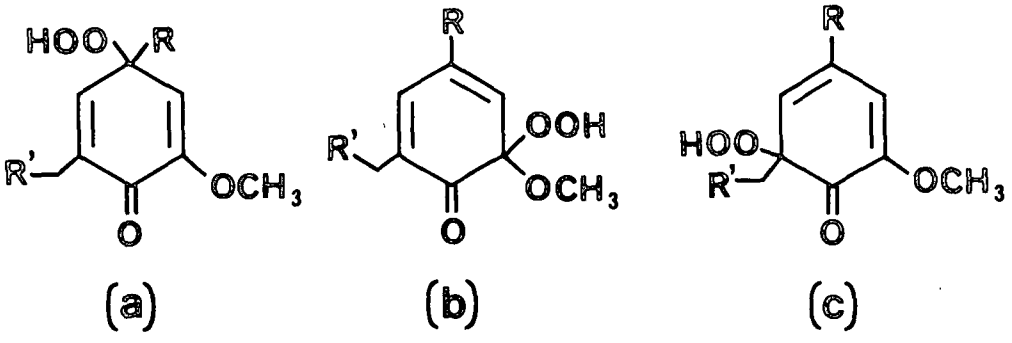

Figure 32. Structures of cyclohexadienone hydroperoxide intermediates of MBB (R,R' as in Fig. 31).

Primary Reaction Products

Hydroperoxides formed during the peroxide oxidation of MBB (Fig. 32) may undergo intramolecular rearrangement via dioxetanes to form epoxy quinol structures (68). This reaction, depicted in Fig. 33, accounts for the formation of product XXI. Formation of other epoxy quinol structures can be visualized, but no others were detected. This finding is analogous to results of other studies (67,68,103). The selectivity is probably due to the electron donating character of the methoxyl group which resonantly deactivates position 4 toward nucleophilic addition (68).

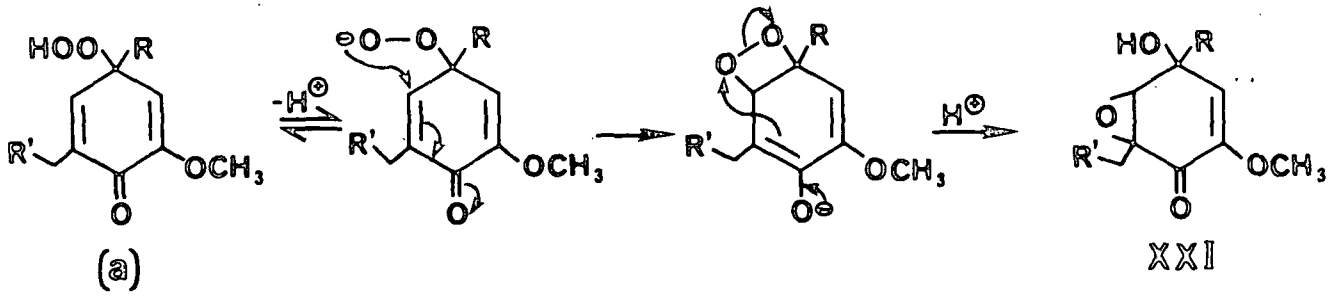

Figure 33. Formation of XXI from rearrangement of cyclohexadienone hydroperoxide-a.

Demethylation of hydroperoxide-b (Fig. 32) and subsequent nucleophilic reactions with hydroperoxy anions result in the formation of XIX and XX (Fig. 34). The mechanism of demethylation shown in Fig. 34 was postulated by Mih (104). Orthoquinones are reactive intermediates which have been detected during the treatment of lignin models under milder alkaline H_2O_2 conditions (59,60).

Product XX likely arises from the cleavage of the orthoquinone via a dioxethane intermediate (58,62), followed by lactonization of the muconic acid (pathway b in Fig. 34). This route is commonly referred to as the muconic acid pathway.

Alternatively, one of the double bonds of the orthoquinone may be epoxidated (by HO_2^-) followed by cleavage between the carbonyl groups (pathway a in Fig. 34). The resulting monoepoxidated dicarboxylic acid is then converted to the corresponding lactonic acid (XIX) by intramolecular nucleophilic attack (82,105).

Both compounds (XIX, XX) are structurally very similar and should exhibit similar reactivities under the oxidative conditions. Since XIX was found in much higher yields than XX (Appendix II: Table 24) it can be concluded that pathway a must dominate. Furthermore, based on the semiquantitative results (Table II), a minimum of 10-20% of the overall reaction proceeds by this pathway.

In a separate experiment oxygen was bubbled through an alkaline solution of MBB without added H_2O_2 (see Experimental). Under these conditions an acidic products mixture containing mainly XI, XIX, XX, and XXI was produced. This result supports the contention that oxygen and hydrogen peroxide attack phenolic lignin units by similar reaction mechanisms (see Background).

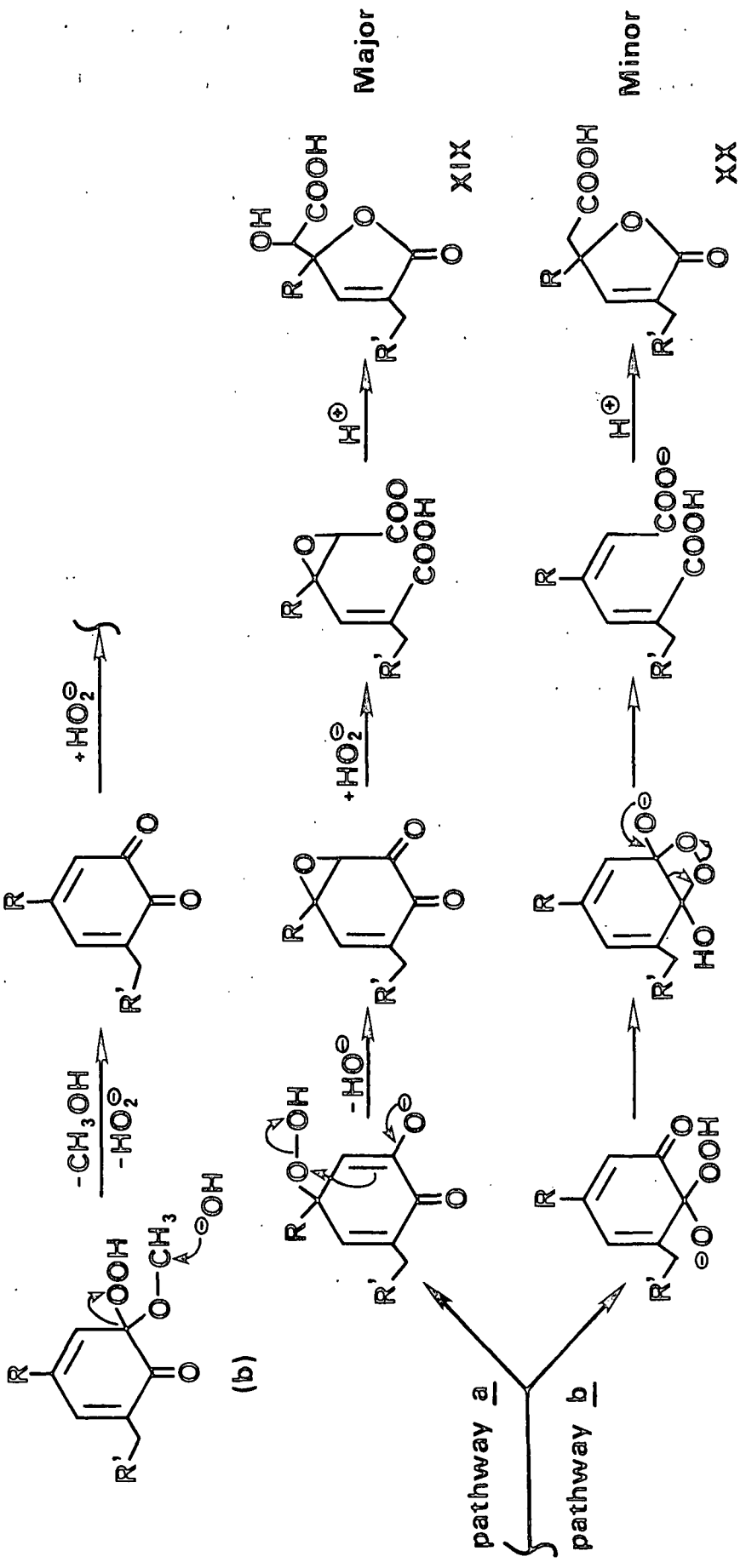

Figure 34. Probable routes to the formation of XIX and XX from cyclohexadienone hydroperoxide-b.

The alkaline stability of these autoxidation products was examined by purging the above reaction solution with nitrogen and sampling after 90 minutes. The results of the experiment, listed in Table 13, show that the decrease in [XIX], and the increase in [XVIII] (after the alkaline treatment), were about the same. This observation indicates the XVIII is formed from XIX via alkali-induced reactions.

Table 13. Alkaline stability of selected products under nonoxidative conditions (pH 11, 45°C).

	Concentration, mM	
Product[a]	Start[b]	End[c]
XI	0.79	0.83
XVIII	0.09	0.17
XIX	0.45	0.38
XX	0.29	0.32
XXI	0.22	0.23

[a]Structures listed in Fig. 4.
[b]After purging 30 mM MBB solution with oxygen for 315 minutes.
[c]After purging starting solution with nitrogen for 90 minutes.

An analogous reaction was observed in the autoxidation of 3,5-di-t-butyl pyrocatechol (105), but no mechanism was postulated. Figure 35 depicts a possible mechanism for the formation of XVIII. Under the alkaline conditions, the opened form of lactone XIX can lose glyoxylic acid via a reverse aldol condensation reaction (67). The driving force for this step is the formation of the allylic carbanion, which, after protonation and tautomerization, gives XVIII.

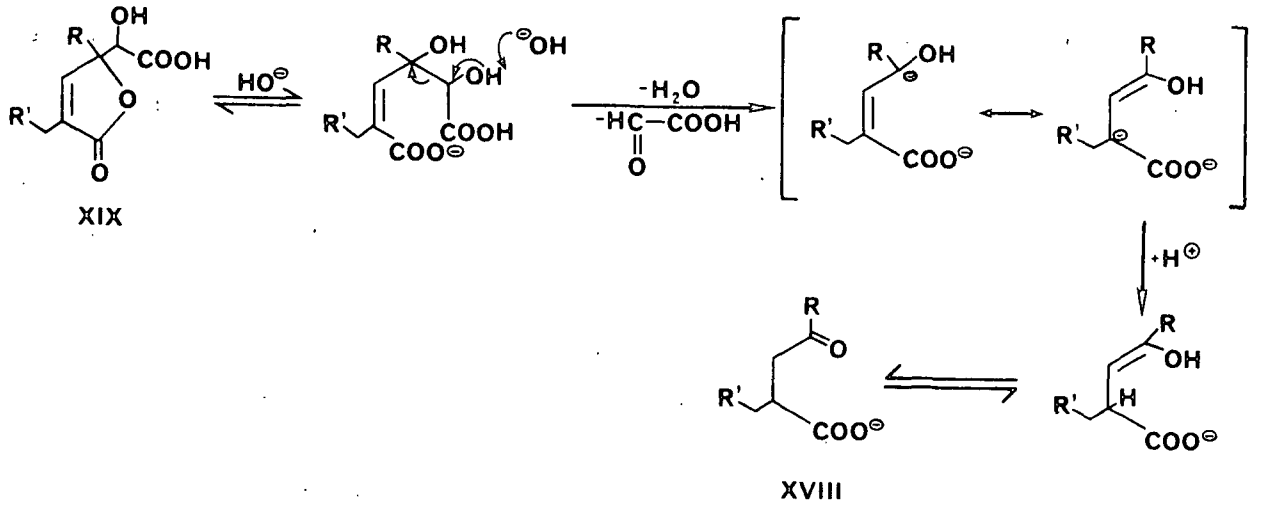

Figure 35. Proposed mechanism for the formation of XVIII from XIX via alkali induced reactions: (1) lactone ring opening, (2) reverse aldol condensation, (3) protonation, and (4) tautomerization.

5-Hydroxymethyl-hydroferulic Acid (XI)

The formation of 5-hydroxymethyl-hydroferulic acid (XI) during MBB degradation is of interest, since it represents the direct cleavage of the diphenylmethane bond - a productive reaction in the context of delignification. Based upon several observations, a plausible mechanism for the formation of XI is outlined in Fig. 36. An intramolecular rearrangement of the phenolate anion of hydroperoxide-c results in the cleavage of the diphenylmethane bond into two reactive intermediates. The arylhydroperoxide intermediate likely rearranges to the orthoquinone which would rapidly undergo further degradation under the reaction conditions (see next section). Addition of hydroxyl anion to the quinone methide intermediate results in the formation of XI.

A similar rearrangement of XXI to yield XI [Fig. 37(a)] can be ruled out based upon the observed stability of XXI in alkali (Table 13). Such a rearrangement would result in the loss of aromaticity of both rings. Note that in the

rearrangement shown in Fig. 36 there is no net loss of aromaticity. Neither hydroperoxide-a nor -b (Fig. 32) can undergo this type of rearrangement due to their structural arrangement of double bonds. Thus, only hydroperoxide-c is the likely precursor of XI.

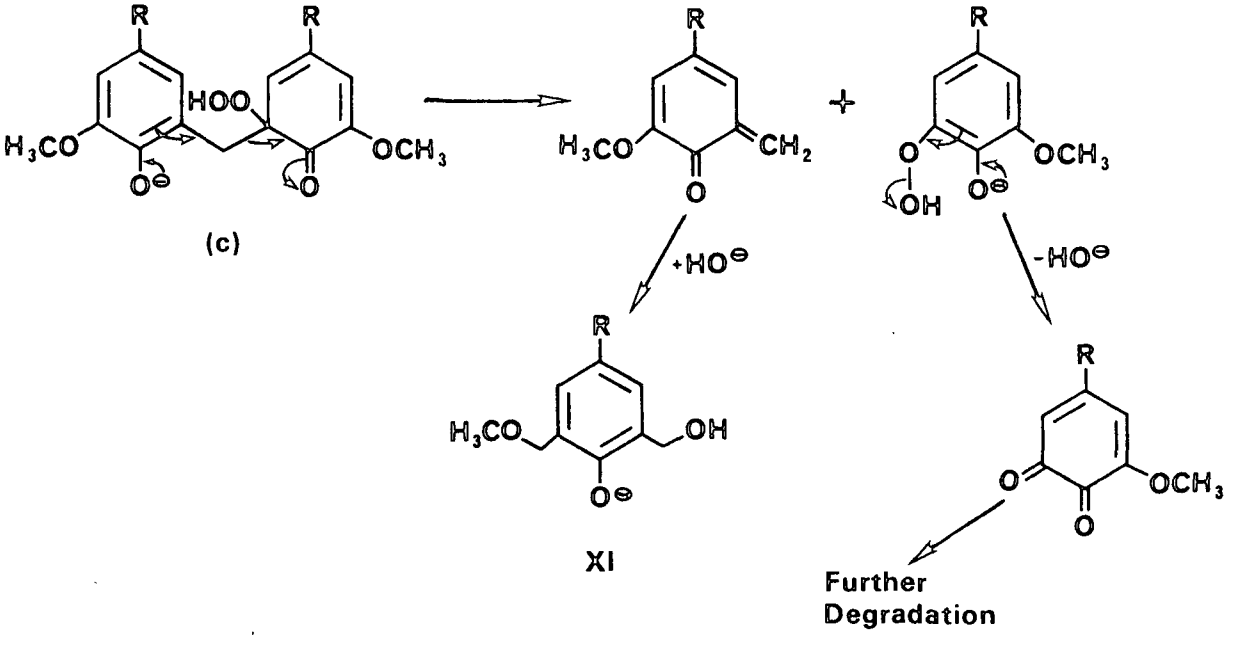

Figure 36. Proposed mechanism for the formation of XI from MBB under alkaline H_2O_2 conditions.

Additional experimental observations supporting the above mechanism were made. The monomethyl ether of MBB was reacted with H_2O_2 under base-line conditions (pH 11, 45°C, 225 minutes). Approximately 25% of this MBB derivative reacted, but neither XI nor the methyl ether of XI was detected among the reaction products. This result indicates that a free phenolic group on both rings is necessary for direct cleavage of the diphenylmethane bond to occur. Furthermore, this observation precludes the possibility of XI formation via nucleophilic attack of hydroxyl or hydroperoxy anions on the bridge carbon of hydroperoxide-c [Fig. 37(b)].

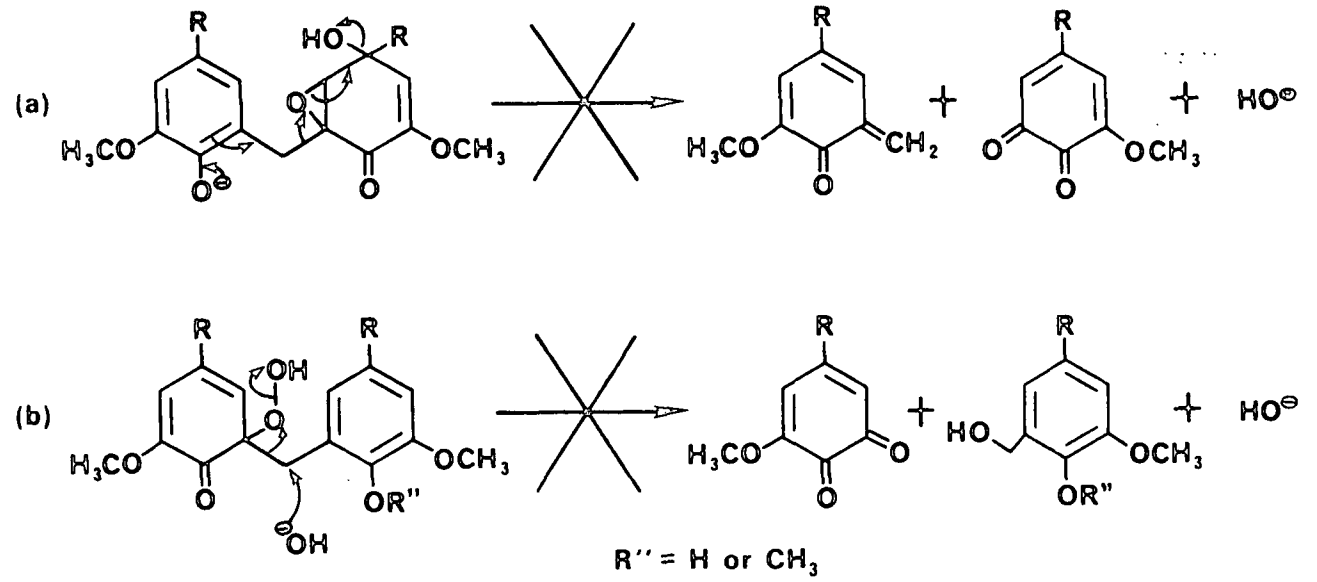

Figure 37. Examples of possible routes to XI formation which were shown not to occur.

Generally 12-20% of the theoretical yield of XI (based on reacted MBB) was detected in the product mixtures from the reactions (Table II). This yield represents a minimum since XI is susceptible to further degradation under the reaction conditions. In order to determine the true yield of XI (i.e., the yield in the absence of XI degradation) a kinetic model was utilized.

The kinetic model, derived for the Control reaction conditions, is detailed in Appendix VI, and the results are presented in Fig. 38. This analysis shows that toward the end of the Control reaction (270 min) the true yield of XI was 24% of the theoretical (1.24 mM) compared to the 13% (0.69 mM) found. Thus, a significant fraction of the overall reaction proceeds through this pathway.

Fragmentation Products

Alkaline hydrogen peroxide degradation of MBB (and its primary products) to lower molecular weight acids is obviously complex. Numerous reaction pathways leading to the observed fragmentation products likely exist. In this study, the

exact reaction routes were not pursued. However, a few plausible reaction schemes are presented below to account for many of the observed products.

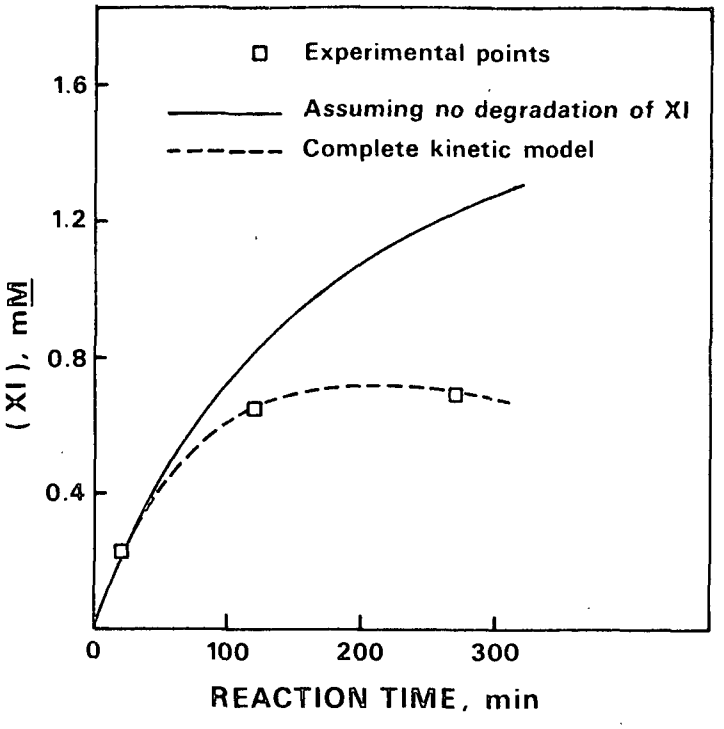

Figure 38. Kinetic plot of XI formation from MBB according to the model (Appendix VI) and the experimental data for the Control reaction.

It was shown in the previous section that ca. one-fourth of the reacted MBB results in the formation of XI. Based on the mechanism depicted in Fig. 36, formation of an equal amount of the orthoquinone is predicted. Also, an additional amount of this orthoquinone can form from the oxidation of XI via a Dakin-like displacement of the α-carbinol side chain (59). Since methoxy-substituted orthoquinones are quite reactive in alkaline hydrogen peroxide (67,82), a significant quantity of the fragmentation products probably arise form this intermediate.

A reaction scheme for the oxidative fragmentation of the orthoquinone is outlined in Fig. 39. This reaction scheme shows possible pathways that lead to

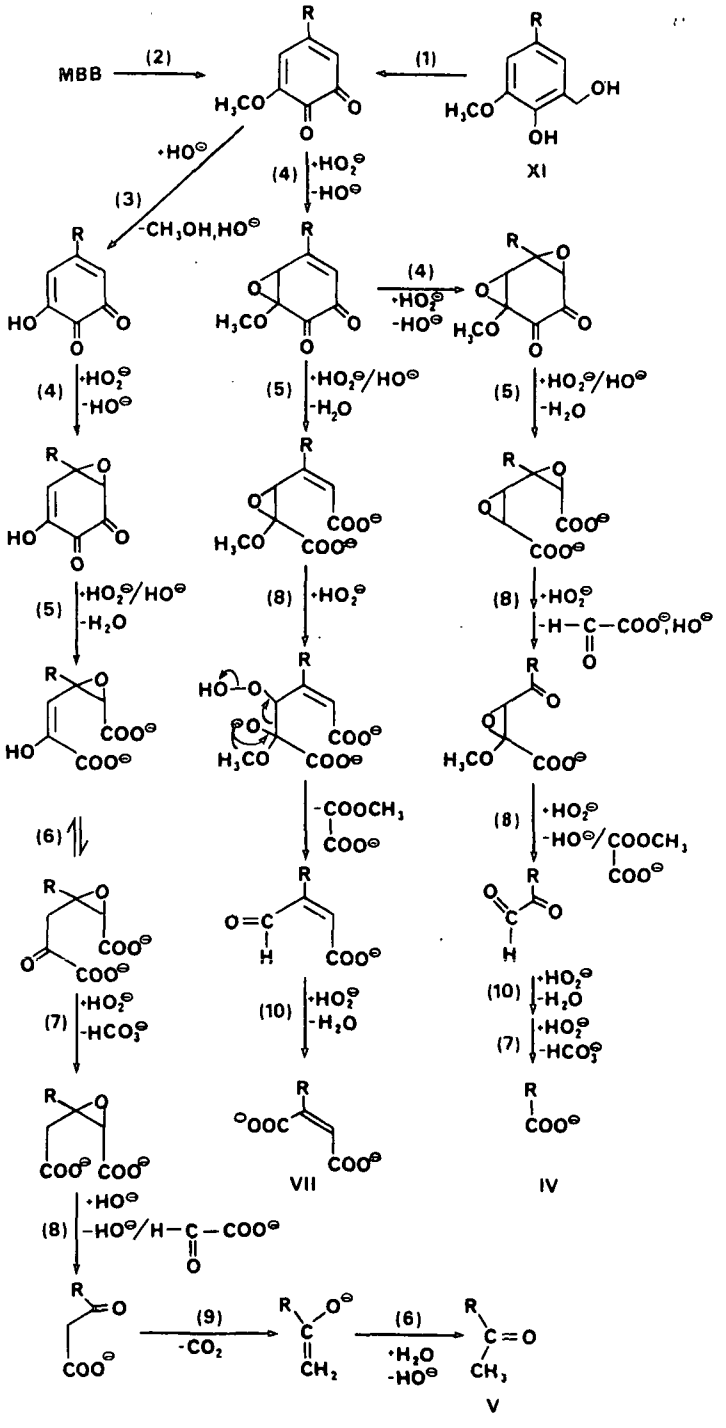

Figure 39. Possible reaction pathways for ring fragmentation reactions: (1) α-carbinol side chain displacement via Dakin-like mechanism (59), (2) diphenylmethane cleavage (Fig. 36), (3) alkaline demethylation (106), (4) epoxidation by hydrogen peroxide (82), (5) ring cleavage (Fig. 34), (6) tautomerization, (7) oxidative decarboxylation of α-keto acid (59,107), (8) oxidative cleavage of epoxide (82), (9) decarboxylation of β-keto acid (60,107), (10) oxidation of aldehyde by HO_2^-.

the formation of the identified products: III, IV, VII, methanol, and carbon dioxide. Products I and XIV also arise from simple ring fragmentation reactions (Fig. 40).

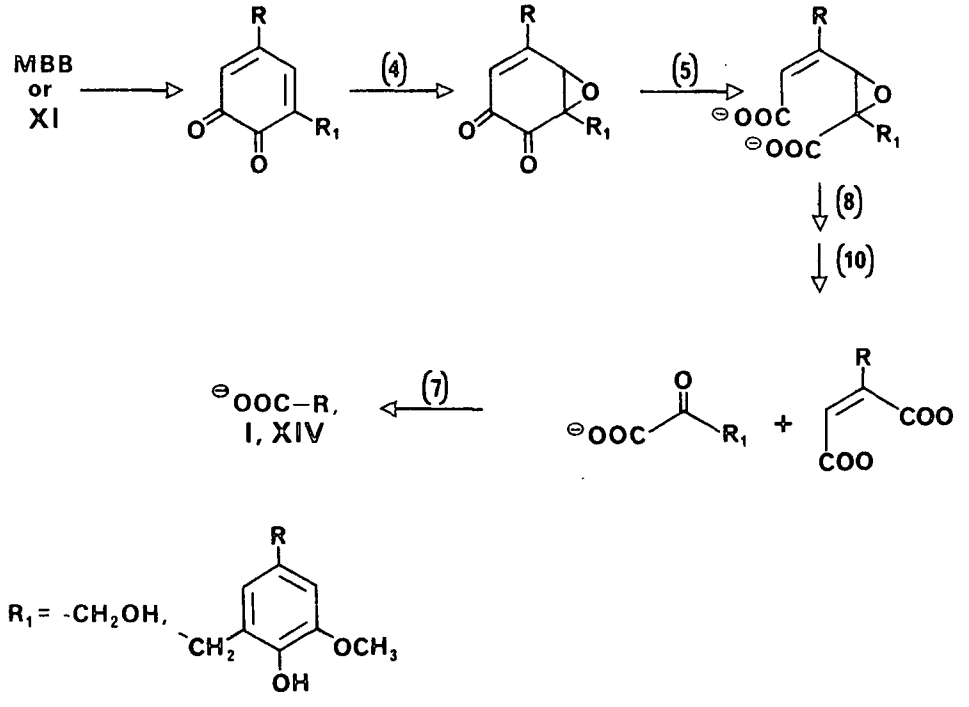

Figure 40. Possible reaction pathway for the formation of I and XIV (reactions numbered as in Fig. 39).

The reaction pathways shown in Fig. 39 and 40 are largely based on the work of Gellerstedt, et al. (82). These researchers isolated several epoxidated acidic products resulting from the alkaline H_2O_2 oxidation of quinone model compounds. Their work was done under mild conditions which facilitated the isolation of these reactive intermediates.

Epoxidation of the quinoid ring appears to be a prerequisite for extensive ring fragmentation to occur. Simple unsaturated carboxylic acids (e.g., 3-phenylpropenoic acid and fumaric acid) are known to be relatively insensitive to alkaline H_2O_2 (108). Therefore ring fragmentation via a muconic acid intermediate (cf. Fig. 3, Background section) is unimportant in this system.

Products VI and VIII obviously occur by more complicated routes (not shown here). Several researchers have reported the isolation of substituted succinic and furoic acids (analogous to VI and VIII) from the peroxide or oxygen reactions of various phenolic lignin models (59,60,66,67,76). A reaction pathway which might account for the formation of VI has been reported by Kratzl and coworkers (62,66).

Gierer and Imsgard (67) found good yields of 4-t-butyl-2-furoic acid from the oxygen-alkali treatment of 5-t-butyl-3-methoxy-o-quinone. These two compounds are structurally related to VIII and the orthoquinone (in Fig. 36), respectively. In the present study, VIII was formed during reaction of either MBB or XI, but not from the oxidation of the monomethyl ether of MBB. These observations suggest that the orthoquinone (in Fig. 36) is the likely precursor to VIII.

To a certain extent ring fragmentation reactions are probably beneficial in peroxide delignification of pulp. These reactions not only contribute to the breakup of the condensed lignin structure (Fig. 41), but also make the lignin fragments more hydrophilic. However, as evident by the reaction schemes (Fig. 39 and 40) and the stoichiometry results (Table 5), extensive fragmentation leads to a large consumption of hydrogen peroxide. In the context of pulp delignification much of this peroxide consumption can be considered wasteful (and expensive).

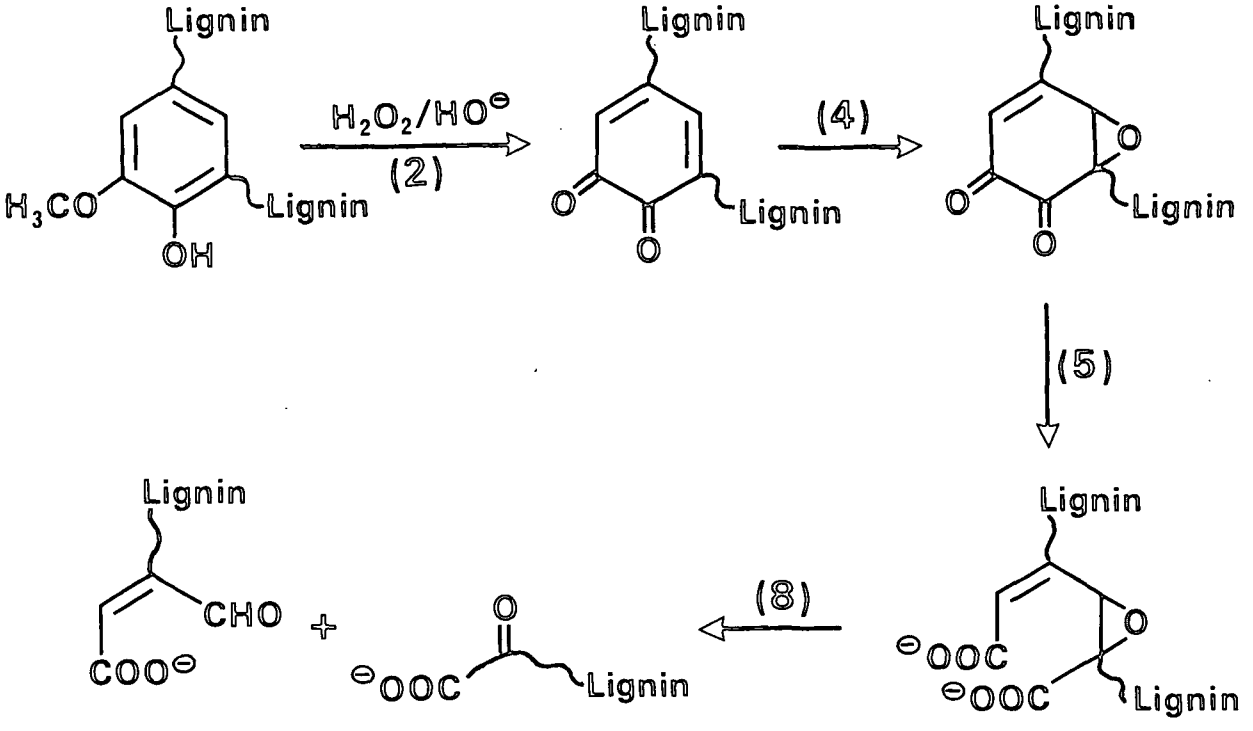

Figure 41. A possible reaction pathway of peroxide delignification.

CONCLUSIONS

Transition metal ions perform two central roles in the alkaline hydrogen peroxide oxidation of MBB (1,1'-methylenebis(2-hydroxy-3-methoxy-5(2-carboxy-ethyl) benzene)). First, they catalyze the decomposition of H_2O_2 into reactive species (viz. $HO^{\bullet}$, $O_2^{\bullet-}$, O_2). This step is necessary for MBB oxidation to occur since MBB was shown not to react with hydroperoxy anions. Second, these metals have the capability to oxidize phenolate anions to phenoxy radicals, which is believed to represent the rate limiting step of phenol degradation under these conditions (68-70).

The presence of catalytic amounts of ferricyanide, Mn, Fe, and Cu ions strongly influence the reaction kinetics of both peroxide decomposition, and MBB oxidation. These additives not only catalyze the rates of the two reactions, but also change the reaction orders (with respect to H_2O_2 concentration) to different extents.

The presence of Cu ions gives the strongest effect. The addition of Cu (12 μM $CuSO_4$) causes the rate of MBB oxidation to become independent of H_2O_2 concentration (in the absence of additives the order is 1.3). It is postulated that the Cu catalyst (and Mn, and Fe to a lesser extent) effectively competes with phenoxy radicals for superoxide anions ($O_2^{\bullet-}$). Thus combination of phenoxy radicals with dissolved oxygen becomes the favored reaction pathway.

Hydrogen peroxide decomposition is catalyzed to a greater extent than MBB oxidation (by a factor of two) by both Fe and Mn ions (both show an equal effect). In contrast, the addition of ferricyanide causes the MBB oxidation rate to increase to a greater extent than the increase in the H_2O_2 decomposition rate. Therefore some metal ion species can favor phenol oxidation over H_2O_2 decomposition.

The presence of added ferricyanide, Mn, Fe, and Cu ions do not induce major changes in the reaction stoichiometries or the types of reaction products formed during MBB degradation. The reaction products identified are consistent with the view that the key reactive intermediate is a cyclohexadienone hydroperoxide. This intermediate, resulting from reaction of superoxide or oxygen with the phenoxy radical of MBB, undergoes alkaline and oxidative conversions and degradations by HO^-/HO_2^- to lower molecular weight products.

Direct cleavage of the diphenylmethane bond of MBB accounts for ca. 24% of the reacted MBB. Based on the experimental evidence accumulated, a mechanism for this reaction is proposed. It involves the initial formation of a cyclohexadienone hydroperoxide (hydroperoxy group at the 1 position). Subsequent electron rearrangement of the ionized phenolic hydroxyl (of the other ring), results in the cleavage of the diphenylmethane bond into an orthoquinone methide and an aryl-hydroperoxide. Addition of hydroxide to the former product results in the formation of 5-hydroxymethyl-hydroferulic acid.

SUGGESTIONS FOR FUTURE WORK

Results of this study show that catalytic amounts of transition metal ions can strongly influence the reaction kinetics of hydrogen peroxide decomposition and MBB oxidation to different degrees. Additional studies are necessary to obtain a more thorough understanding of this phenomenon. The nature of the metal ion species (except ferricyanide) present in the reactions of this study were largely unknown and probably changed during the course of the reaction. Future kinetic studies would benefit by the use of well-defined catalysts such as complexed metal ions (homogeneous catalysis), and/or supported metal oxides (heterogeneous catalysis).

Improvements in the economics of peroxide delignification and resulting pulp quality should be gained from a better understanding of the chemistry involved. For instance, it might be possible to increase the extent (and rate) of delignification (for a given H_2O_2 charge) by controlling the levels and types (and location ?) of metal ion species in the pulp. Since H_2O_2 is a relatively expensive bleaching chemical, it must be used to its maximum benefit. In a similar manner, an increase in selectivity might be achieved. Certain catalysts might be found which preferentially direct peroxide attack to the lignin fraction, thus minimizing damage to the carbohydrates.

EXPERIMENTAL

GENERAL ANALYTICAL PROCEDURES

Melting points were determined on a Thomas Hoover capillary melting point apparatus which had been calibrated with known compounds.

The pH measurements were made with a Fisher Electrometer (Model 380) equipped with a polymer body, sealed reference combination pH electrode (Sensorex, Westminster, California, Part No. S300C). The setup was calibrated prior to each reaction with two pH standards which bracket pH 11: (1) a pH 10 standard buffer solution (Sargent-Welch), and (2) a saturated calcium hydroxide solution prepared according to Bates (109). The two solutions at 45°C had pH values of 9.85 and 11.84, respectively.

Ultraviolet (UV) spectra were recorded with a Perkin-Elmer Model 320 UV-visible spectrometer.

Nuclear magnetic resonance (^{1}H-NMR and ^{13}C-NMR) spectra were taken with a Jeol FX-100 pulse Fourier transform nuclear magnetic resonance (FT-NMR) spectrometer equipped with a Texas Instruments 980B computer.

Infrared and ion chromatographic analyses were conducted by the Institute's Analytical Group using a Nicolet FT-IR spectrometer and Dionex Ion Chromatograph.

Thin-layer chromatography (TLC) was conducted on microscope slides coated with Silica gel 60 GF (E. Merck). The slides were generally developed with dichloromethane:p-dioxane:acetic acid (90:10:1, v/v/v), and the spots visualized by placing the slide in a closed jar containing iodine crystals.

Quantitative gas-liquid chromatography (GLC) was performed on a Perkin-Elmer (PE) Model 3920 or Hewlett-Packard (HP) Model 5840A gas chromatograph equipped

with a hydrogen flame ionization detector. The chromatographs were interfaced with a PE Sigma-10 and HP 5840A-GC digital integrators, respectively.

Preparative GLC was done on a Varian Aerograph 202 gas chromatograph equipped with a thermal conductivity detector. The fractions were collected in V-shaped glass tubes loosely packed with glass wool.

Mass spectral analyses were conducted on a Hewlett-Packard 5985 GC/MS System interfaced with a jet separator to a HP 5840A gas chromatograph.

Column descriptions and GLC operating conditions, and mass spectrometer control settings, respectively, are listed in Appendixes VII and IX.

SOLUTIONS AND REAGENTS

Water

Triply-distilled (3-D) water was used in preparing reaction solutions and cleaning the reaction apparatus. The second distillation was from alkaline permanganate to remove any organic contaminants. The distillation system was all-glass.

Sodium Hydroxide

An ultrapure grade of sodium hydroxide was used to prepare the reaction solutions. It was purchased as a 30% solution in a polyethylene bottle from Alfa Division, Ventron Corp. (Danvers, Massachusetts). In order to minimize carbonate formation, the bottle was stored in a sealed jar containing Ascarite.

Hydrogen Peroxide

Ultrapure hydrogen peroxide (30%) was purchased in a 450 mL polyethylene bottle from J. T. Baker Chemical Co. (Phillipsburg, New Jersey). The bottle was stored in the dark at 4°C.

Additives

The following analytical reagent grade chemicals were used as additives to catalyze or inhibit hydrogen peroxide decomposition: $CuSO_4 \cdot 5H_2O$, $MnSO_4 \cdot H_2O$, $FeSO_4 \cdot 7H_2O$, $K_3Fe(CN)_6$, $MgSO_4\ 7H_2O$, $Na_2SiO_3 \cdot 9H_2O$.

Internal Standard Solutions

n-Octacosane

An analytical standard grade of n-octacosane was purchased from Alltech Associates (Deerfield, Illinois). Chloroform (14 g) and n-octacosane (112 mg) were directly weighed into a 15 mL Hypo-vial. The vial was fitted with a Teflon-lined silicone septum and sealed with an aluminum crimp top.

Vanillic Acid

Vanillic acid (Pfaltz & Bauer, Inc.) was purified by three recrystallizations from benzene/ethanol. An aqueous solution (5.95 mM) was prepared by first dissolving 250 mg of vanillic acid in 15 mL of 0.1N NaOH and 3 mL of ethanol (with warming). This solution was quantitatively transferred to a 250 mL volumetric flask and diluted with distilled water.

Ethanol

A weighed amount of reagent grade ethanol (95%) was diluted with distilled water to give a 3-10 mM solution.

PREPARATION OF COMPOUNDS

The mass spectra of the TMS derivatives of the following synthesized compounds (except hydroferulic acid) are contained in Appendix IX.

Hydroferulic Acid

Hydroferulic acid (3-(4-hydroxy-3-methoxybenzene)propanoic acid) was prepared by the catalytic hydrogenation of 4-hydroxy-3-methoxy-cinnamic acid

(ferulic acid). Ferulic acid (Aldrich Chemical Co.) was dissolved in absolute ethanol containing a small quantity of catalyst (10% Pd on powdered charcoal, Sargent-Welch). The mixture was hydrogenated at ambient temperature and pressure for several hours. The product was recovered from the mixture and purified via column chromatography using silica gel 60 (70-230 mesh ASTM, E. Merck) adsorbent and dichloromethane:acetic acid (100:1 —> 10, v/v) solvent system. White crystals were obtained after recrystallization from dichloromethane/hexane mixture (60% yield): m.p. 89-90.5°C, λ_{max}(methanol) 280, 227 nm. Literature: m.p. 89-90°C (110), λ_{max}(methanol) 281, 225 nm (111).

5-Hydroxymethyl-Hydroferulic Acid (XI)

This compound was prepared by the alkaline phenol-formaldehyde condensation (112,113) of hydroferulic acid. Hydroferulic acid (10 mmol) and 1.6 mL of 37% aqueous formaldehyde (20 mmol) were added to 9 mL of 2N NaOH. The solution was purged with nitrogen and the vessel sealed. After 2 days at room temperature, the solution was carefully acidified to pH 2 with 4N HCl and extracted with chloroform. The chloroform extract was dried over $CaSO_4$, filtered, and evaporated to dryness in vacuo. Two recrystallizations from chloroform/petroleum ether afforded 1.2 g of fluffy, white crystalline product shown to be pure by GLC analysis. ^{1}H-NMR (100 MHz, $CDCl_3$): δ 2.67(m, 2H, β-CH_2), 2.84(m, 2H, α-CH_2), 3.85(s, 3H, OCH_3), 4.69(s, 2H, Ar-CH_2-OH), 6.67(s, 2H, Ar).

MBB

MBB was synthesized by a general phenol-formaldehyde condensation procedure (112,113). Hydroferulic acid (130 mmol) and 22 mL of 37% aqueous formaldehyde solution (260 mmol) was added to 120 mL of cold 2.2N NaOH. The solution was continuously purged with helium and heated at reflux for 3 hours. At the end of

this time, the solution was carefully acidified to pH 2 with 50% HCl. The product, present as a light tan, creamy precipitate, was taken up in ethyl acetate. After drying over Na_2SO_4, the ethyl acetate extract was evaporated to dryness in vacuo. The light yellow product obtained was purified via column chromatography (using the same conditions as described above for hydroferulic acid). The recovered product was then recrystallized from distilled water to give finely divided white crystals: m.p. 168-169°C. Analyses by GLC and TLC showed the product to be pure. ^{1}H-NMR (100 MHz, $CDCl_3$): δ 2.57(m, 4H, β-CH_2), 2.87(m, 4H, α-CH_2), 3.84(s, 8H, OCH_3 and Ar-CH_2-Ar), 6.58(d, 6H, Ar and Ar-OH).

Monomethyl Ether of MBB

This compound was prepared by selective methylation of MBB. A solution of MBB (2.1 mmol) dissolved in 9.3 mL of a 10% tetraethylammonium hydroxide (TEAH) solution (6.5 mmol) was evaporated to dryness in vacuo to give the tri-(tetraethylammonium) salt of MBB. Due to the fairly wide spread in the pK_a's of the two phenolic hydroxyls (Appendix X), the salt of only one of the phenolic groups (and both carboxylic acid groups) was formed. The light yellow, crystalline residue was dissolved in 20 mL of chloroform and 5 mL of methanol, and the solution was refluxed with excess methyl iodide (1.6 mL) for two hours. This treatment produced the dimethyl ester/monomethyl ether of MBB. After cooling, the solvents were removed in vacuo, and the residue was dissolved in 5% TEAH and heated at 90°C for one hour under a nitrogen atmosphere. This step hydrolyzed the methyl esters to carboxylic acids and gave the desired product. The solution was acidified to pH 3 with 4N HCl and the precipitated product was taken up in ether. A suitable solvent system for crystallization of the product could not be found, so the material was only purified by column chromatography. The recovered product was an off-white, glassy material which was found to contain

ca. 5% impurities by GLC analysis. ^{1}H-NMR (100 MHz, $CDCl_3$): δ 2.57(m, 4H, β-CH_2), 2.83(m, 4H, α-CH_2), 3.82,3.86(two s, 11H, OCH_3 and Ar-CH_2-Ar), 6.54(m, 4H, Ar).

REACTION PROCEDURES AND SOLUTION ANALYSIS

Reactor System

The reactor system used in this study provided means for adding reactants to, or removing samples from, the reaction vessel, and monitoring pH and oxygen evolution over the course of the reaction. The Teflon-lined reaction vessel was adapted from a previous study (97) and is diagrammed in Fig. 42.

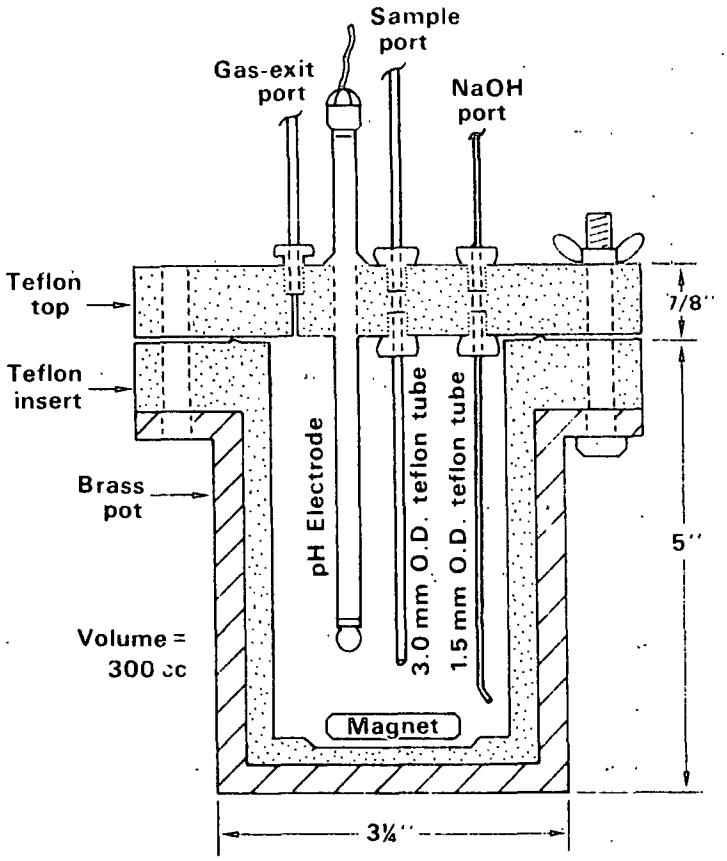

Figure 42. Teflon-lined reaction vessel.

The reaction vessel was raised and lowered into a well-stirred temperature controlled water bath via a rack and pinion mechanism. The temperature was maintained (45 ± 0.2°C) by a knife heater controlled through a Precision Scientific Relay activated by a CRC thermoregulator. The water bath was positioned over a mechanically driven magnetic stirrer which enabled the reaction solution to be continuously stirred.

A schematic of the system used to measure the volume of evolved oxygen is shown in Fig. 43. The entire reactor system was gas tight. In order to assure water vapor saturation of the collected gas, ca. 2 mL of water was placed atop the mercury in the water-jacketed gas buret. As oxygen evolved from the reaction solution, ambient pressure (indicated by the manometer) in the gas buret and reaction vessel was maintained by adjusting the height of the mercury reservoir attached to the pulley system.

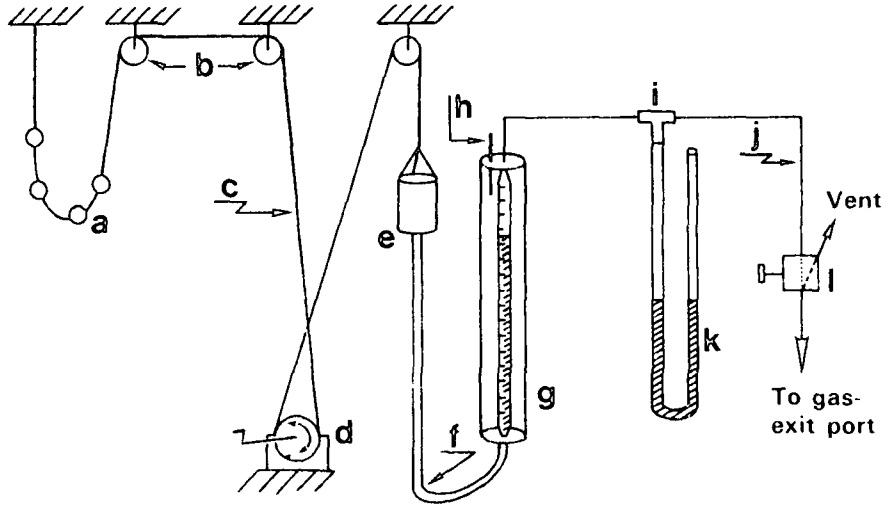

Figure 43. System for measuring evolved gas: (a) counterweights, (b) pulleys, (c) nylon cord, (d) rotatable shaft, (e) Hg reservoir made of PVC, (f) thick-walled rubber tubing, (g) water-jacketed 100 mL gas buret, (h) thermometer, (i) tee connector, (j) Teflon tubing, (k) water manometer, (l) 3-way slide valve.

Figure 44 depicts the remaining parts of the reactor system. The valves were turned to the 1-2 configuration when reactants were added to, or samples removed from, the reaction vessel. During the reaction both valves were placed in the 1-3 configuration.

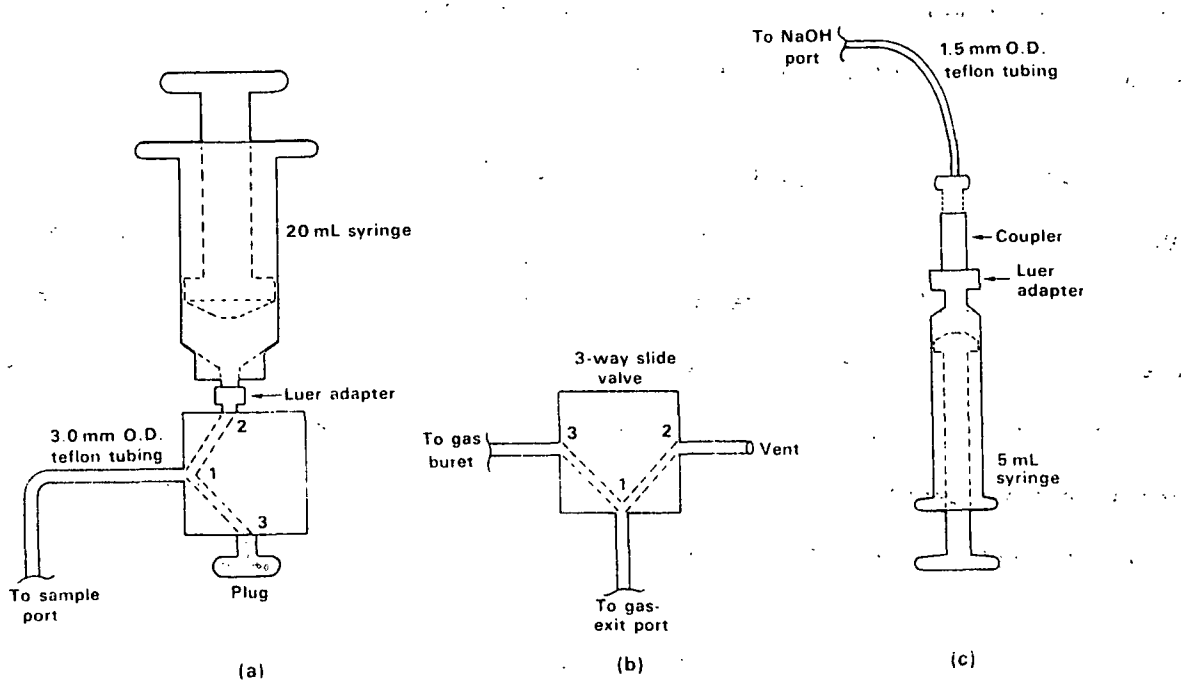

Figure 44. Schematic of remaining parts of reactor system: (a) sampling system, (b) gas buret valve, and (c) NaOH addition syringe.

Preparation of Reaction Solutions

The Teflon reactor surfaces, pH electrode body, and all labware used to prepare the reaction solutions were cleaned by successive washings with Alconox solution, distilled water, acetone, aqua regia or 35% nitric acid (v/v), and copious quantities of 3-D water.

In each of the reaction runs, appropriate quantities of MBB, H_2O_2, NaOH and 3-D water were added to the reaction vessel to give a solution (155 mL) initially containing 20.0 mM MBB and 100 mM H_2O_2 at pH 11.0. The reaction solutions were prepared by adding weighed amounts of MBB and cooled, boiled-out 3-D water to

the reactor. Additives, if present, were included at this point along with sufficient 30% ultrapure NaOH solution (ca. 0.8 mL) to just dissolve the MBB (pH 8-9). The catalysts were added as 1 mL aliquots of stock metal ion solutions.

The reactor, with the cover bolted in place, was then lowered into the water bath. As the reactor reached thermal equilibrium (ca. 2 h), the solution was purged through the sample line with a slow stream of nitrogen. A calculated amount of H_2O_2 stock solution was weighed into the sample syringe (plunger removed), and the reaction was initiated by injecting the H_2O_2 into the reactor with nitrogen pressure. A small amount of preheated 3-D water was also added through the syringe to insure that all of the H_2O_2 reached the reactor. The valves were then closed (configuration 1-3), and NaOH solution was added via the NaOH addition syringe (Fig. 44) to give a pH of 11.0 ± 0.05. The syringe plunger was then pulled back to its original position in order to prevent diffusion of excess NaOH into the reactor. Addition of hydrogen peroxide and adjustment of the pH required 1-2 minutes to complete.

The hydrogen peroxide decomposition kinetic runs were performed by the procedure given above (except MBB was not added).

The Control-A reaction solution was prepared in a different manner. The sealed reactor, containing only 3-D water, was lowered into the water bath. Hydrogen peroxide stock solution was injected into the reactor and the pH adjusted to 10.9. The concentration of H_2O_2 (ca. 150 mM) was determined by iodometric titration, and the decomposition was followed by monitoring the evolved oxygen. When the required peroxide concentration was reached, the reaction was initiated by injecting a warmed, concentrated aqueous solution of MBB (10 mL) (followed by rinse water) into the reactor, and adjusting the pH to 11.0.

Reaction Sampling

The reaction solution was periodically sampled by the following procedure: The system was first adjusted to ambient pressure and the valves turned to the 1-2 configuration (Fig. 44). After withdrawing ca. 15 mL of reaction solution, the syringe was disconnected from the valve, and solution remaining in the sample line drained back into the reactor. The valves were immediately returned to the 1-3 configuration. The entire sampling procedure was completed within 30 seconds.

The sample was injected into a clean, dry test tube which was placed in an ice bath to slow further reaction. Portions of the cooled sample were immediately taken for the various analyses.

Analysis of Reaction Solution

Oxygen Evolution

Hydrogen peroxide decomposition was followed over the course of the reaction by measuring the volume of evolved oxygen. The number of millimoles of oxygen (O_2, mmol) evolved is given by Eq. (33).

$$O_2, \text{ mmol} = (Vg/22.4) \cdot (273/(273+T)) \cdot ((P-Pv)/760) + \text{dissolved} \qquad (33)$$

where

Vg = oxygen volume, mL

T = temperature of water jacket, °C

P = atmospheric pressure, mm of Hg

Pv = vapor pressure of water, mm of Hg

dissolved = $(\alpha) \cdot (Vi/22.4) \cdot (P/760)$, where $\alpha = 0.02$ [Bunsen absorption coefficient extrapolated from work of Bruhn (114)], and Vi = initial reaction solution vol., mL

Taking into account the stoichiometry of the decomposition reaction [Eq. (18)], the concentration (mM) of decomposed hydrogen peroxide ($[H_2O_2]d$) was calculated by Eq. (34).

$$[H_2O_2]d = (2000) \cdot (O_2, \text{ mmol})/(Vs) \quad (34)$$

where

Vs = reaction solution volume, mL

Hydrogen Peroxide Analysis

The concentration of residual H_2O_2 in the reaction solution was determined by a standard iodometric titration procedure (115). A 1 mL aliquot of cooled reaction solution was added (via an auto-pipetter) to a freshly prepared solution containing: 20 mL of 2N H_2SO_4, 10 mL of 3% potassium iodide (w/w), and 3 drops of 10% ammonium molybdate (w/w). The liberated iodine was immediately titrated with standard 0.01N sodium thiosulfate to a starch endpoint. The endpoint was reached within 30 seconds of addition of the sample. The concentration of H_2O_2 was calculated by Eq. (35), and the average of duplicate samples are reported in Appendix II.

$$[H_2O_2] \text{ mM} = (\text{mL of titrant}) \times 5 \quad (35)$$

MBB Analysis

Reaction solution (ca. 1 mL) was added to a tared 8-mL vial containing a quench solution (0.3 mL of 1.4M KH_2PO_4 and 0.3 mL of 0.75M $NaAsO_2$). The vial was weighed and internal standard solution (n-octacosane in chloroform) was added via a glass hypodermic syringe. After reweighing the vial, the mixture was transferred to a separatory funnel (60 mL) with a pipet and acidified (pH 2) with a few drops of 2N H_2SO_4. Chloroform (5 mL) was used to rinse the inside

surfaces of the vial and pipet. This solvent was transferred to the separatory funnel via the pipet and used to extract the mixture. This process was repeated three times in order to assure complete transfer and extraction of the sample and internal standard.

The combined chloroform extracts were dried over Na_2SO_4, decanted, and evaporated in vacuo to ca. 2 mL in a pear-shaped flask. The solution was transferred to a 4-mL screw-top vial, and after evaporation to dryness, the sample was stored over P_2O_5 in a vacuum desiccator for a few hours to remove the last traces of water.

The sample vial was fitted with a septum, and the residue was dissolved in 0.5 mL of chloroform (dried over Molecular Seive 4A). The mixture was then treated with 0.2 mL of N,O-bis-(trimethylsilyl)-acetamide (BSA; Pierce Chemical Co.) and heated (50°C) for two hours prior to analysis by GLC (Appendix VII, conditions A). Duplicate samples (injected in triplicate) were averaged and reported in Appendix II.

Methanol Analysis

Reaction solution (ca. 1 mL) and internal standard solution (aqueous ethanol) were gravimetrically added to a tared 8-mL vial containing quench solution (see above). The sample was then analyzed directly by GLC (Appendix VII, conditions B).

Acidic Products Analysis

A 10 mL aliquot of reaction solution was directly added to a 25 mm x 200 mm test tube (in an ice bath) and neutralized with carbon dioxide delivered via a gas dispersion tube. A 1 mL aliquot of internal standard solution (aqueous

vanillic acid) was added, and the residual H_2O_2 decomposed by addition of 1 mL of a freshly prepared aqueous solution (0.3%, w/w) of catalase (beef liver; P-L Biochemicals, Milwaukee, Wisconsin).

The solution was deionized by batch addition of ca. 3 mL of Dowex 50W-x8 (H^+) cation exchange resin (20-50 mesh). This lowered the solution pH (ca. 3) and caused unreacted MBB to precipitate from solution. The mixture was filtered through a sintered glass funnel and the resin/MBB solids were rinsed with distilled water (2 x 5 mL). The filtrate was adjusted to pH 5-6 by addition of a few drops of aqueous 10% tetraethylammonium hydroxide (Eastman Kodak Co.), and evaporated in vacuo (< 45°C) to ca. 2 mL in a pear-shaped flask. The solution was transferred to a 4-mL screw-top vial, and after evaporation to dryness, the sample was stored over P_2O_5 in a vacuum desiccator for several hours to remove the last traces of water.

The sample vial was fitted with a septum, and the residue was dissolved in 0.2 mL of silylation grade DMSO (Pierce Chemical Co.). The mixture was then treated with 0.5 mL of Tri-Sil concentrate (hexamethyldisilazane trimethylchlorosilane mixture; Pierce Chemical Co.) and heated (50°C) for four hours prior to analysis by GLC (Appendix VII, conditions C), or GLC/MS (Appendix IX).

Methylation and Hydrogenation of Acidic Products

For the purposes of product identification (see Appendix VIII), samples of the acidic products mixture were treated by the procedures described below.

Selected samples were methylated by dissolving the residue (obtained after normal workup) in 20 mL of dichloromethane and refluxing for 2 h in the presence of methyl iodide. After evaporation, the residue was dissolved in diethyl ether

and filtered. The solution, containing carboxylic methyl esters, was analyzed by GC/MS. Any free hydroxyl groups on the products were converted to TMS ethers by treating a portion of this solution with Tri-Sil concentrate.

A sample of the acidic products mixture was hydrogenated by the following procedure. The residue (obtained after normal workup) was dissolved in 10 mL of absolute ethanol. A small scoop of catalyst (10% Pd on charcoal) was added and hydrogen gas was bubbled through the solution (with good agitation) for 6 h. After filtering, and evaporating the solvent, the residue was silylated (as above) and analyzed by GC/MS.

Test of Product Stability in Alkali

Oxygen gas was bubbled through an aqueous solution of MBB (30 mM) kept at pH 11 and 45°C. After 315 minutes the reaction solution was sampled (5 mL) and nitrogen (in place of oxygen) was used to purge the solution. After 90 minutes under these nonoxidative alkaline conditions, the solution was again sampled. Both samples were prepared and analyzed according to the Acidic Products Analysis procedure.

ACKNOWLEDGMENTS

The guidance, advice, and support extended during the course of this thesis by the members of my advisory committee - Drs. T. J. McDonough (Chairman), N. S. Thompson, and W. F. W. Lonsky - is genuinely appreciated. Also, I thank the many Institute staff and faculty members and students who were always willing and able to help me out when needed.

The financial support and educational experiences which the Institute and its member companies have provided is gratefully acknowledged.

Finally, I wish to thank my wife, Lee Ann, for her unending love, and the sacrifices she made during the completion of this thesis. This work is dedicated to my father, whose memory has provided a constant source of inspiration during the pursuit of my academic goals.

LITERATURE CITED

1. Allison, R. W., Paperi Puu 65(2):71-7(1983).

2. Kempf, A. W., U. S. pat. 4,410,397(Oct. 18, 1983).

3. Gellerstedt, G.; Petterson, I., J. Wood Chem. Technol. 2(3):231-50(1982).

4. Lachenal, D.; de Choudens, C.; Soria, L.; Monzie, P. 1982 TAPPI Int'l. Pulp Bleaching Conf. Proceedings. TAPPI Press, Atlanta, GA, 1982:145-51.

5. Ruhanen, M.; Dugal, H. S. 1981 Environmental Conf. Proceedings. TAPPI Press, Atlanta, GA, 1981. p. 93. Tappi 65(9):107-11(1982);

6. Lachenal, D.; de Choudens, C.; Monzie, P., CPPA Annual Mtg. (Montreal) Preprints, Jan. 31-Feb. 3, 1978:A153-9; Transactions CPPA 4(4):TR98(1978).

7. Lachenal, D.; de Choudens, C.; Monzie, P., Paperi Puu 63(4):301-8(1981); Svensk Papperstid. 83(17):494-7(1980); Tappi 63(11):59-62(1980); Revue ATIP 34(7):319(1980); Revue ATIP 31(1):16(1977).

8. Lachenal, D.; de Choudens, C.; Monzie, P., Tappi 63(4):119-22(1980).

9. Carles, J. E.; Lemoyne, H.; Logan, W. R. 1980 TAPPI Pulping Conf. Proceedings. TAPPI Press, Atlanta, GA, 1980:325-32.

10. Germgard, U.; Larsson, S., Paperi Puu 65(14):287-90(1983).

11. Teder, A.; Tormund, D., Svensk Papperstid. 83(4):106-9(1980).

12. Erdey, L., Acta Chim. Acad. Sci. Hung. 3:81(1953); Chem. Abstr. 47:10399f (1953).

13. Duke, F. R.; Haas, T. W., J. Phys. Chem. 65:304-9(1961).

14. Roberts, J. L.; Morrison, M. M.; Sawyer, D. T., J. Am. Chem. Soc. 100(1): 329-30(1978).

15. Stanley, J. P., J. Org. Chem. 45(8):1413-8(1980).

16. Agnemo, R.; Gellerstedt, G., Acta Chem. Scand. B33:337-42(1979).

17. Makkonen, H. P. Decomposition of hydrogen peroxide in dilute alkaline aqueous solutions. Doctoral Dissertation. University of Washington, Seattle, WA, 1974.

18. Nicoll, W. D.; Smith, A. F., Ind. Eng. Chem. 47(12):2548-54(1958).

19. Galbacs, Z. M.; Csanyi, L. J., J. Chem. Soc. Dalton Trans. 1983:2353-7.

20. Spalek, O.; Balej, J.; Paseka, I., J. Chem. Soc. Faraday Trans. I 78:2349-59(1982).

21. Koubek, E.; Haggett, M. L.; Battaglia, C. J.; Ibne-Rasa, K. M.; Pyun, H. Y.; Edwards, J. O., J. Am. Chem. Soc. 85(8):2263-8(1963).

22. Walling, C., Accts. Chem. Res. 8:125-31(1975).

23. Gilbert, A. F.; Pavlovova, E.; Rapson, W. H., Tappi 56(6):95-9(1973).

24. Strunk, W. G., Pulp Paper 54(6):156(1980).

25. Andrews, D. H., Pulp Paper Can. 60(11):T273(1968).

26. Gellerstedt, G.; Agnemo, R., Acta Chem. Scand. B34:275-80(1980).

27. Csanyi, L. J.; Galbacs, Z. M.; Nagy, L., J. Chem. Soc. Dalton Trans. 2:237-45(1982).

28. Kitajima, N.; Fukuzumi, S.; Ono, Y., J. Phys. Chem. 82(13):1505-9(1978).

29. Barb, W. G.; Baxendale, J. H.; George, P.; Kargrave, K. R., Trans. Faraday Soc. 47:462-500, 591-616(1951).

30. Draganic, I. G.; Draganic, Z. D. The radiation chemistry of water. New York, Academic Press, 1971:102-16.

31. Spinks, J. W. T.; Woods, R. J. An introduction to radiation chemistry. 2nd ed. New York, John Wiley & Sons, Inc., 1976:256-360

32. Rabani, J.; Nielsen, S. O., J. Phys. CHem. 73:3736(1969).

33. Goldstein, S.; Czapski, G., J. Am. Chem. Soc. 105(25):7276-80(1983).

34. Bull, C.; McClune, G. J.; Fee, J. A., J. Am. Chem. Soc. 105(16):5290-5300 (1983).

35. Dorfman, L. M.; Adams, G. E. Reactivity of the hydroxyl radical in aqueous solutions, NSRDS-NBS 46. Washington, D. C., U. S. Government Printing Office, 1973:20-38.

36. Bielski, B. H. J.; Allen, A. O., J. Phys. Chem. 81(11):1048-50(1977).

37. Sawyer, D. T.; Valentine, J. S., Accts. Chem. Res. 14:393-400(1981).

38. Bielski, B. H. J.; Richter, H. W., J. Am. Chem. Soc. 99(9):3019-23(1977).

39. Khan, A. U., Sci. 164:476-7(1970).

40. Khan, A. U., J. Am. Chem. Soc. 103:6516-7(1981).

41. Guiraud, H. J.; Foote, C. S., J. Am. chem. Soc. 98(7):1984-6(1976).

42. Agnemo, R.; Gellerstedt, G.; Lindfors, E., Acta Chem. Scand. B33:154-5 (1979).

43. Smith, L. L.; Kuling, M. J., J. Am. Chem. Soc. 98(4):1027-9(1976).

44. Aubry, J. M.; Rigaudy, J., J. Am. Chem. Soc. 103:4965-6(1981).

45. Nilsson, R.; Kearns, D. R., J. Phys. Chem. 78:1681(1974).

46. Foote, C. S.; Shook, F. C.; Abakerli, R. A., J. Am. Chem. Soc. 102(7): 2503-4(1980).

47. Haber, T.; Weiss, J. J., Proc. R. Soc. London, Ser. A. 147:332(1932).

48. Wilshire, J.; Sawyer, D. T., Accts. Chem. Res. 12:105-10(1979).

49. Weinstein, J.; Bielski, B. H. J., J. Am. Chem. Soc. 101(1):58-62(1979).

50. Christensen, H.; Sehested, K.; Corfitzen, H., J. Phys. Chem. 86:1588-90 (1982).

51. Suwalski, J. P.; Bobrowski, K.; Zagorski, Z. P., Proc. Tihany Symp. Radiat. Chem. 4:911-6(1976); Chem. Abstr. 88:113249(1968).

52. Gall, B. L.; Dorfman, L. M., J. Am. Chem. Soc. 91(9):2199-2204(1969).

53. Schaumb, W. C.; Satterfield, C. N.; Wentworth, R. L. Hydrogen peroxide. ACS Monograph Series, No. 128. New York, Reinhold Publishing Corp. 155:470.

54. Bobtelsky, M.; Simchen, A. E., J. Am. Chem. Soc. 64:2492-8(1942).

55. Walling, C.; Goosen, A., J. Am. Chem. Soc. 95(9):2987-91(1973).

56. Bodini, M. E.; Sawyer, D. T., J. Am. Chem. Soc. 98(26):8366-71(1976).

57. Lim, P. K.; Cha, J. A.; Fagg, B. S., Ind. Eng. Chem. Fundam. 23:29-33 (1984).

58. Gierer, J.; Imsgard, F., Svensk Papperstid. 80(16):510-8(1977).

59. Bailey, C. W.; Dence, C. W., Tappi 52(3):491-500(1969).

60. Kempf, A. W.; Dence, C. W., Tappi 58(6):104-8(1975).

61. Gierer, J.; Imsgard, F.; Noren, I., Acta Chem. Scand. B31(7):56-72(1977).

62. Holocher-Ertl, M.; Fricko, P.; Kratzl, K. Int'l. Symp. on Wood & Pulping Chem. Proceedings. Stockholm, June 9-12, 1981. p. II:83-9.

63. Holocher-Ertl, V. M.; Kratzl, K., Holzforsch. 36(1):11-6(1982).

64. Omori, S.; Dence, C. W. Int'l. Symposium on Wood & Pulping Chem. Stockholm, June 9-12, 1981. p. II:112-5; Wood Sci. Technol 15:67-79, 113-23(1981).

65. Agnemo, R.; Gellerstedt, G.; Lindsfor, E. Canadian Wood Chem. Symp. Preprints. Harrison Hot Springs, 1979:14-5.

66. Fricko, P.; Holocher-Ertl, M.; Kratzl, K., Monatsh. Chem. 111(5):1025-41 (1980).

67. Gierer, J.; Imsgard, F., Acta Chem. Scand. B31:537-45, 546-60(1977).

68. Eckert, R. C.; Chang, H.; Tucker, W. P., Tappi 56(6):134-8(1973).

69. Landucci, L. L., Trans. Tech. Sect. CPPA 4:25-9(1978).

70. Kratzl, K.; Claus, P.; Lonsky, W.; Gratzl, J. S., Wood Sci. Technol. 8:35-49(1974).

71. Kratzl, K.; Claus, P.; Gratzl, J. S.; Schilling, P., Monatsh. Chem. 98(3): 891(1967).

72. Landucci, L. L., Tappi 62(4):71-4(1979).

73. Steelink, C., J. Am. Chem. Soc. 87(9):2056-7(1965).

74. Haynes, G. C.; Turner, A. H.; Waters, W. A., J. Chem. Soc. 1956:2823-31.

75. Stone, T. J.; Waters, W. A., J. Chem. Soc. 1964:213,4301.

76. San Clemente, M. R.; Sarkanen, K. V.; Sundin, S. E., Svensk Papperstid. 84:R1-5(1981).

77. Neta, P.; Schuler, R. H., J. Am. Chem. Soc. 97(4):912-3(1975).

78. Land, E. J.; Ebert, M., Trans. Faraday Soc. 63:1181(1967).

79. Moro-oka, Y.; Foote, C. S., J. Am. Chem. Soc. 98(6):1510-4(1976).

80. Sawyer, D. T.; Nanni, E. J. In Oxygen and oxy-radicals in chemistry and biology; Rodgers, M. A. J. and Powers, E. L., ed. New York, Academic Press, 1981:31-3.

81. Starnes, W. H. In Chemistry of delignification with oxygen, ozone, and peroxides; Gratzl, J. S., Nakano, J., and Singh, R. P., ed. Tokyo, Japan, Uni Publishers Co., Ltd., 1980:12-24.

82. Gellerstedt, G.; Hardell, H.; Lindsfor, E., Acta Chem. Scand. B34:669-73 (1980).

83. Gierer, J., Svensk Papperstid. 73(18):571-96(1970).

84. Shinoda, Y.; Inaba, M.; Tajma, T. 1983 Int'l. Symp. on Wood & Pulping Chem., Proceedings, 4:99-102(1983).

85. Terashima, N.; Araki, H.; Suganuma, N., J. Jap. Wood Res. Soc. 23(7):343-7 (1977).

86. Gierer, J.; Lindeberg, O., Acta Chem. Scand. B33:580-2(1979).

87. Gierer, J., Holzforsh. 36(1):43-51(1982).

88. Ekman, K. H., Tappi 48(7):398(1965).

89. Araki, H.; Terashima, N., J. Jap. Wood Res. Soc. 27(5):414-8(1981).

90. Morck, R.; Kringstad, K.; Mansson, P. 1982 Canadian Wood Chemistry Symp., Preprints. p. 161-8.

91. Kringstad, K P.; Morck, R., Holzforsh. 37(5):237-44(1983).

92. Weiser, H. B. Inorganic colloid chemistry. New York, John Wiley & Sons, Inc., 1935:69, 153, 331.

93. Baes, C. F.; Mesmer, R. E. The hydrolysis of cations. New York, John Wiley & Sons, Inc., 1976:224, 237, 273.

94. Bamford, C. H.; Tipper, C. F. H. Comprehensive chemical kinetics. New York, Elsevier Publishing Co., Vol. 1, Chap. 5, 1969.

95. Laidler, K. J. Chemical kinetics. 2nd ed. New York, McGraw-Hill, Chap. 1, 1965.

96. Hill, C. G. An introduction to chemical engineering kinetics and reactor design. New York, John Wiley & Sons, Inc., 1977. p. 86.

97. Weaver, J. W. The alkaline hydrogen peroxide reaction of methyl β-D-glucopyranoside and methyl 4-D-methyl-β-D-glucopyranoside. Doctoral Dissertation. Appleton, WI, The Institute of Paper Chemistry, 1976.

98. Sinkey, J. D. The function of magnesium compounds in an oxygen-alkali-carbohydrate system. Doctoral Disseration. Appleton, WI, The Institute of Paper Chemistry, 1973.

99. Isbell, H. S.; Frush, H. L., Carb. Res. 59:C25-31(1977).

100. Graves, D. P. The influence of cobalt ion concentration on the degradation of methyl-β-D-glucopyranoside in oxygen-alkali. Doctoral Dissertation. Appleton, WI, The Institute of Paper Chemistry, 1981.

101. Rabani, J.; Klug-Roth, D.; Lilie, J., J. Phy. Chem. 77(9):1169-75(1973).

102. Zehavi, D.; Rabani, J., J. Phy. Chem. 76(25):3703-9(1972).

103. Hewgill, F. R.; Lee, S. L., J. Chem. Soc. C:2080(1969).

104. Mih, J. F. The effect of liquor composition on the rate of reaction of a lignin model compound (acetovanillone) under oxygen-alkali conditions. Doctoral Dissertation. Appleton, WI, The Institute of Paper Chemistry, 1982.

105. Grinstead, R. R., Biochem. 3(9):1308-14(1964).

106. Gitzpatrick, J. D.; Steelink, C., J. Org. Chem. 37:762(1972).

107. March, J. Advanced organic chemistry. 2nd ed. New York, McGraw-Hill Book Co., 1977:571, 1087.

108. Weitz, E.; Scheffer, A., Ber. 54B:2327(1921); Chem. Abstr. 16:1232(1922).

109. Bates, R. G. Determination of pH. New York, John Wiley & Sons, Inc., 1964:129-30.

110. Handbook of Chemistry and Physics. 56th ed. Cleveland, OH, CRC Press, 1975:C-450.

111. Nakagawa, Y., Anal. Biochem. 7(3):374-8(1964).

112. Troughton, G. E.; Manville, J. F., Can. J. Forest Res. 2:271-5(1972).

113. Marton, J.; Marton, T.; Falkehag, S. I.; Adler, E., Adv. Chem. Ser. No. 59, 1966:125-44.

114. Bruhn, G.; Gerlach, J.; Pawlek, F., A. Anorg. Allgem. Chem. 337(1-2):68-79 (1965).

115. Kolthoff, I. M.; Sandel, E. B. Textbook of quantitative inorganic chemistry. 3rd ed. New York, MacMillan, 1956. p. 600.

116. Ziegel, E. R.; Gorman, J. W., Technometrics 22:139-51(1980).

117. Sullivan, J. J.; O'Brien, M. J. In modern practice of gas chromatography, Grob, R. L., ed. New York, John Wiley & Sons, Inc., 1977. p. 253.

118. Pierce, A. E. Silylation of organic compounds. Rockford, IL, Pierce Chemical Publishing Co., 1979.

119. Atlas of spectral data and physical constants for organic compounds, Grasselli, J. G., ed. Cleveland, OH, CRC Press, 1973. p. B-548.

120. Silverstein, R.; Bassler, G.; Morrill, T. Spectrophotometric identification of organic compounds. 3rd ed. New York, John Wiley & Sons, Inc., 1974. p. 103.

121. Albert, A.; Serjeant, E. P. In ionization constants of acids and bases. New York, John Wiley & Sons, Inc., 1962:69-92.

122. Francis, D. J.; Yeddanapalli, L. M., Indian J. Chem. 2(4):166(1964).

APPENDIX I

HYDROGEN PEROXIDE DECOMPOSITION DATA

Table 14. Hydrogen peroxide decomposition runs with no additives (45°C).

Time, min	$[O_2]$, as $[H_2O_2]$, mM	$[H_2O_2]$ mM by: Titration	$[H_2O_2]$ mM by: O_2 Meas.[a]	Ratio[b]	pH
Run B-1					
0	--	151	--	1.00	--
10	4.8	--	146	--	11.05
20	8.6	141	142	1.01	--
40	16.6	133	134	1.01	--
60	23.6	126	127	1.01	11.10
80	29.2	--	122	--	--
100	34.6	114	116	1.02	11.20
130	40.4	--	111	--	--
150	44.4	104	107	1.03	11.30
180	49.6	--	101	--	--
220	55.2	93.4	95.8	1.03	11.35
330	67.6	81.8	83.4	1.02	--
350	69.3	--	81.7	--	--
500	80.1	67.5	70.9	1.05	11.65
Run B-3					
0	--	153	--	1.00	10.90
10	5.2	--	148	--	10.90
20	9.7	--	143	--	--
30	14.1	--	139	--	10.90
40	18.1	--	135	--	--
50	21.3	--	132	--	11.00
60	24.6	127	128	1.01	11.05
75	29.0	--	124	--	11.10
90	33.0	--	120	--	--
105	36.8	--	116	--	11.10
120	40.1	111	113	1.02	11.10
140	44.4	--	109	--	--
160	48.1	--	105	--	11.15
180	51.3	99.4	102	1.03	11.20
200	54.4	--	98.6	--	--
465	--	71.5	--	--	11.35
490	--	68.8	--	--	11.37

[a] $[H_2O_2]_i - [O_2]$, as $[H_2O_2] = [H_2O_2]_{O_2}$ i = initial.
[b] Ratio = $[H_2O_2]_{O_2}/[[H_2O_2]_t$ t = titration.

Table 15. Hydrogen peroxide decomposition runs with no additives. $[H_2O_2]$ measured by titration method; pH 11.0-11.4 ± 0.1.

Time, min	$[H_2O_2]$, mM	Time, min	$[H_2O_2]$, mM
Run B-10		Run B-11	
0	29.81	0	15.73
10	29.61	10	15.77
20	29.60	20	15.68
30	29.48	40	15.61
45	29.21	60	15.53
60	29.09	110	15.35
80	28.87	125	15.31
100	28.52	140	15.30
180	27.73	155	15.22
190	27.65	200	15.06
200	27.57	230	14.96
210	27.42		
220	27.28	Run B-14	
Run B-9		0	152.3
		12	146.3
0	61.6	30	137.2
10	61.0	50	130.9
20	60.0	80	122.3
30	59.9	120	114.0
40	59.3	150	107.5
60	58.2	205	97.8
80	57.4	235	93.7
100	57.2	270	90.2
205	52.4	330	84.3
240	51.8		
250	51.3	Run B-8	
260	51.3		
270	50.9	0	837
285	50.5	4	695
300	49.7	8	606
320	49.4	12	545
340	48.5	16	507
360	48.0	20	474
		25	457

Table 16. Hydrogen peroxide decomposition runs with $FeSO_4$ or $CuSO_4$ added. $[H_2O_2]$ measured by titration method; pH 11.0-11.4 ± 0.1, 45°C.

Time, min	$[H_2O_2]$, mM
Run C-3 (1.8 μM Cu)	
0	154.7
10	142.0
15	135.4
20	129.6
25	124.1
30	118.5
35	113.8
45	105.0
50	100.8
55	96.8
60	92.5
70	84.9
80	78.2
90	72.0
100	66.1
170	30.7
Run C-4 (285 μM Cu)	
0	149.7
5	134.8
15	104.5
20	90.7
25	77.2
30	64.0
35	51.2
45	24.7

Time, min	$[H_2O_2]$, mM
Run F-2 (1.8 μM Fe)	
0	150.5
10	142.8
20	135.9
30	129.8
40	124.3
50	118.9
60	114.4
70	111.5
80	108.0
100	101.6
120	96.2
150	90.3
175	85.4
210	78.7
Run C-2 (9.1 μM Cu)	
0	133.4
10	121.1
20	112.2
30	102.8
45	90.0
60	78.8
75	67.0
85	60.0
145	22.5

Time, min	$[H_2O_2]$, mM
Run C-1 (18.2 μM Cu)	
0	148.8
10	134.6
15	131.2
20	125.9
25	120.7
30	113.3
35	108.1
40	105.0
50	95.8
Run F-1 (18.2 μM Fe)	
0	150.7
5	147.3
15	142.8
20	140.0
30	134.7
50	125.3
60	120.9
70	117.1
90	109.8
100	106.3
125	99.1
170	88.6
200	82.7
Run F-3 (285 μM Fe)	
0	147.3
8	142.1
15	138.6
20	134.8
28	126.4
38	118.0
48	113.2
70	99.2
80	93.9

Table 17. Hydrogen peroxide decomposition runs with $MnSO_4$ added (45°C).

Time, min	$[O_2]$, as $[H_2O_2]$, mM	$[H_2O_2]$ mM by: Titration	O_2 Meas.[a]	Ratio[b]	pH
Run M-2 (1.8 μM Mn)					
0	--	154	--	1.00	10.9
10	5.3	--	149	--	--
20	12.3	140	142	1.01	11.0
30	16.7	--	137	--	--
40	20.5	--	133	--	11.0
50	24.3	126	130	1.03	--
60	27.9	--	126	--	11.1
70	32.2	120	122	1.02	--
80	35.8	--	118	--	--
90	38.8	--	115	--	--
110	47.3	108	107	0.99	11.15
130	54.0	--	100	--	--
170	58.9	96.3	95.1	0.99	11.20
200	65.5	--	88.5	--	--
260	69.8	--	84.2	--	11.30
350	75.6	70.6	78.4	1.11	11.40
Run M-3 (9.1 μM Mn)					
0	--	151	--	1.00	10.9
10	9.5	--	141	--	--
20	16.8	136	134	0.99	11.05
30	23.1	--	128	--	11.10
45	31.9	--	119	--	11.30
60	40.0	112	111	0.99	11.40
75	47.3	--	104	--	11.5
90	54.0	--	97.0	--	11.55
105	60.6	--	90.4	--	11.60
120	66.1	83.6	84.9	1.02	11.65
135	71.7	--	79.3	--	--
150	76.7	--	74.3	--	11.70
165	81.5	--	69.5	--	11.70
180	86.1	63.0	64.9	1.03	--
195	90.5	--	60.5	--	11.75
210	94.5	--	56.5	--	--
225	98.5	50.3	52.5	1.04	11.75

See end of table for footnotes.

Table 17 (Continued). Hydrogen peroxide decomposition runs with $MnSO_4$ added (45°C).

Time, min	$[O_2]$, as $[H_2O_2]$, mM	$[H_2O_2]$ mM by: Titration	O_2 Meas.[a]	Ratio[b]	pH
Run M-1 (18.2 μM Mn)					
0	--	139	--	1.00	10.9
10	24.4	--	123	--	--
15	33.7	--	113	--	--
20	40.7	--	106	--	11.2
25	45.9	--	101	--	--
30	49.6	--	97.3	--	--
35	52.6	--	94.4	--	11.25
45	59.2	--	87.8	--	11.25
50	62.3	--	84.7	--	--
60	68.1	--	78.9	--	11.45
70	73.8	72.0	73.2	1.02	11.50
80	79.2	--	67.8	--	11.55
90	84.0	--	63.0	--	--
100	88.9	--	58.1	--	--
120	97.9	47.4	49.4	1.04	11.60
190	117.8	--	20.2	--	11.65

[a] $[H_2O_2]_i - [O_2]$, as $[H_2O_2] = [H_2O_2]_{O_2}$ i = initial.
[b] Ratio = $[H_2O_2]_{O_2}/[[H_2O_2]_t$ t = titration.

APPENDIX II

HYDROGEN PEROXIDE/MBB REACTION DATA (45°C)

Table 18. Control reaction: no additives.

Time, min	$[H_2O_2]$, mM			MBB, mM	MeOH, mM	pH
	Residual	Decomposed	Consumed			
0	100	--	--	20.0	--	11.02
5	--	2.4	--	--	--	11.02
10	--	4.6	--	--	--	11.03
15	--	6.9	--	--	--	11.04
20	87.1	8.6	4.5	18.6	1.23	11.06
30	--	12.0	--	--	--	11.08
45	--	16.4	--	--	--	11.11
60	63.9	20.1	16.0	17.6	2.94	11.14
75	--	23.1	--	--	--	11.15
90	--	25.8	--	--	--	11.18
120	43.1	29.6	27.3	16.0	4.77	11.21
135	--	31.1	--	--	--	11.22
165	--	33.5	--	--	--	11.24
200	27.0	35.4	37.6	15.1	6.41	11.23
270	18.0	37.5	44.5	14.8	7.34	11.22

Table 19. Control-A reaction: no additives.

Time, min	$[H_2O_2]$, mM			MBB, mM	MeOH, mM	pH
	Residual	Decomposed	Consumed			
0	100	--	--	20.0	--	--
15	--	7.4	--	--	--	11.00
30	78.1	11.7	8.2	19.0	1.57	--
45	--	15.6	--	--	--	11.04
60	63.7	18.7	15.6	17.9	2.99	11.05
80	--	22.0	--	--	--	11.06
110	45.4	25.7	26.9	16.7	4.55	11.10
140	--	28.0	--	--	--	11.12
160	32.6	29.6	35.8	15.8	5.84	--
200	25.0	31.4	41.6	15.0	6.80	11.14
240	19.4	32.6	46.0	13.6	7.60	11.14

Table 20. Fe reaction: 300 μM $FeSO_4$ added.

Time, min	$[H_2O_2]$, mM			MBB, mM	MeOH, mM	pH
	Residual	Decomposed	Consumed			
0	100	--	--	20.0	--	11.02
5	--	6.2	--	--	--	11.07
10	--	11.0	--	--	--	11.10
15	81.0	15.7	3.3	18.6	0.95	11.14
25	--	23.8	--	--	--	11.21
30	65.7	27.1	7.2	18.1	1.66	11.22
40	--	32.7	--	--	--	11.26
50	50.5	37.4	12.1	17.6	2.75	11.29
60	--	41.2	--	--	--	11.32
70	--	44.3	--	--	--	11.34
75	36.6	45.6	17.8	17.1	3.58	11.36
90	--	49.2	--	--	--	11.39
110	--	52.6	--	--	--	11.42
120	20.8	53.8	25.4	16.5	4.80	11.44

Table 21. FC reaction: 300 μM $K_3Fe(CN)_6$ added.

Time, min	$[H_2O_2]$, mM			MBB, mM	MeOH, mM	pH
	Residual	Decomposed	Consumed			
0	100	--	--	20.0	--	11.02
10	--	8.9	--	--	--	11.05
20	--	14.5	--	--	--	11.08
30	67.5	19.0	13.5	17.2	3.06	11.10
45	--	23.8	--	--	--	11.14
60	--	27.5	--	--	--	11.18
80	38.2	31.1	30.7	15.2	5.62	11.24
100	--	33.7	--	--	--	11.26
130	22.5	36.1	41.1	14.4	7.45	11.28

Table 22. Cu reaction: 12 μM $CuSO_4$ added.

Time, min	$[H_2O_2]$, mM			MBB, mM	MeOH, mM	pH
	Residual	Decomposed	Consumed			
0	100	--	--	20.0	--	11.00
5	--	6.9	--	19.9	1.05	11.02
10	--	10.9	--	--	--	11.04
15	77.6	15.2	7.2	18.6	2.48	11.06
20	--	18.6	--	--	--	11.08
25	--	22.1	--	--	--	11.09
30	--	25.1	--	--	--	11.11
36	--	28.4	--	--	--	11.14
40	37.0	30.3	32.7	15.9	6.52	11.16
50	24.8	33.4	41.8	14.9	7.69	11.20
60	--	35.4	--	--	--	11.26
70	7.3	36.9	55.8	13.1	10.20	11.30
77	--	37.4	--	--		11.32

Table 23. Mn reaction: 21 μM $MnSO_4$ added.

Time, min	$[H_2O_2]$, mM			MBB, mM	MeOH, mM	pH
	Residual	Decomposed	Consumed			
0	100	--	--	20.0	--	11.05
5	83.4	12.4	4.2	19.1	0.62	11.10
10	--	19.0	--	--	--	11.10
15	--	24.9	--	--	--	11.12
20	55.8	30.7	13.5	18.1	1.98	11.18
30	--	39.6	--	--	--	11.22
35	--	43.4	--	--	--	11.27
40	32.6	46.8	20.6	17.1	3.30	11.31
50	--	52.3	--	--	--	11.38
60	17.4	56.6	26.0	--	4.26	11.44
75	10.0	60.9	29.1	15.8	4.92	11.50

Table 24. Acidic products distributions with time.

Reaction[a]	Control			Fe			FC	Mn			Cu		
Reaction time, min	20	120	270	30	75	120	130	40	60	75	15	40	70
MBB reacted, %	7.3	20.0	26.0	9.5	14.3	17.9	28.0	15.0	18.5	21.0	6.8	20.4	34.8
Acidic Product[b]	Estimated Concentration of Product, mM x 10[c]												
I	0.0	2.9	2.3	2.2	3.7	5.1	8.2	2.6	1.5	1.4	2.2	3.3	4.4
II	0.0	0.0	0.6	0.0	0.0	0.0	0.1	0.0	0.0	0.0	0.0	0.2	0.4
III	0.0	1.1	3.7	0.0	0.0	0.4	2.4	0.0	0.0	0.5	0.0	1.6	2.6
IV	0.9	8.5	10.3	1.5	2.7	4.0	11.6	2.9	4.4	5.1	3.8	12.0	16.6
V	0.4	3.2	8.3	0.0	0.6	1.7	6.2	0.4	0.4	1.0	0.5	3.4	5.7
VI	0.6	2.9	4.2	1.1	1.5	2.1	2.5	1.3	1.0	1.3	0.8	1.4	1.9
VII	1.2	5.5	6.9	1.0	2.0	3.0	8.9	4.8	3.7	4.4	3.0	8.5	12.1
VIII	0.8	3.7	5.0	1.1	1.8	2.6	6.2	3.1	3.5	4.6	2.1	5.9	10.2
IX	0.0	0.5	1.5	0.0	0.0	0.2	0.8	0.0	0.0	0.0	0.0	0.3	0.6
X	0.0	1.8	3.3	0.8	0.8	1.2	2.6	1.1	1.5	2.0	0.4	1.5	2.6
XI	2.3	6.5	6.9	3.2	4.2	4.8	6.7	5.4	5.7	6.0	5.0	8.3	8.7
XII	0.2	1.1	1.6	0.0	0.5	0.6	1.6	0.6	0.9	1.6	0.7	2.9	4.6
XIII	0.4	1.6	2.1	0.5	0.7	1.3	2.2	1.2	1.8	2.3	0.5	1.7	3.7
XIV	0.2	1.6	2.4	0.5	0.7	0.9	2.0	0.2	0.4	1.0	0.3	1.1	1.4
XVIII	0.0	0.1	1.1	0.0	0.0	0.0	0.3	0.0	0.0	0.3	0.0	0.0	0.3
XIX	1.2	5.7	6.5	1.1	3.0	3.6	6.3	5.0	3.3	6.3	0.2	8.2	10.3
XX	0.1	0.1	0.2	0.0	0.0	0.0	0.2	0.1	0.0	0.1	0.4	0.4	0.3
XXI	0.0	0.1	0.2	0.0	0.0	0.0	0.2	0.5	0.4	1.1	0.0	0.2	1.0

Reaction Conditions: 45°C, pH 11.0-11.4, $[H_2O_2]$ = 100 mM, [MBB] = 20.0 mM

[a]Reaction/addtive: control/none; Fe/300 μM $FeSO_4$; FC/300 μM Fe $(CN)_6^{-3}$; Mn/21 μM $MnSO_4$; Cu/12 μM $CuSO_4$.
[b]See Table 10 for product identities.
[c]Product concentrations estimated by GLC analysis of silylated product mixtures using response factors listed in Appendix VI. For a given acidic product, the standard deviation for duplicate silylations was generally in the range of ± 10-20%.

APPENDIX III

CALCULATION OF TOTAL ACIDIC GROUPS FORMED

The total concentration of organic acid groups formed during the oxidation reactions was calculated based on the following derivation.

The following equilibria and ions exist in the reaction solution:

$$H_2O_2 \rightleftharpoons H^+ + HO_2^- \quad (36)$$

$$H_2O \rightleftharpoons H^+ + HO^- \quad (37)$$

$$MBB_2 \rightleftharpoons H^+ + MBB_2^- \quad (38)$$

$$MBB_2^- \rightleftharpoons H^+ + MBB_2^= \quad (39)$$

$$A\text{-}H \longrightarrow H^+ + A^- \quad (40)$$

$$NaOH \longrightarrow H^+ + HO^- \quad (41)$$

where

MBB_2 = dianion of MBB (both carboxylic acid groups ionized)

MBB_2^-, $MBB_2^=$ = phenoxy mono- and di-anions of MBB_2, respectively

A-H = organic acids formed by oxidation of MBB.

A balance of the ionic charges described in these equations gives:

$$[Na^+] + [H^+] = [HO^-] + [HO_2^-] + [MBB_2^-] + MBB_2^=] + [A^-] \quad (42)$$

This equation can be reduced to Eq. (43) based on the following assumptions:

1. $[H^+]$ is negligible at pH 11
2. Equation (38) and (39) can be neglected since the two ionized MBB_2 species are not likely protonated after oxidation.

$$[Na^+]_o = [HO^-] + [HO_2^-] + [A^-] \quad (43)$$

where $[Na^+]_o$ = initial $[Na^+]$ when $[A^-] = 0$ and $[MBB_2^{-,-2}]$ are neglected.

The $[A^-]$ can now be evaluated using the reaction data and the following procedure. The $[Na^+]_o$ is first calculated using the known initial conditions (pH and $[H_2O_2]$) and Eq. (44) and (45). For a given reaction time, the $[A^-]$ is then calculated by using the measured pH and $[H_2O_2]$, and again Eq. (44) and (45). Table 25 summarizes the results of these calculations on the data from the Control reaction.

$$pH = \log[HO^-] + pK_w \tag{44}$$

$$pH = pK_a + \log([HO_2^-]/([H_2O_2]-[HO_2^-])) \tag{45}$$

where

$pK_w = 13.4$ and $pK_a = 11.31$

Table 25. Summary of values used to calculate total acids formed during control reaction.

Time, min.	$[H_2O_2]$, mM	pH	$[HO_2^-]$, mM	$[HO^-]$, mM	$[A^-]$, mM	$[Na^+]_o$, mM
0	100	11.02	33.9	4.2	0	38.1
20	87.1	11.06	31.4	4.6	2.1	38.1
60	63.9	11.14	25.8	5.5	6.8	38.1
120	43.1	11.21	19.1	6.5	13.5	38.1
200	27.0	11.23	12.3	6.8	19.0	38.1
270	18.0	11.22	8.1	6.6	23.4	38.1

APPENDIX IV

KINETIC RATE DATA AND PLOTS

Table 26. Hydrogen peroxide decomposition rate data in the absence of MBB or added metal ions.

Run No.	$[H_2O_2]$, mM	$-d[H_2O_2]/dt$,[a] mM/min
B-11	15.74	0.003365
B-10	29.81	0.01124
B-9	51.8	0.03142
B-9	61.6	0.05142
B-1	80.7	0.106
B-3	89.5	0.119
B-1	98.6	0.167
B-1	119.5	0.263
B-3	122	0.294
B-3	146	0.380
B-8	486	7.14
B-8	519	9.64
B-8	582	16.4
B-8	652	22.4
B-8	728	30.3
B-8	827	39.5

[a]Rates determined by measuring slopes of tangents on the $[H_2O_2]$ *vs.* time plots of data from Appendix I.

Table 27. Peroxide decomposition rate data in the presence of MBB. The rates were measured from the slopes of tangents of [Ox] vs. time plots for the reactions with the MBB present.

([Ox] = O_2 as [H_2O_2])

Reaction Time, min.	[H_2O_2], mM [Ox]	[H_2O_2], mM Residual	d[Ox]/dt mM/min • 10
Control			
0	0	100	5.50
26.8	11.2	83.0	3.31
56.3	19.4	66.0	2.31
86.2	25.2	53.5	1.63
145	31.8	37.5	0.85
215	36.1	24.0	0.35
Fe rxn.			
0	0	100	14.0
10.6	12.0	86.0	9.73
23.2	22.7	72.0	7.35
35.2	30.2	61.5	5.56
61.6	41.9	44.0	3.30
103	51.3	25.5	1.51
FC rxn.			
0	0	100	6.51
15.6	12.6	81.5	5.38
26.0	17.3	71.5	4.03
46.3	23.1	55.0	2.94
61.8	27.9	46.5	2.14
102	37.0	30.0	1.06
Mn rxn.			
0	0	100	71.6
7.1	15.9	78.5	14.9
14.4	24.8	63.5	11.7
20.5	31.1	55.0	9.51
31.5	40.6	42.0	8.10
56.5	55.1	20.0	3.94
Cu rxn.			
0	0	100	15.9
5.1	6.77	92.5	10.0
7.5	8.85	89.5	8.93
12.8	13.2	81.5	8.27
25.6	22.7	60.0	6.55
36.6	28.7	42.5	4.63
45.3	32.1	29.5	3.18
671.8	35.6	14.0	1.54

Table 28. Rate data measured from the slope of tangents on the [MBB] vs. time plots.

Reaction Time, min.	[MBB], mM	Residual $[H_2O_2]$, mM	-d[MBB]/dt, mM/min · 100
Control			
16.1	19.1	89.0	4.83
25.0	18.7	84.0	4.49
34.3	18.3	73.0	4.17
50.4	17.7	69.5	3.58
73.2	17.0	58.5	2.85
102	16.3	48.5	1.97
125	15.9	42.0	1.60
Fe rxn.			
6.9	19.2	90.5	9.01
11.8	18.8	85.0	6.53
15.9	18.6	80.0	4.78
19.3	18.4	76.0	3.60
22.0	18.3	73.5	3.35
26.1	18.2	69.5	3.05
37.4	17.9	60.0	2.41
52.2	17.5	49.5	2.15
62.2	17.3	43.5	1.99
FC rxn.			
12.0	18.7	85.5	9.73
19.7	18.0	78.0	7.47
29.3	17.3	68.5	6.66
50.4	16.2	36.5	2.67
84.6	15.2	52.5	4.01
93.9	14.7	33.0	1.73
Mn rxn.			
5.7	19.1	82.5	10.61
7.8	18.9	77.5	9.51
12.3	18.5	67.5	7.13
20.6	18.0	55.0	5.51
39.8	17.1	34.0	4.63
52.8	16.5	23.0	3.66
Cu rxn.			
17.6	18.3	73.0	11.1
23.7	17.7	63.0	10.9
31.1	16.9	51.0	10.5
42.0	15.7	34.0	10.2
57.2	14.3	17.5	8.76

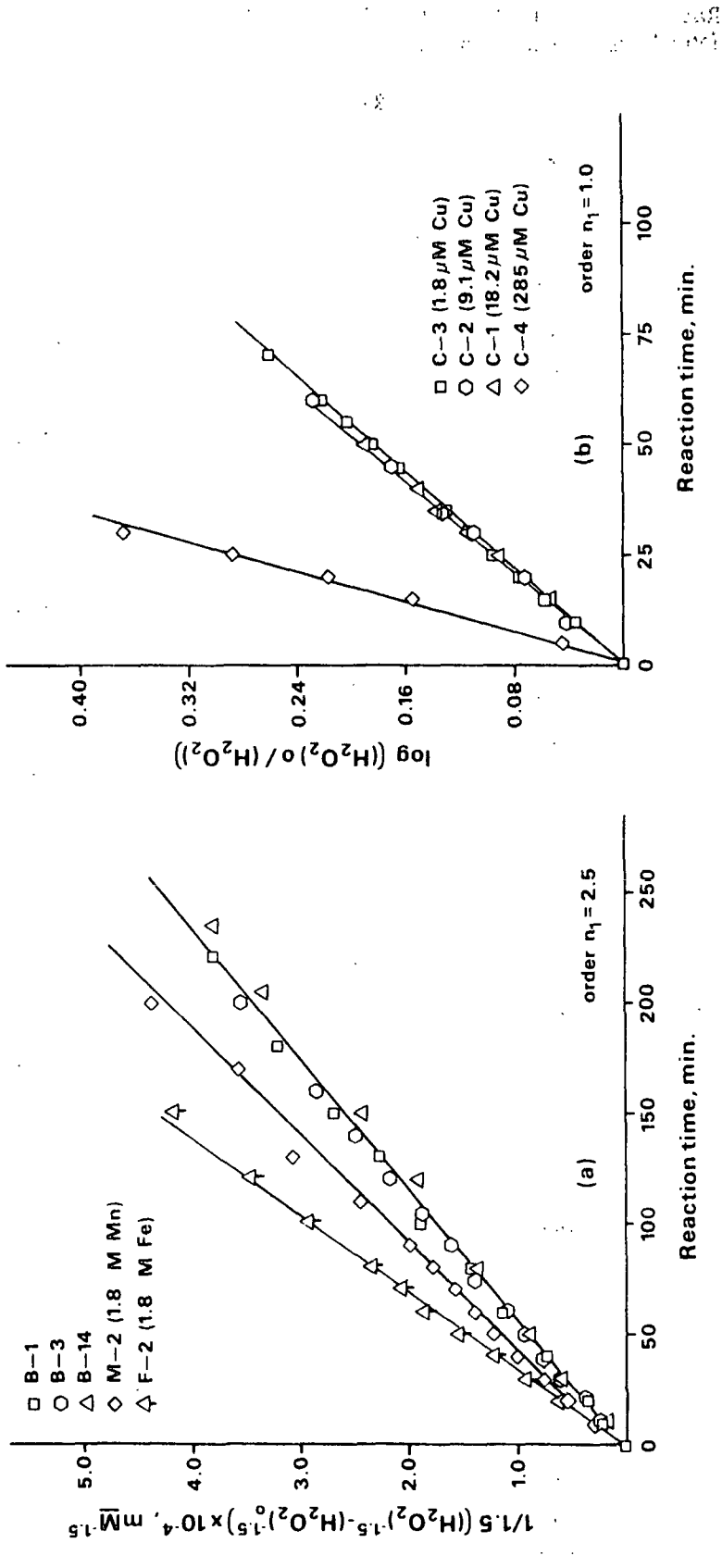

Figure 45. Kinetic plots of hydrogen peroxide decomposition data in the absence of MBB. Data plotted according to the integral method with reaction orders of: (a) $n_1 = 2.5$; (b) $n_1 = 1.0$.

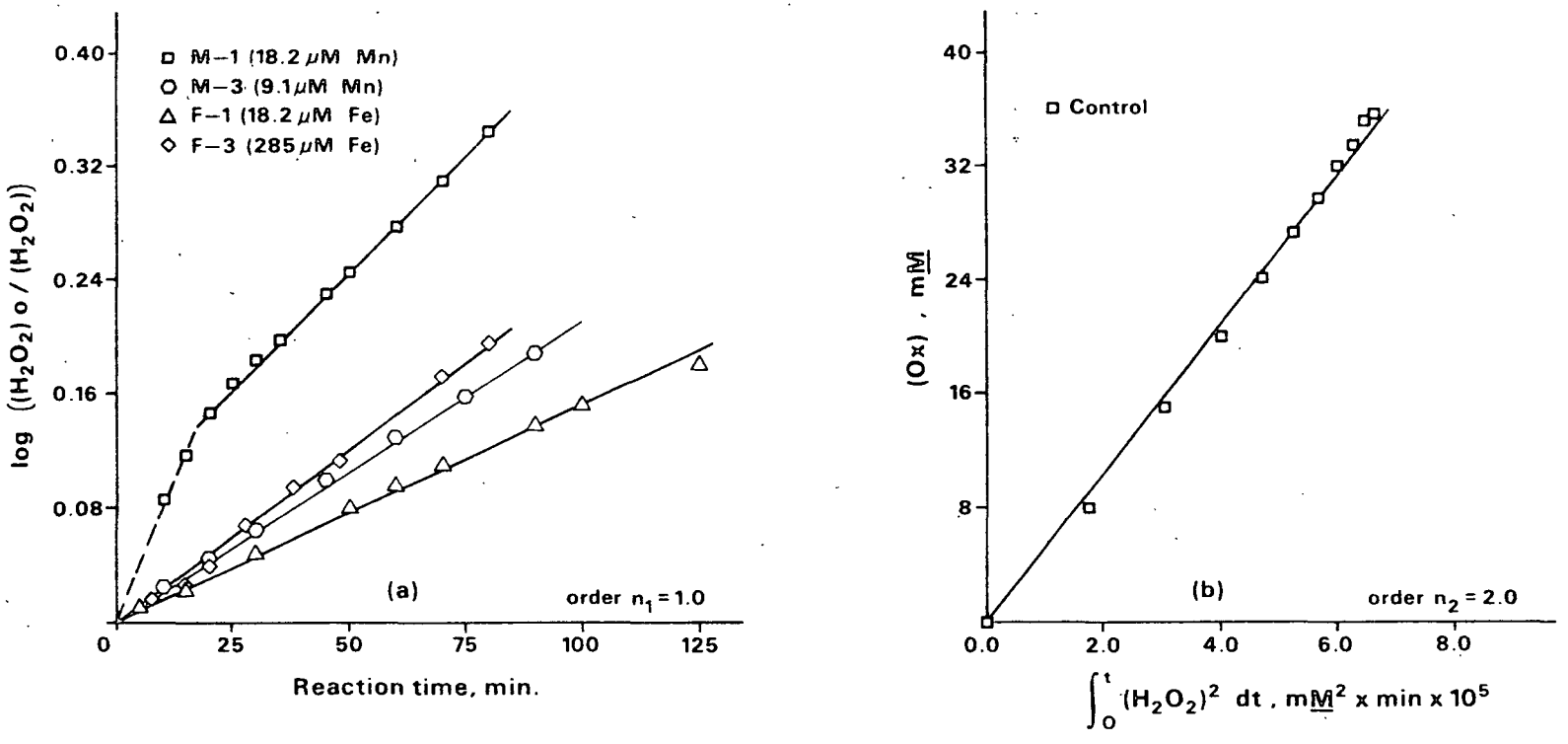

Figure 46. Kinetic plots of hydrogen peroxide decomposition data according to the integral method: (a) with MBB absent, n_1 = 1.0; (b) with MBB present (Control reaction) n_2 = 2.0.

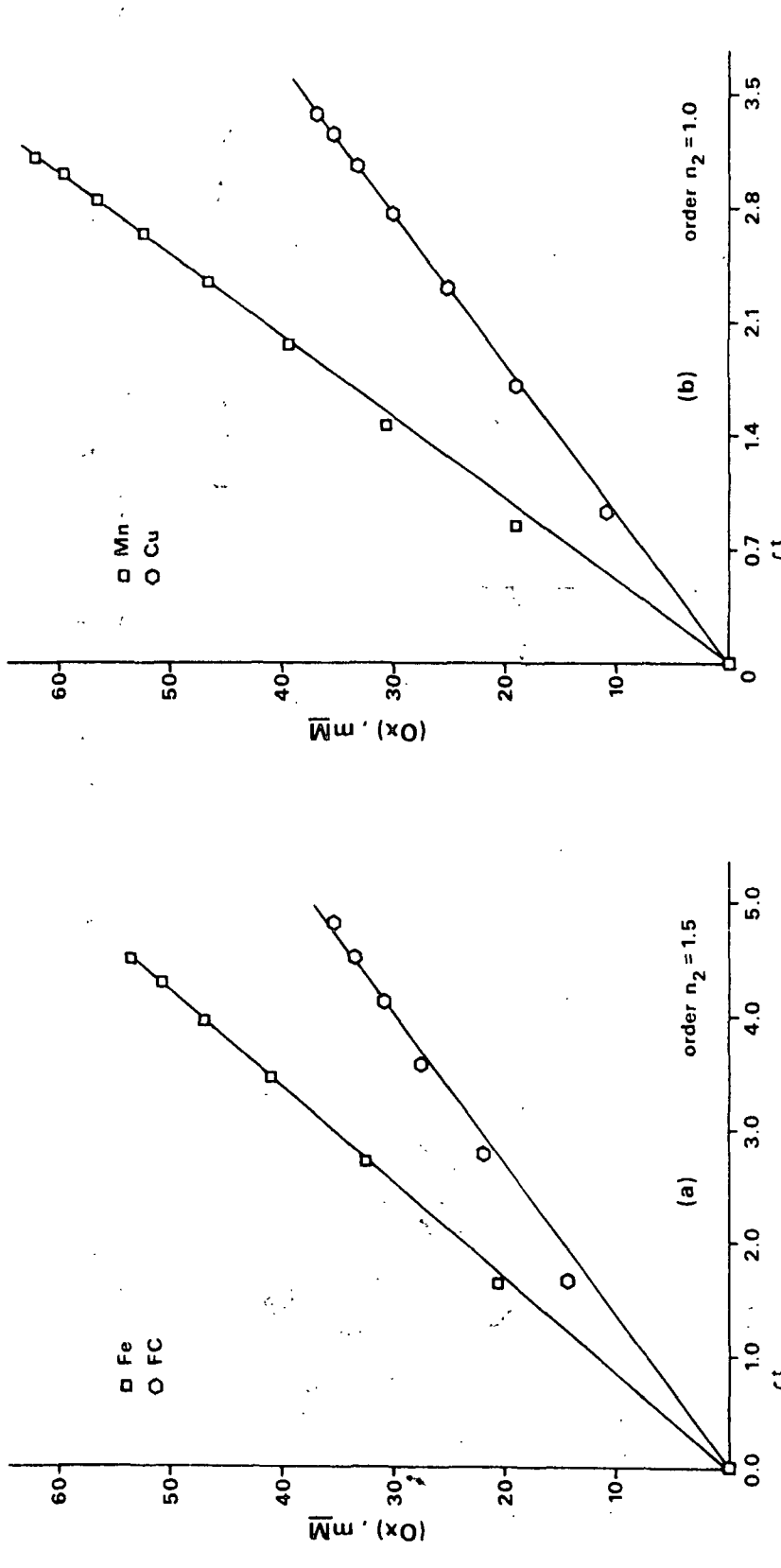

Figure 47. Kinetic plots of hydrogen peroxide decomposition data according to the integral method: (a) with MBB present (Fe and FC reactions), n_2 = 1.5; (b) with MBB present (Mn and Cu reations), n_2 = 1.0.

APPENDIX V

KINETIC MODEL ANALYSIS OF MBB/H_2O_2 REACTION

The computer programs used in the kinetic model analysis are stored in the Institute's Computer Center tape library, and are only briefly described here. Optimal values of k_5, k_6 (or k_4, k_7) for the kinetic model defined by Eq. (28), (29) [or (24), (30)] were obtained by using a multiresponse parameter estimation (MRPEST) computer program (116). This program was coupled with an IMSL subroutine (DVERK) which evaluated the differential rate expressions. Experimental data ([MBB], [H_2O_2] vs. time), and k_2, n_2 (Table 7) from each reaction were the main inputs to the program. The MRPEST program uses a parameter estimation procedure which involves the minimization of the determinant based on the residuals for the two responses ([MBB], [H_2O_2]).

A separate program using DVERK was employed to produce calculated reactant concentration-time data from the given kinetic model using the appropriate rate constants (Table 29). These calculated values were plotted as curves in Fig. 48-52 along with the experimental data from Appendix II.

Table 29. Values of rate constants used in the kinetic models.

Reaction	Rate Constants[a]				
	k_2	k_4	k_5	k_6	k_7
Control	5.42E-05	--	2.69E-05	2.06E-04	--
Cu	1.08E-02	5.90E-03	--	--	4.95E-02
Fe	1.16E-03	--	3.60E-05	2.30E-04	--
FC	7.28E-04	--	5.39E-05	3.78E-04	--
Mn	1.95E-02	--	8.60E-05	7.23E-04	--

[a]Units: k_4, k_7, k_2 (Cu), k_2(Mn) - min^{-1}

k_5, k_6, k_2 (Control) - $\underline{mM}^{-1} \cdot min^{-1}$

k_2 (FC, Fe) - $\underline{mM}^{-0.5} \cdot min^{-1}$

NOTE: k_2 values are from Table 7; all other values obtained from MRPEST program.

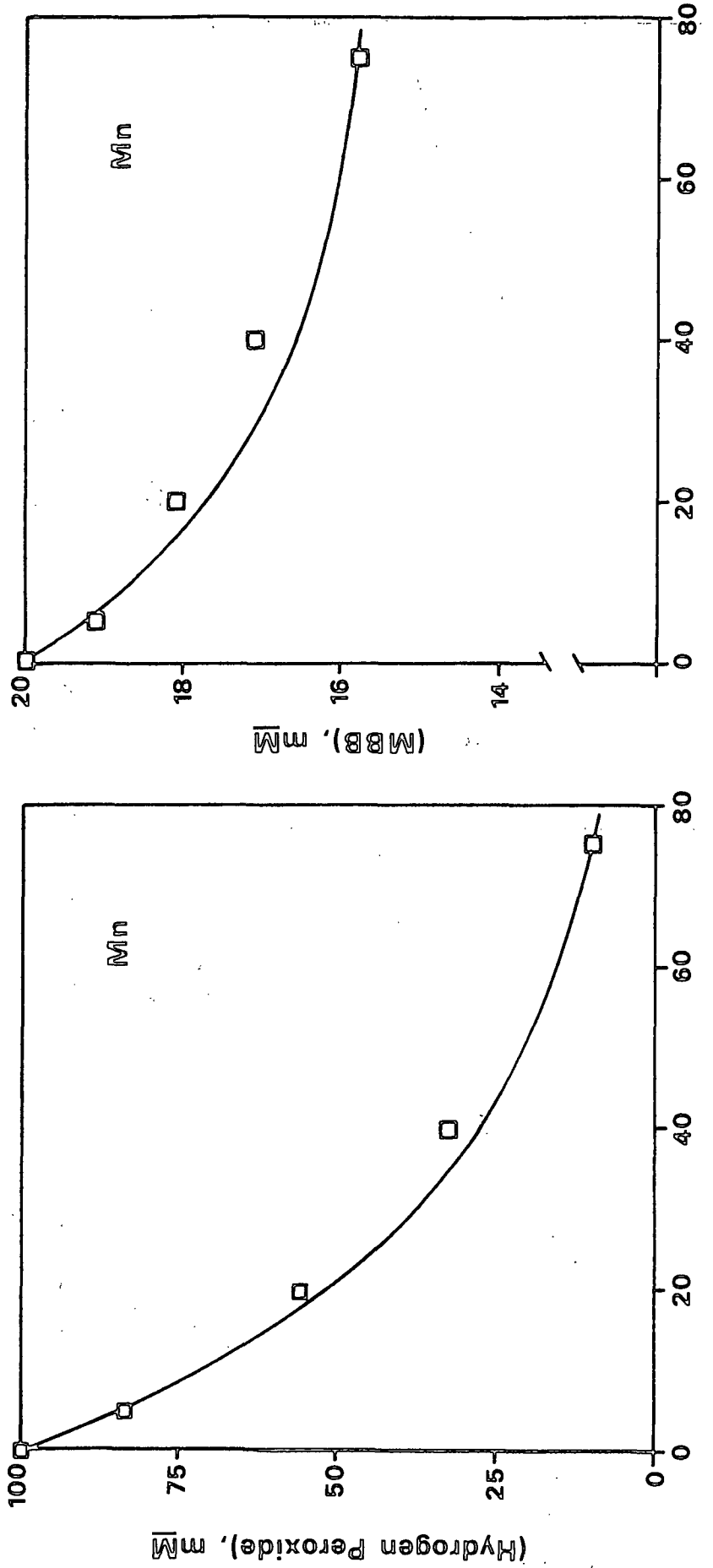

Figure 48. Comparison of experimental data (□) to the calculated (——) reactant concentration - time curves for the Mn reaction. The curves were calculated using Eq. (28) and (29), and the rate constants in Table 29.

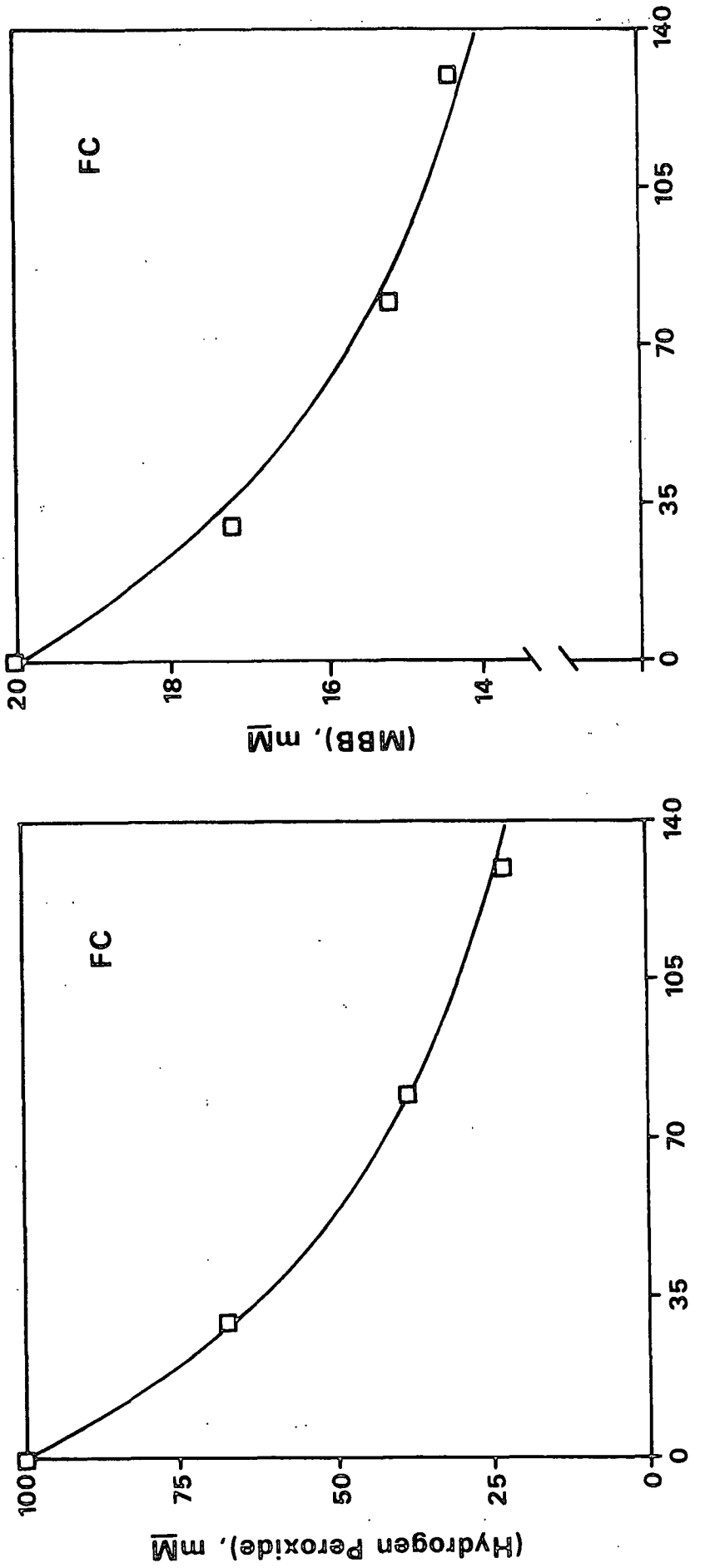

Figure 49. Comparison of experimental data (□) to the calculated (——) reactant concentration - time curves for the FC reaction. The curves were calculated using Eq. (28) and (29), and the rate constants in Table 29.

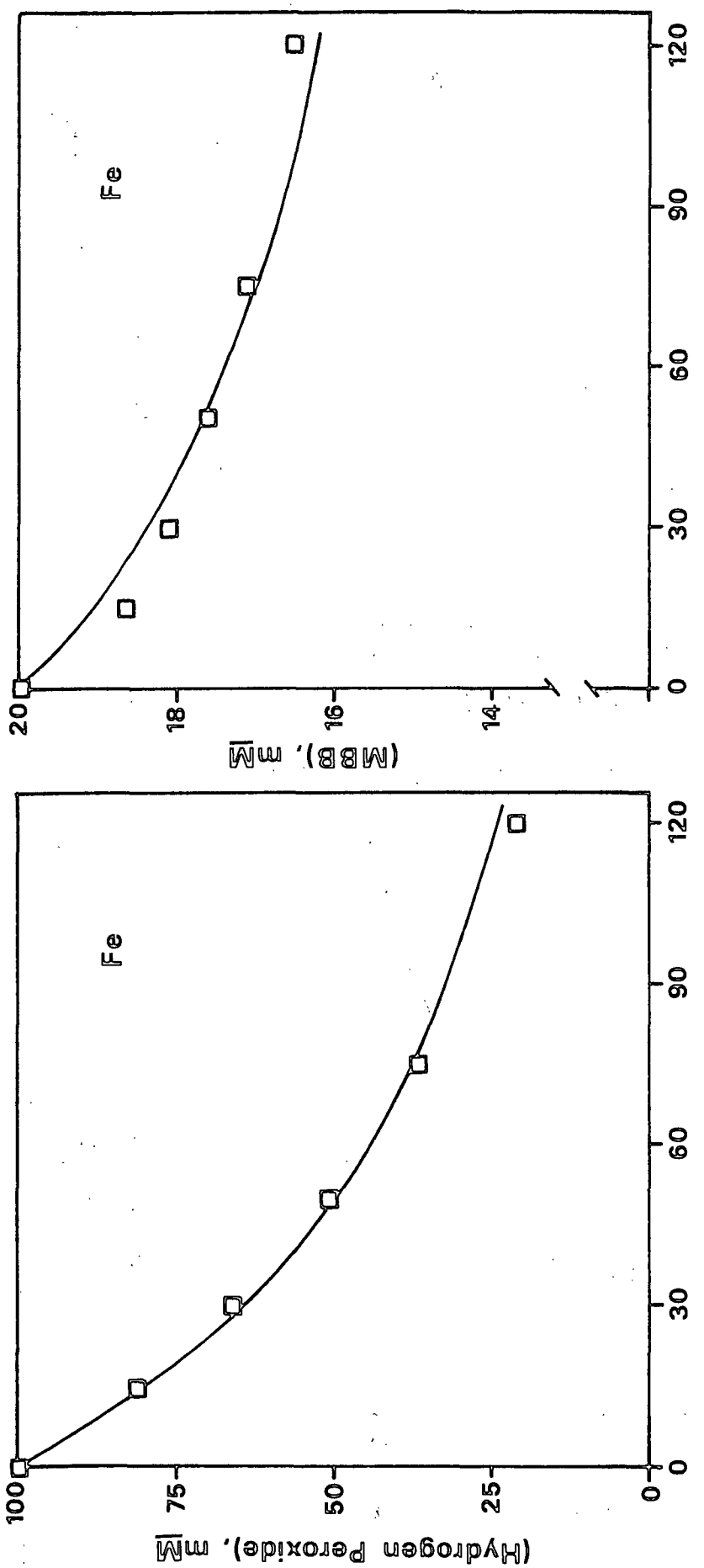

Figure 50. Comparison of experimental data (□) to the calculated (——) reactant concentration - time curves for the Fe reaction. The curves were calculated using Eq. (28) and (29), and the rate constants in Table 29.

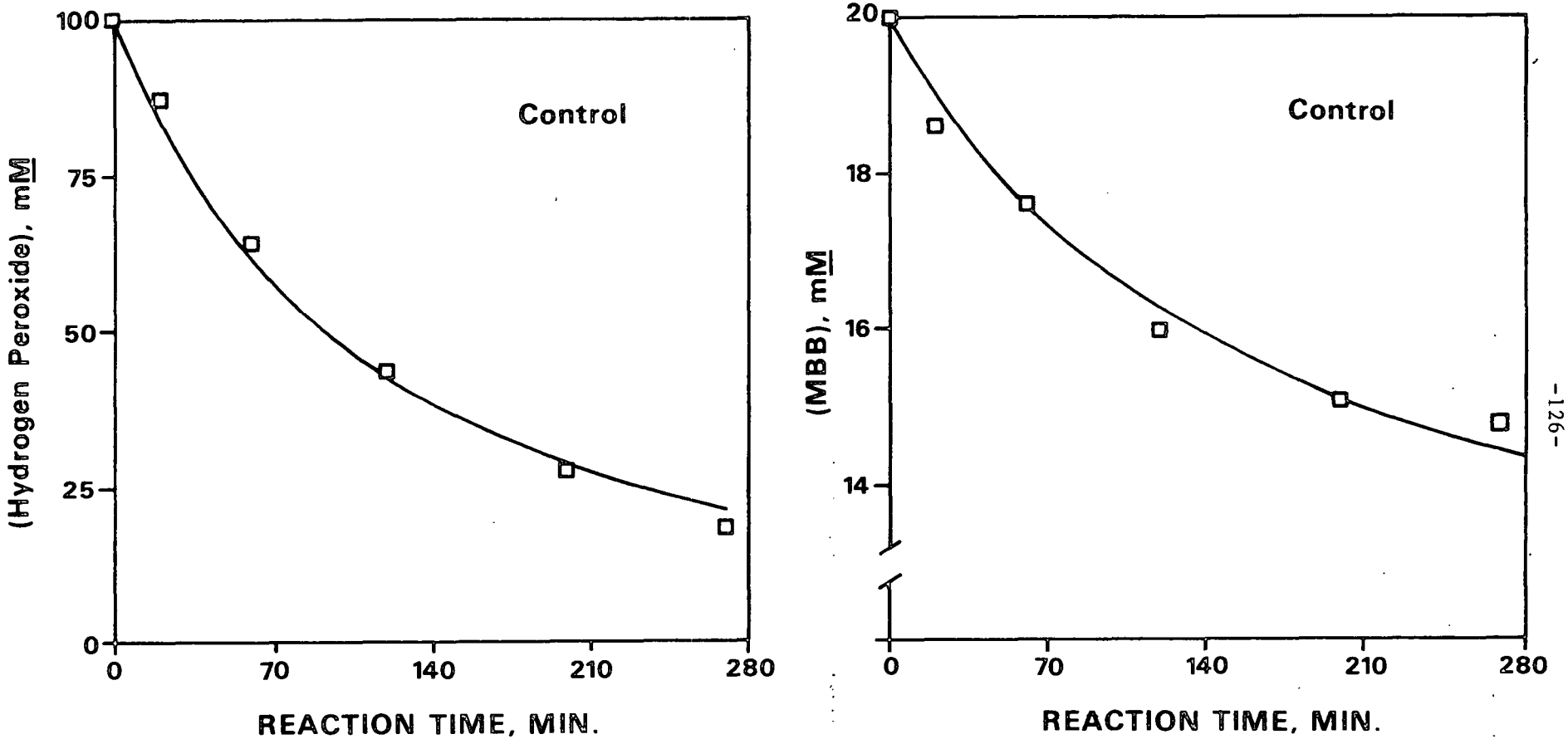

Figure 51. Comparison of experimental data (□) to the calculated (——) reactant concentration - time curves for the Control reaction. The curves were calculated using Eq. (28) and (29), and the rate constants in Table 29.

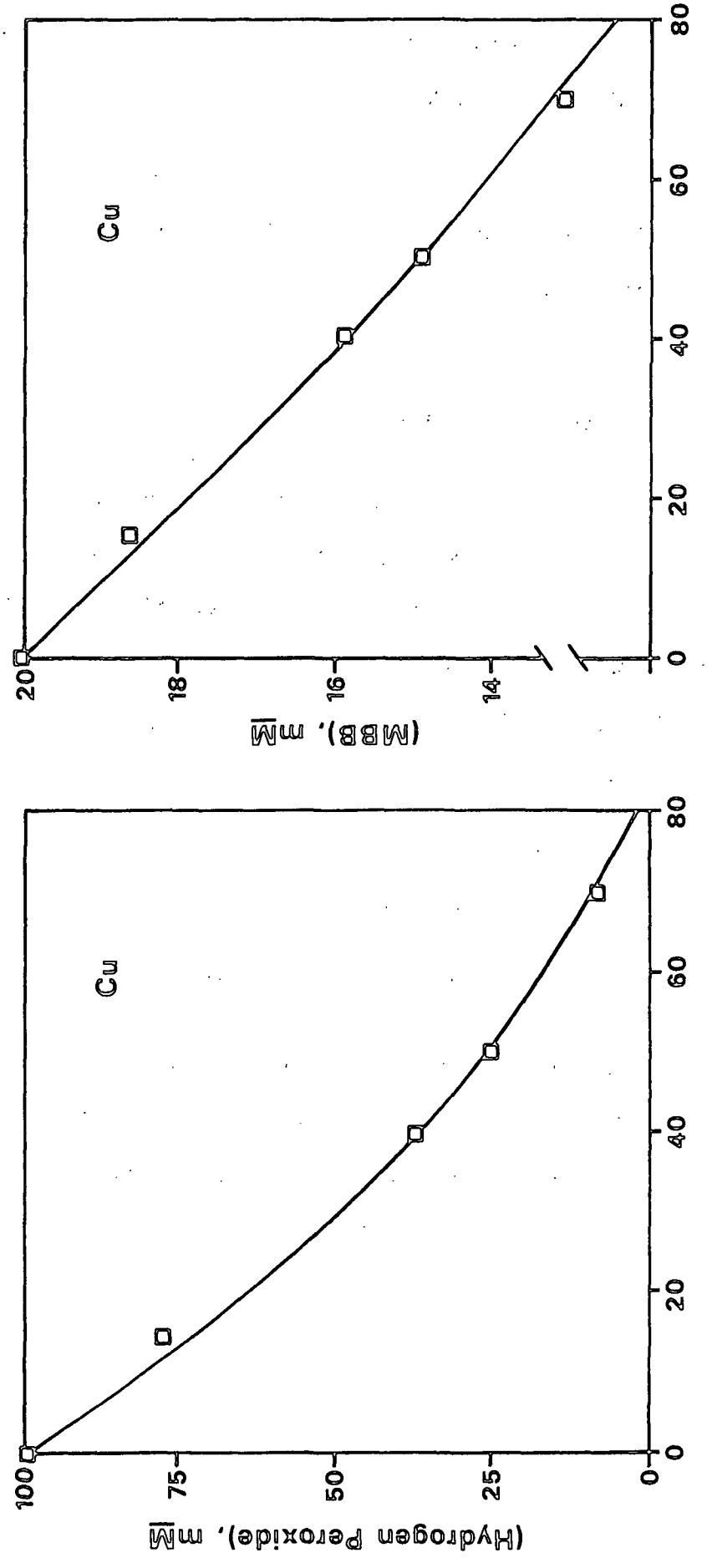

Figure 52. Comparison of experimental data (□) to the calculated (——) reactant concentration - time curves for the Cu reaction. The curves were calculated using Eq. (28) and (29), and the rate constants in Table 29.

APPENDIX VI

KINETIC MODEL FOR XI FORMATION

A kinetic model which describes the rate of formation of 5-hydroxymethyl-hydroferulic acid (XI) under the Control reaction conditions was derived in the following manner. The overall rate equation for the observed formation of XI was assumed to be:

$$d[XI]/dt = k_f[H_2O_2][MBB] - k_d[XI] \quad (46)$$

Rate constant, k_d, represents the pseudo-first-order rate constant for the disappearance of XI in the presence of a large excess of H_2O_2 (a condition which exists over most of the reaction). This constant was evaluated in separate, duplicate experiments by following the degradation of XI (5 mM) in alkaline hydrogen peroxide (50 mM H_2O_2, pH 11.0, 45°C), and applying the integral method of kinetic analysis (Fig. 53).

Rearrangement of Eq. (46) gives an expression [Eq. (47)] which can be used to evaluate k_f. The data for this calculation are presented in Table 30.

$$k_f = (d[XI]/dt + k_d[XI])/[H_2O_2][MBB] \quad (47)$$

With the values for k_f and k_d determined, Eq. (46) was combined with Eq. (28) and (29) (Kinetic section) to define the kinetic model. Using the method described in Appendix V, the model gave calculated [XI] - time curves (Fig. 38). For the case in which no degradation of XI was assumed, k_d was set equal to zero.

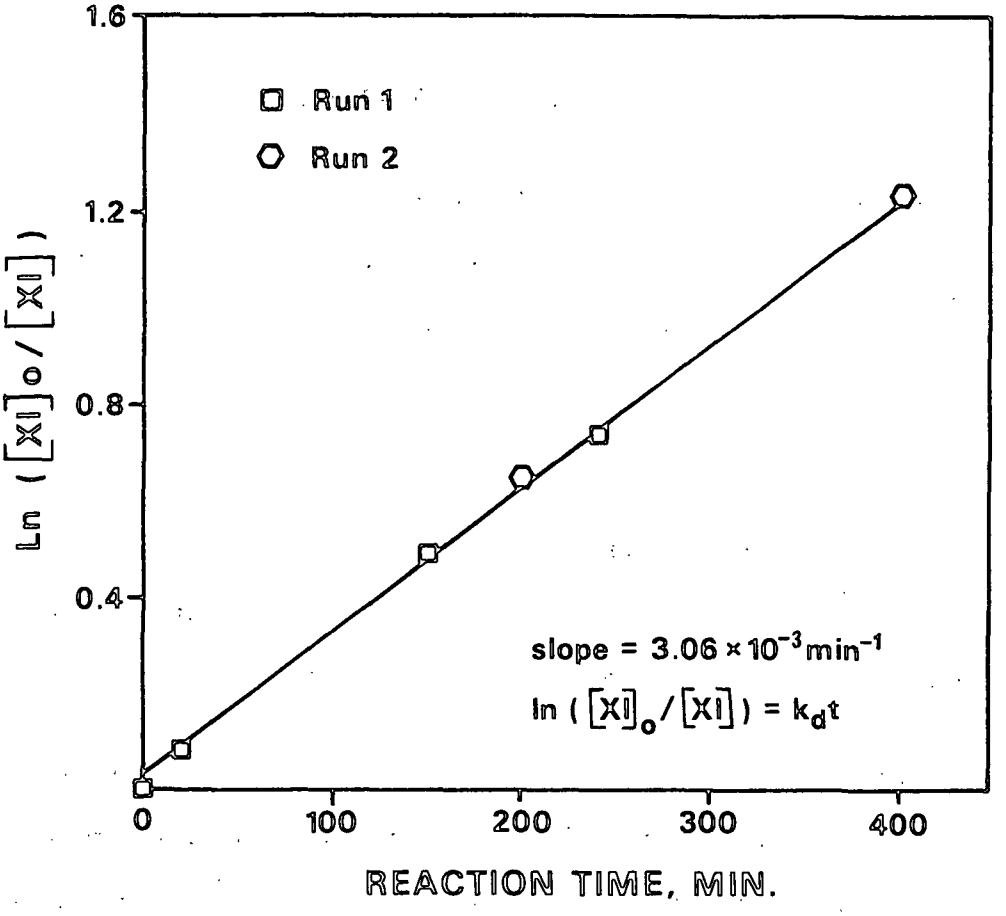

Figure 53. Kinetic plot of XI degradation data according to the integration method (45°C, 50 mM H_2O_2, 5 mM XI, pH 11.0).

Table 30. Summary of data used to calculate k_f.

Time, min	d[XI]/dt[a] • 10^3	[XI]	[H_2O_2]	[MBB]	k_f • 10^6
22	7.82	0.24	85.5	18.5	5.41[b]
60	4.75	0.48	64.0	17.4	5.57
82	5.52	0.57	55.0	16.9	7.82
143	0.53	0.68	38.0	15.7	4.35
270	0.00	0.69	18.0	14.8	7.93
				Average	6.22
				Std. dev.	1.59

[a]Rates measured from slopes of tangents along the observed [XI] vs. time curve for the Control reaction.
[b]Units: $mM^{-1} \cdot min^{-1}$.

APPENDIX VII

GAS-LIQUID CHROMATOGRAPHY

The method of internal standardization was employed for the quantitative and semiquantitative GLC analysis. Molar response factors relative to an internal standard were calculated according to Eq. (48).

$$F_X = A_r \times M_r \tag{48}$$

where

F_X = response factor for compound X relative to the internal standard

A_r = ratio of GLC peak areas of compound X to the internal standard

M_r = mole ratio of the internal standard to compound X

Response factors were experimentally determined by subjecting a series of solutions, prepared with varied mole ratios, to the appropriate workup and analysis procedure. These samples were then analyzed by GLC in triplicate, and response factors were calculated as an average of the values obtained. For semiquantitative GLC analysis, estimated response factors were calculated based on the effective carbon numbers of the compound and the internal standard (117).

The concentration of a given compound in the reaction solution was calculated according to Eq. (49).

$$[X] = (A_r)(IS)(D)/(S)(F_X) \tag{49}$$

where

[X] = concentration of compound X, mM

IS = internal standard, mmoles

D = density of reaction solution, mg/mL

S = sample weight, g

Table 31 describes the various GLC conditions and columns used in this work, and Table 32 lists the retention times and response factors of the associated compounds.

Table 31. Gas-liquid chromatographic conditions.

Conditions	A	B	C	D
Instrument	PE-3920	PE-3920	HP-5840A	Varian 202
Column type	OV-1[a]	Poropak[b]	OV-17[c]	OV-17[d]
Derivative	TMS	None	TMS	TMS
Column temp., °C	250	75	50 —> 290 at 4°/min	Varied as necessary
Injector temp., °C	290	150	310	335
Detector temp., °C	290	175	320	335
Carrier gas[e]	N_2	N_2	He	He
Carrier gas flow rate, mL/min	32	27	30	85

[a]Glass column (3 ft x 0.25 inch, 2 mm ID) rigged for off-column injection and packed with 3% OV-1 on 80/100 mesh Chromosorb W-HP (L. C. Company, Inc.).
[b]Teflon column (2 ft x 0.12 inch, 1.6 mm ID) rigged for off-column injection and filled with Poropak Super-Q 80/100 mesh (All-tech Associates).
[c]Glass column (6 ft x 0.25 inch, 2 mm ID) packed with 3% OV-17 on 80/100 Supelcoport (Supelco, Inc.).
[d]Nickel column (8 ft x 0.25 inch) rigged for off-column injection and filled with 10% OV-17 on 50/60 mesh Chromosorb W-AW DMCS.
[e]Gases: prepurified nitrogen or high purity helium (Matheson Gas).

Table 32. Retention times (T_r) and response factors (F_x).

Conditions	Compound	T_r, min	F_x
A	MBB	1.8	a) 0.942 ± 0.025
	n-Octacosane	5.7	a) 1.000
B	Methanol	0.9	b) 0.520 ± 0.006
	Ethanol	3.3	b) 1.000
C	Glycolic acid (I)	6.6	c) 0.53
	3-Hydroxypropanoic acid (II)	8.2	c) 0.63
	Oxalic acid (III)	9.6	c) 0.51
	Levulinic acid (IV)	10.5	c) 0.53
	Succinic acid (V)	14.5	d) 0.61 ± 0.03
	Vanillic acid	28.1	d) 1.000
	3-Carboxy-hexanedioic acid (VI)	29.3	c) 1.14
	cis-3-carboxy-2-hexenedioic acid (VII)	30.4	c) 1.13
	4-(2)carboxyethyl)-2-furoic acid (VIII)	31.3	c) 0.98
	Unknown (IX)	33.8	e) 1.0
	Unknown (X)	35.2	e) 1.0
	5-Hydroxymethyl-hydroferulic acid (XI)	37.5	d) 1.13 ± 0.01
	Unknown (XII)	39.9	e) 1.0
	Unknown (XIII)	40.6	e) 1.0
	5-Carboxymethyl-hydroferulic acid (XIV)	41.3	c) 1.42
	5-(2,6-dicarboxy-4-oxo-hexane)-hydroferulic acid (XVIII)	56.2	e) 2.0
	MBB	58.8	d) 2.04 ± 0.09
	Lactone - XIX	60.0	e) 2.0
	Lactone - XX	61.1	e) 2.0
	Epoxy quinol - XXI	61.9	e) 2.0

[a]Calculated relative to n-octacosane under the specified conditions.
[b]Calculated relative to ethanol under the specified conditions.
[c]Estimated on an effective carbon number basis relative to vanillic acid.
[d]Calculated relative to vanillic acid under the specified conditions.
[e]Assumed response factor relative to vanillic acid.

NOTE: Error values (± standard deviation) are only shown for the experimentally determined response factors.

APPENDIX VIII

PRODUCT IDENTIFICATIONS

INTRODUCTION

This Appendix presents a detailed examination of the experimental evidence used to identify the acidic reaction products. The main technique used for the identifications was GC/MS analysis of the derivatized acidic product mixtures. Three different methods of derivatization were employed (see Experimental): (1) trimethylsilylation, (2) methylation, and (3) methylation followed by trimethylsilylation.

In the first method, the TMS derivatives of all hydroxyl and carboxylic acid functions of the products were formed. In the second method, only the carboxylic acid groups were methylated, leaving the hydroxyl groups underivatized. These free hydroxyl groups were converted to TMS ethers by the third method. Mass spectra of all of the products derivatized by the latter two methods were not obtainable. However, use of these three derivatization methods did greatly aid in the identification of many of the acidic products by GC/MS.

Preparative GLC was used to a limited extent to isolate small quantities of selected products for nuclear magnetic resonance (NMR) and infrared (IR) spectroscopic analyses.

PRODUCTS FOR WHICH KNOWNS WERE AVAILABLE

Some of the acidic products (I-V) were identified by comparing the mass spectra of their TMS derivatives with reference spectra of known compounds. The reference spectra are from the Wiley Library stored in the computer of the GC/MS system. Figures 71-75 (Appendix IX) present the comparisons of the mass spectra

of the products to the references. These products also showed the same relative GLC retention times as the known compounds (II not tested).

The relative GLC retention time and the mass spectrum of the TMS derivative of XI was identical to that of the known compound obtained by direct synthesis.

PRODUCTS FOR WHICH KNOWNS WERE NOT AVAILABLE

The structural assignment of many of the remaining acidic products are examined in this section. These identifications must be considered tentative since known compounds were unavailable, and complete spectral and chemical analyses were not performed. However, the structures proposed here are consistent with the spectral data obtained, and are analogous to products identified in other studies of oxidation of lignin models (see MBB Oxidation Products section).

The mass spectra of TMS derivatives contain certain common peaks which are useful for the interpretation (118). The m/e (mass to charge ratio) of the base peak of a silylated compound is usually 73 (TMS+). A relatively intense peak at m/e 147 indicates the compound contains more than one TMS ester and/or ether group (m/e 147, $(CH_3)_2$-Si=O-TMS+).

Identification of the molecular ion (M) is usually aided by the presence of a prominent M-15 ($\cdot CH_3$) peak. In addition, M-90 (HO-TMS), M-90-15, M-117 ($\cdot$COOTMS) and M-118 (HCOOTMS) are peaks commonly present which aid in the recognition of M.

Figures 54 and 55 show the mass spectra and fragmentation patterns for the TMS derivatives of VI and VII. Upon catalytic hydrogenation (see Experimental) VII was quantitatively converted to VI - an observation which is consistent with the assigned structures.

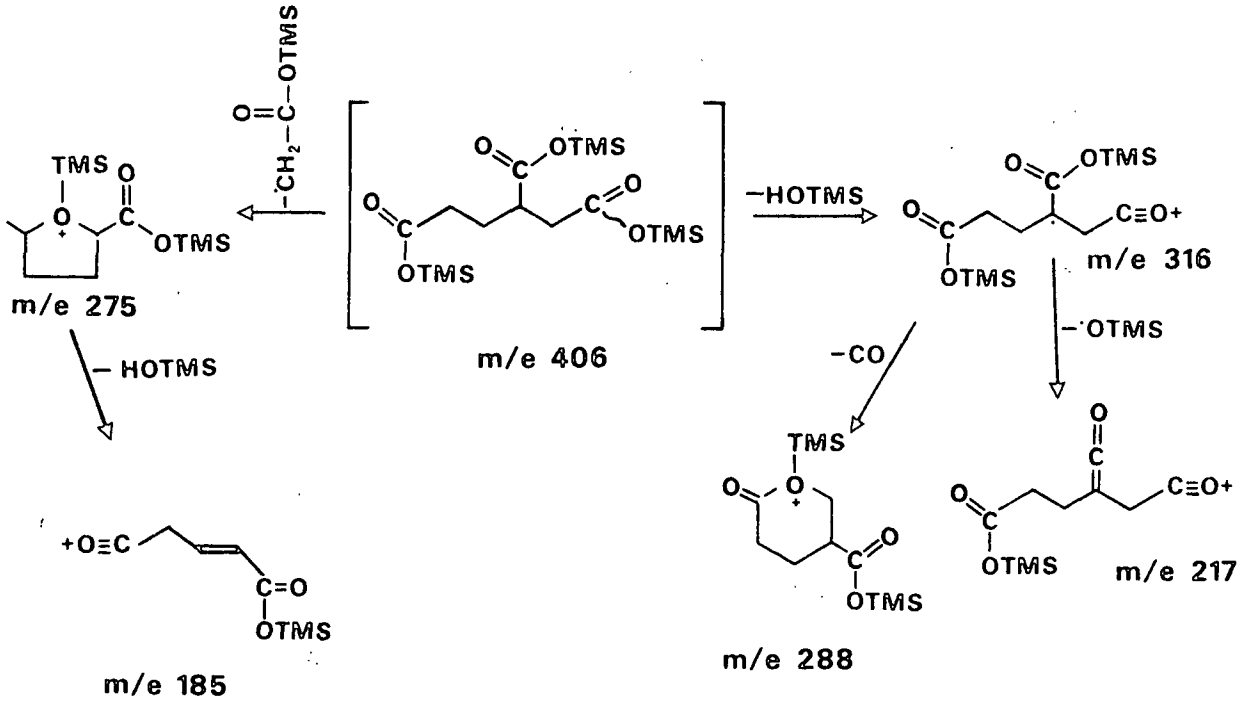

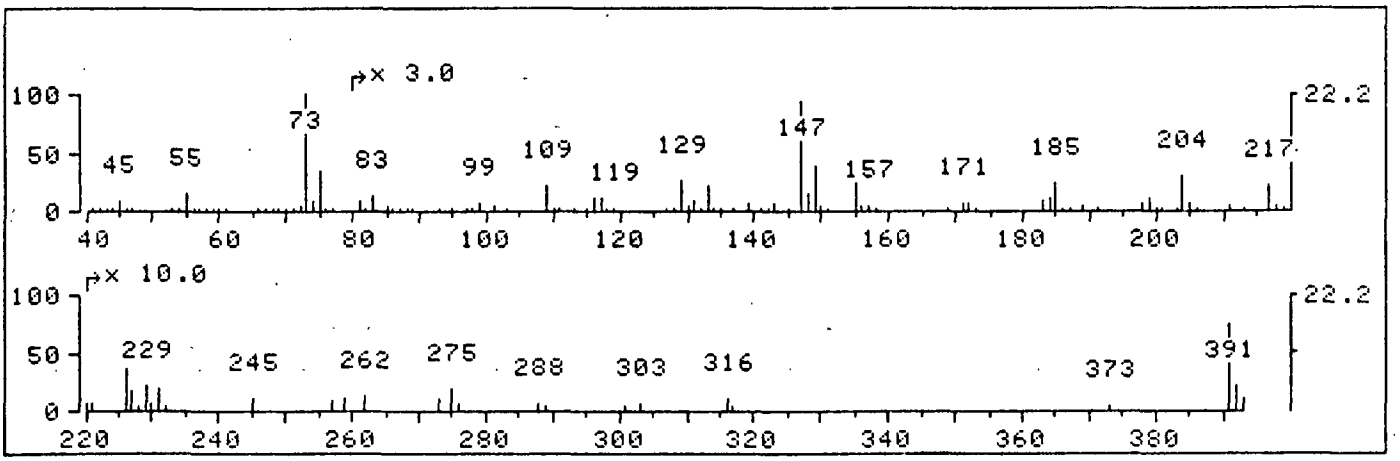

Figure 54. Mass spectrum and fragmentation pattern of the TMS derivative of VI.

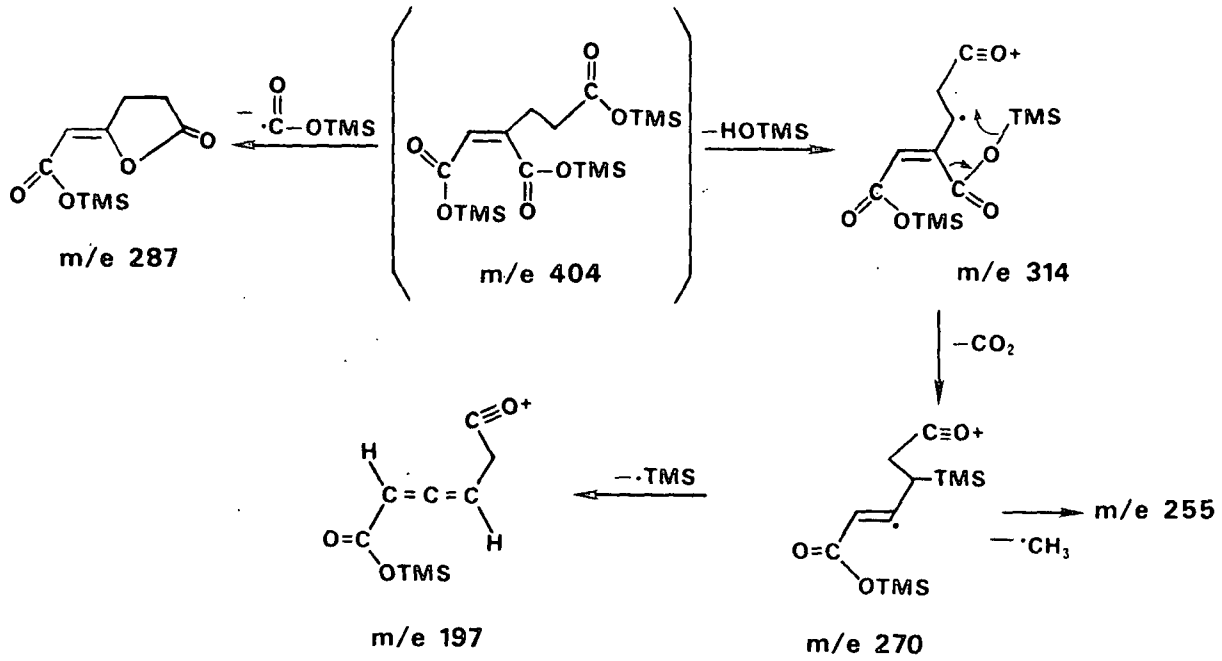

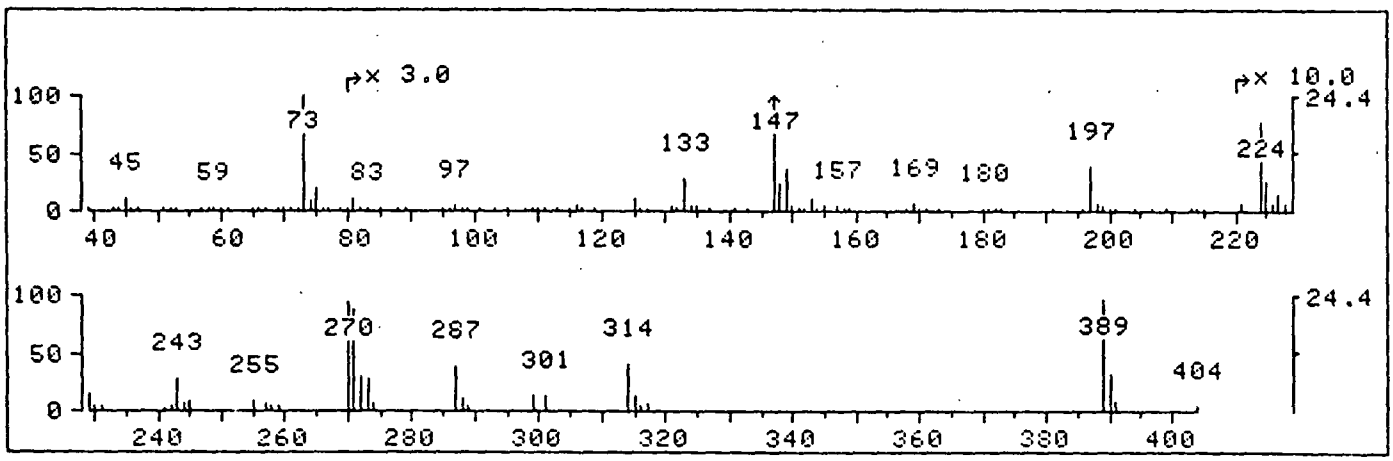

Figure 55. Mass spectrum and fragmentation pattern of the TMS derivative of VII.

Figure 56(a) depicts the mass spectrum and fragmentation pattern of the TMS derivative of VIII. The prominent molecular ion (m/e,%:328,13.2) is consistent with VIII being aromatic. The methylated derivative of VIII has a molecular weight of 212 [Fig. 56(b)] which indicates the compound contains two acid groups and no hydroxyls. The underivatized product was left unchanged after catalytic hydrogenation. The IR and ^{1}H-NMR spectra of the TMS derivative of VIII further supports the assigned structure. The IR spectrum (Fig. 57) showed a strong absorbance at 1692 cm^{-1} which is characteristic of the carbonyl stretch of the ring conjugated carboxyl group of 2-furoic acids (119). In the NMR spectrum (not shown) the ring protons gave singlet peaks at 7.6 and 7.2δ, and the methylene protons of the propanoic acid side chain produced a multiplet at 2.65δ (acetone-d_6 solvent).

The mass spectra and fragmentation patterns of the TMS derivatives of XIV and XVIII are shown in Fig. 58 and 59, respectively. The prominent molecular ions (m/e,%:470,13.9; 670,25.7) are consistent with these compounds containing an aromatic ring.

Figures 60 and 61 show the mass spectra and fragmentation patterns of the TMS and methyl/TMS derivatives of XIX. The IR spectrum of the TMS derivative of XIX showed two strong carbonyl stretching bands at 1710 cm^{-1} and 1742 cm^{-1} (Fig. 62). These bands are assigned to the TMS ester and the unsaturated γ-lactone carbonyls (120), respectively.

The mass spectrum and fragmentation pattern of the TMS derivative of XX is shown in Fig. 63(a). The methyl/TMS derivative of XX has a molecular weight of 536 [Fig. 63(b)] which is consistent with a structure containing three carboxylic acid groups and one hydroxyl group. The IR spectrum of the TMS derivative of XX (Fig. 64) showed a strong carbonyl stretching band at 1710 cm^{-1} (TMS ester

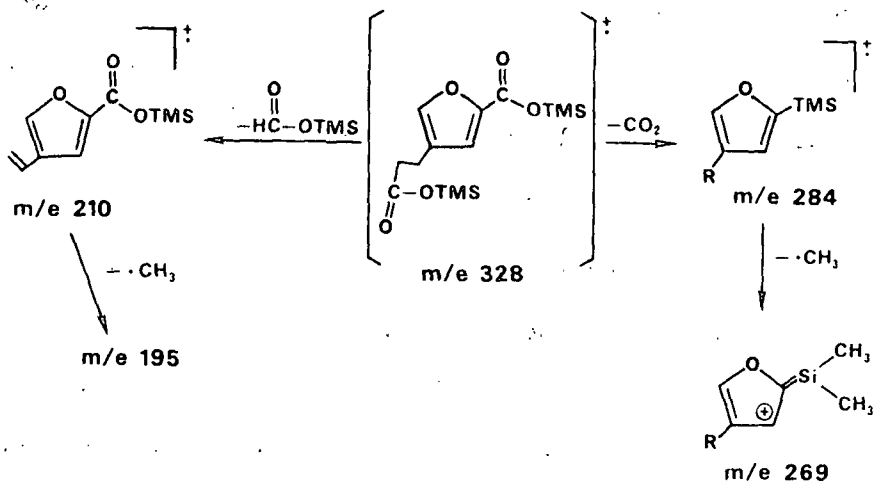

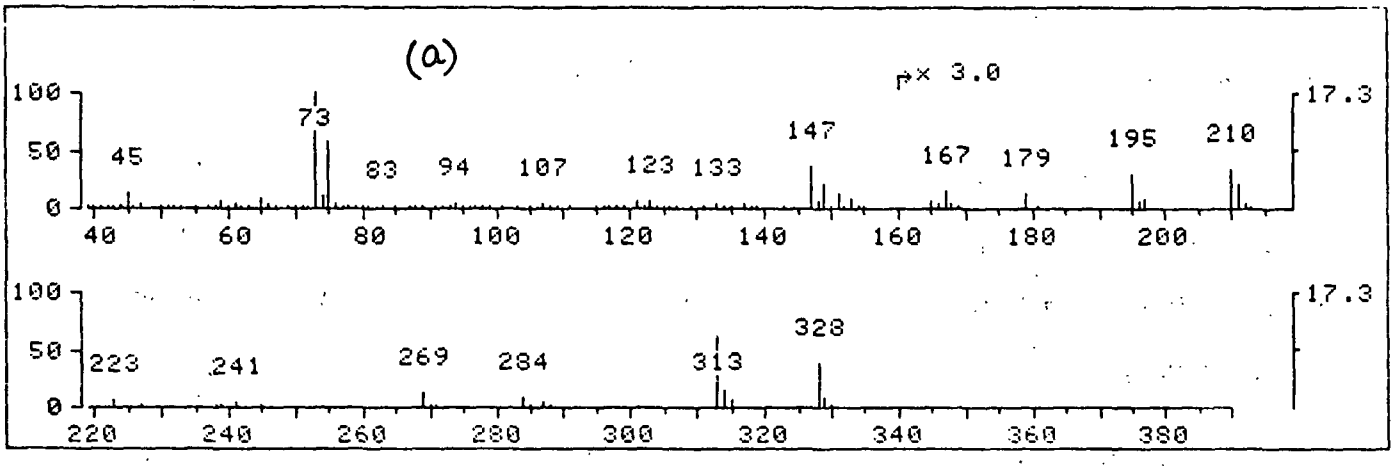

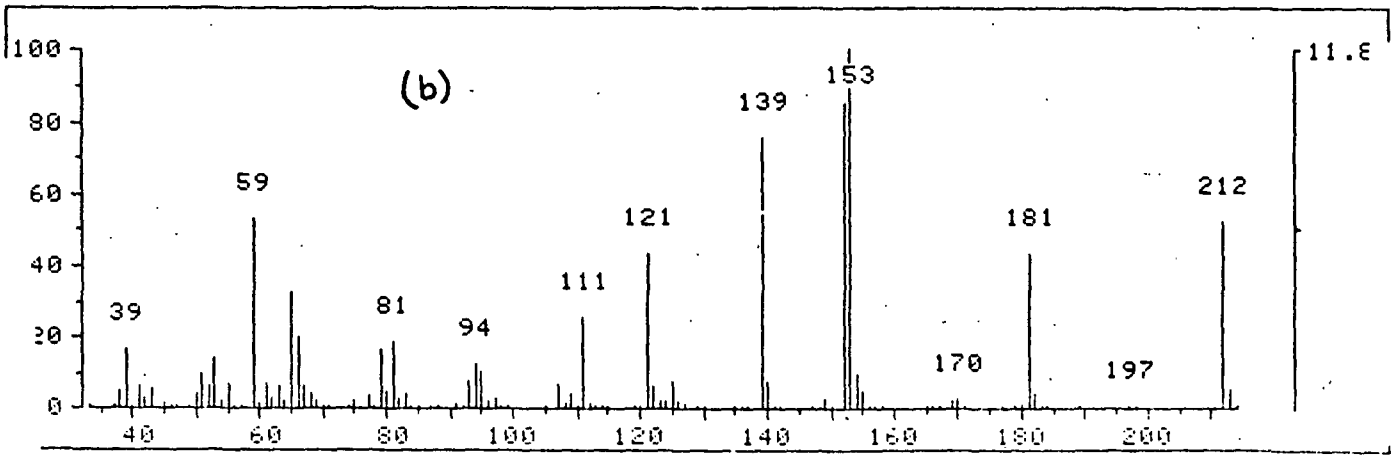

Figure 56. (a) Mass spectrum and fragmentation pattern of the TMS derivative of VIII. (b) Mass spectrum of methylated/silylated derivative of VIII.

groups). The shoulder seen on the higher frequency side of this peak is consistent with the presence of a lactone carbonyl.

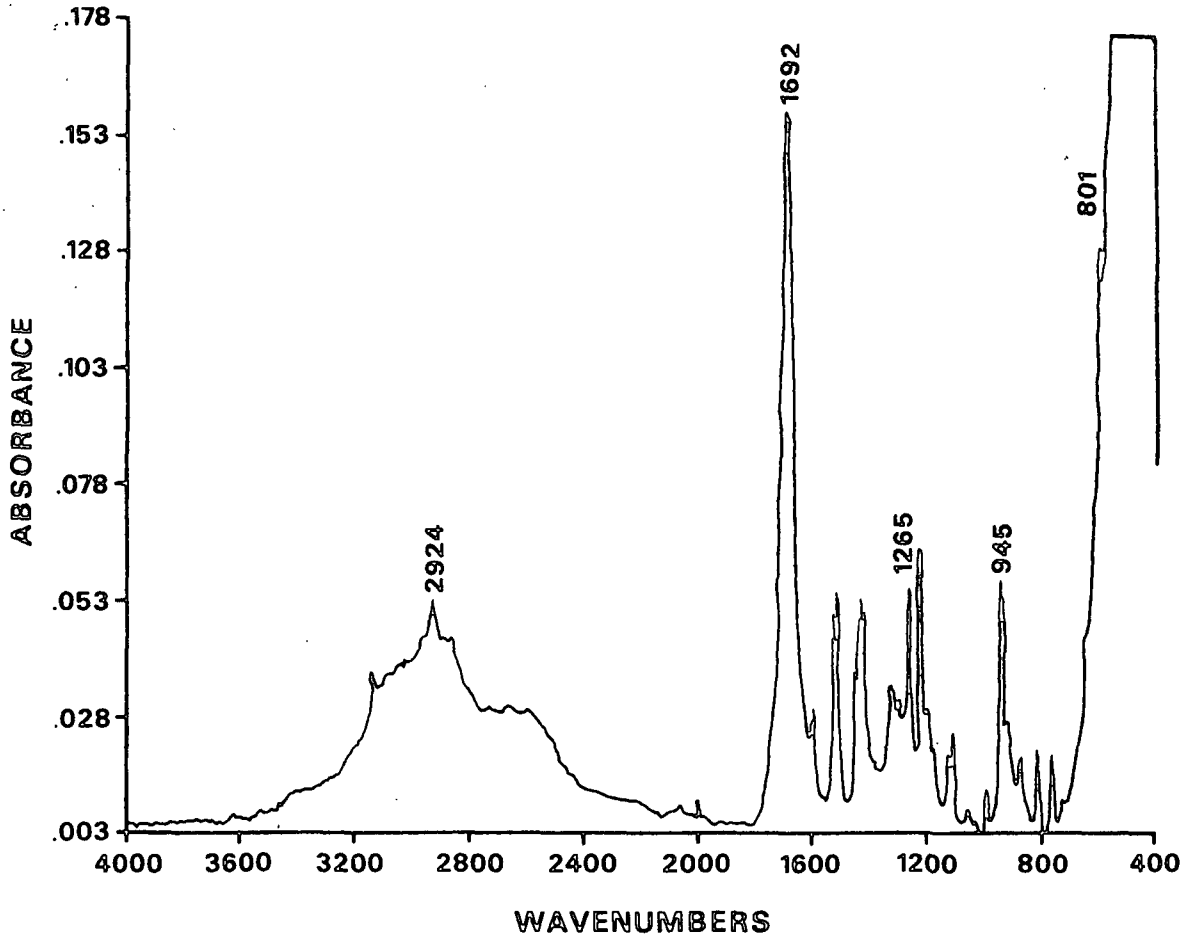

Figure 57. IR spectrum of TMS derivative of VIII isolated by prep-GLC.

Figure 65 shows the mass spectrum and fragmentation pattern of the TMS derivative of XXI. The M-90 and M-90-15 peaks help establish m/e 724 as the molecular ion. Interestingly, the spectrum does not contain a peak for M-15 (loss of $\cdot CH_3$). Loss of H-O-TMS (M-90) must lead to a very stable structure since this step occurs before the facile loss of $\cdot CH_3$. The structure shown in Fig. 65 for M-90 (m/e 634) shows that increased resonance is gained through extension of the unsaturated α,β-carbonyl system.

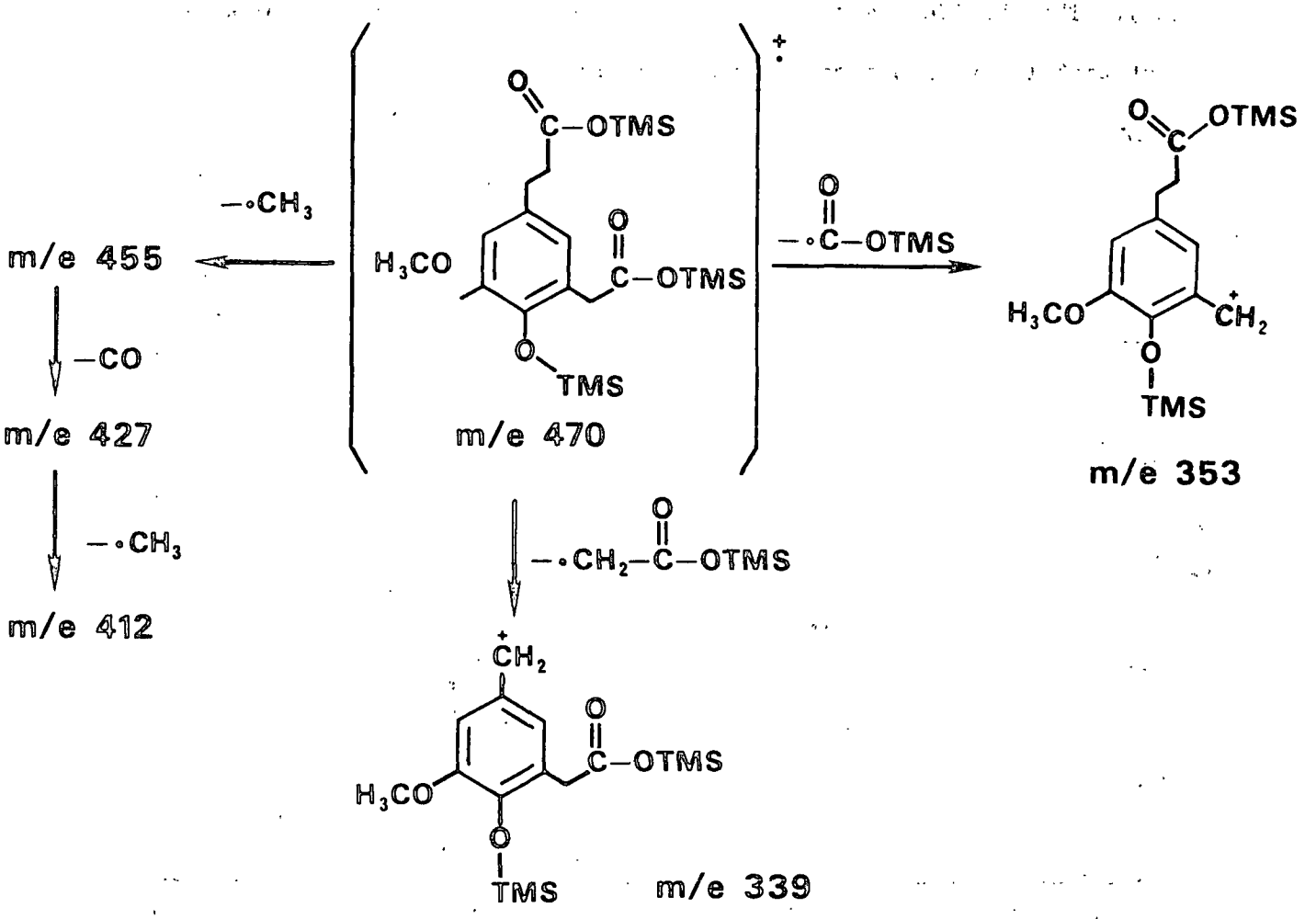

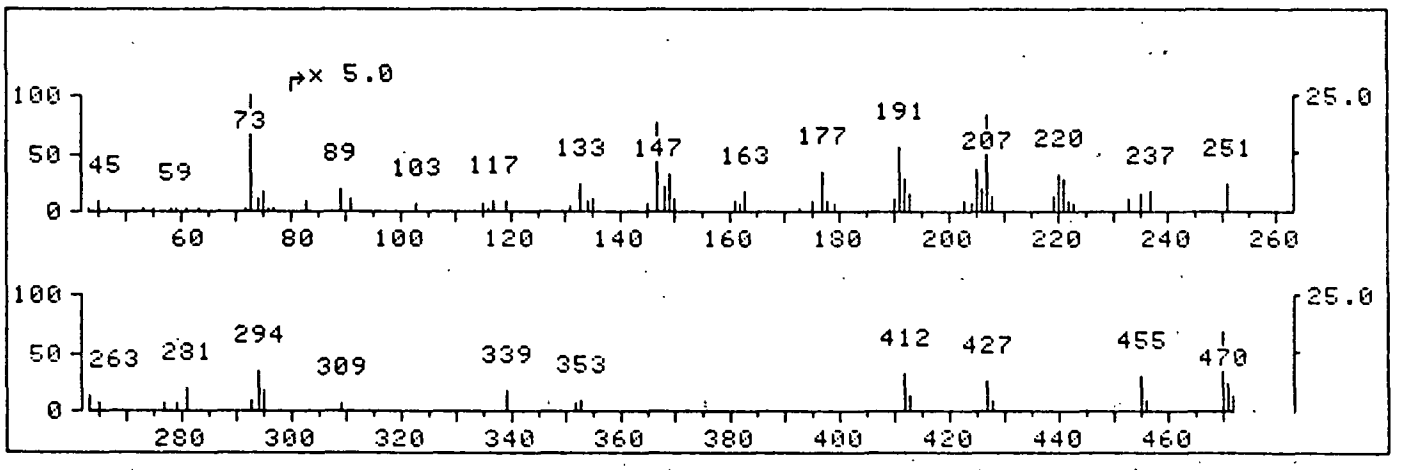

Figure 58. Mass spectrum and fragmentation pattern of the TMS derivative of XIV.

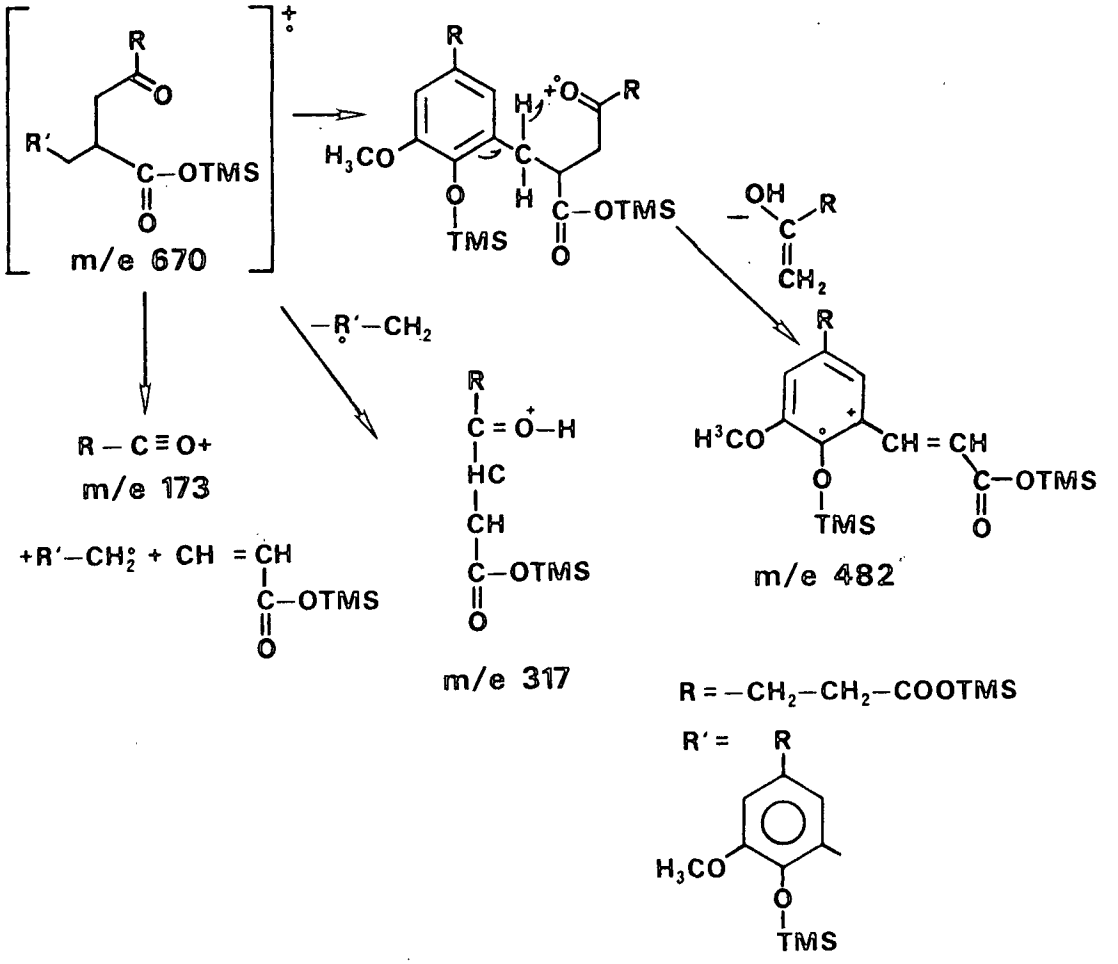

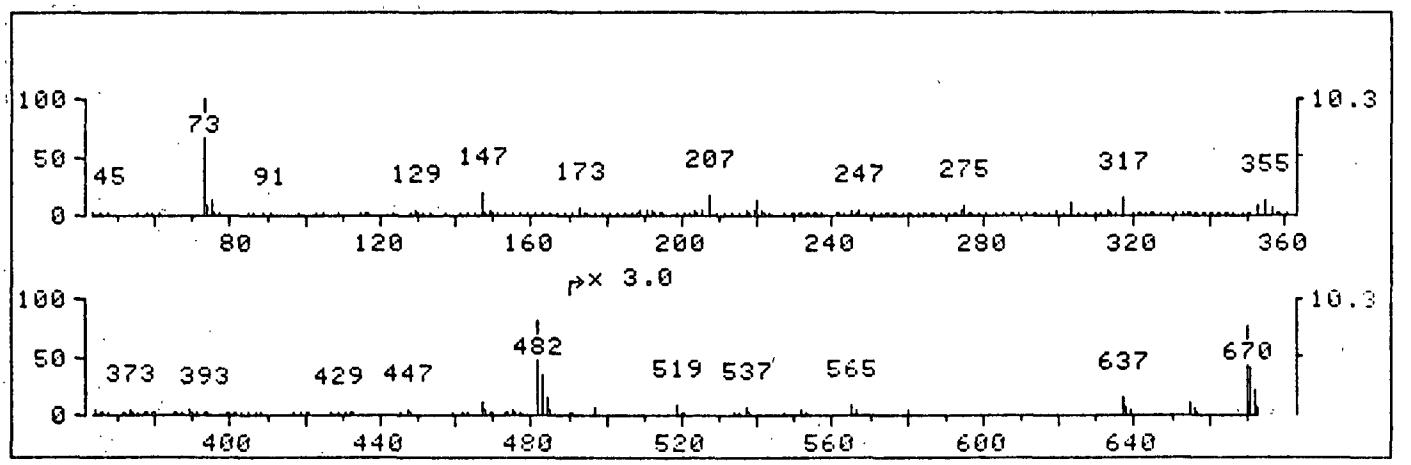

Figure 59. Mass spectrum and fragmentation pattern of the TMS derivative of XVIII.

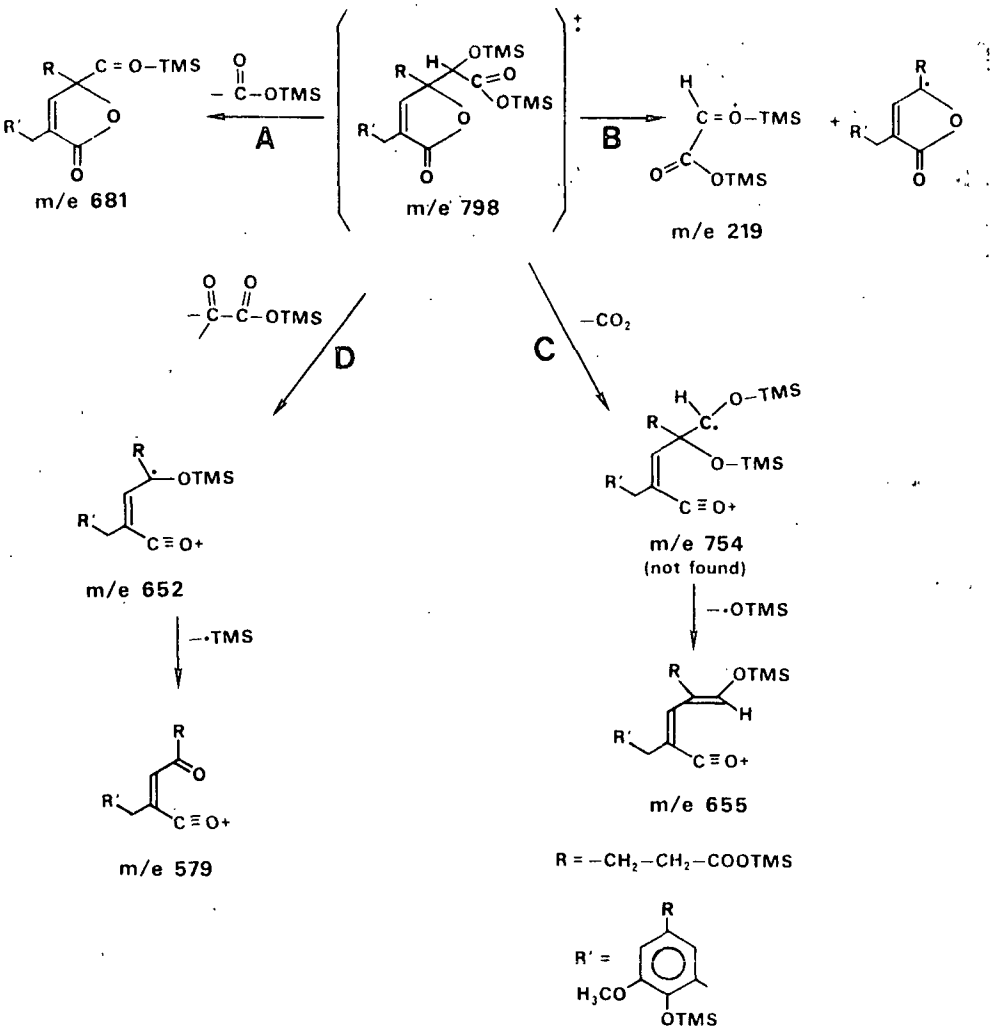

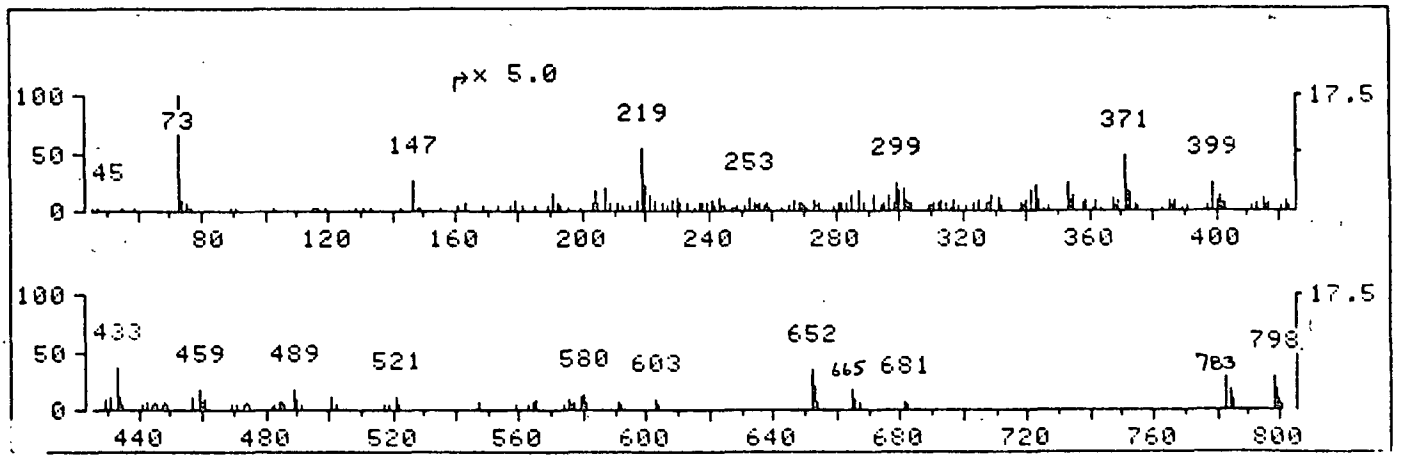

Figure 60. Mass spectrum and fragmentation pattern of the TMS derivative of XIX.

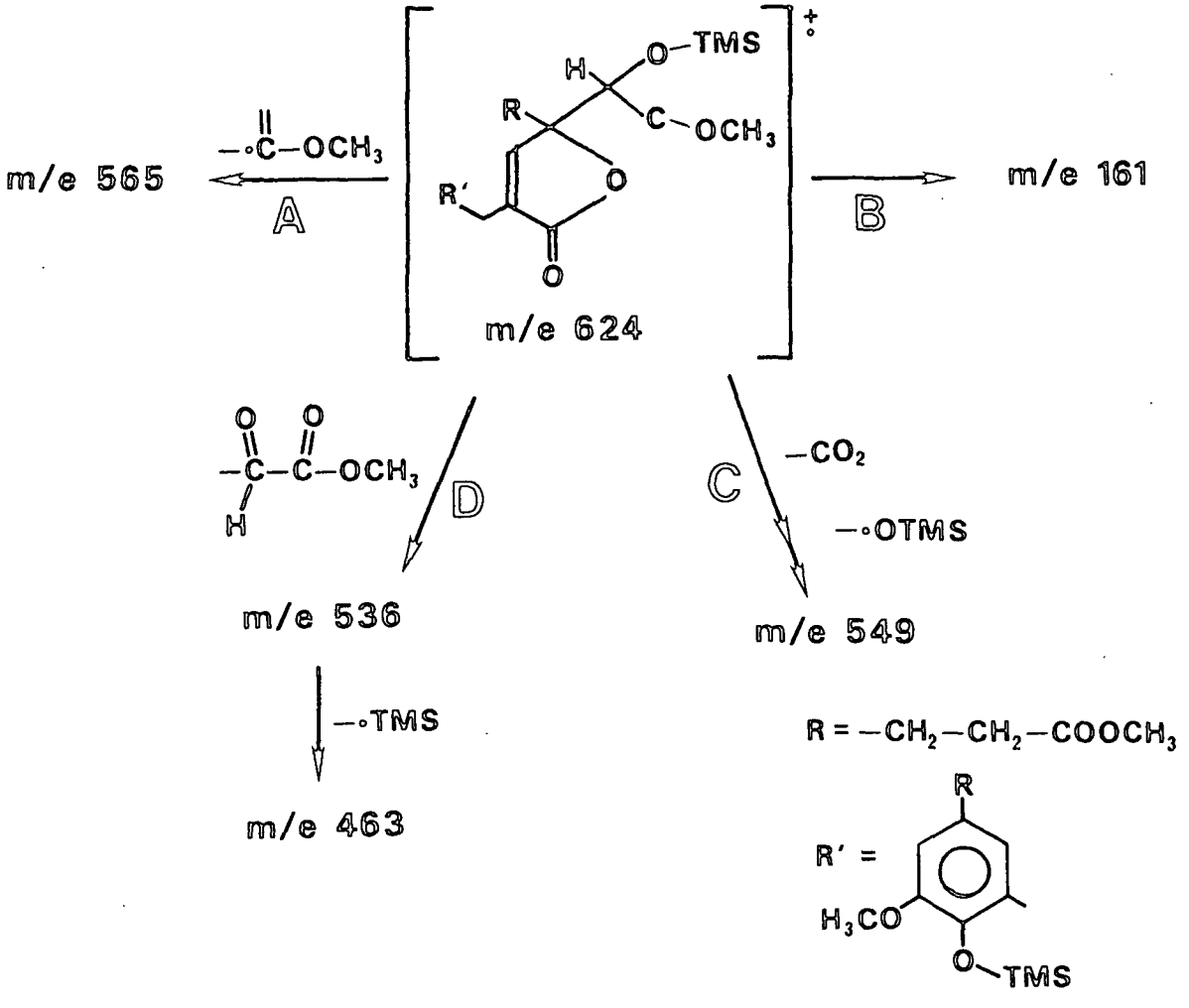

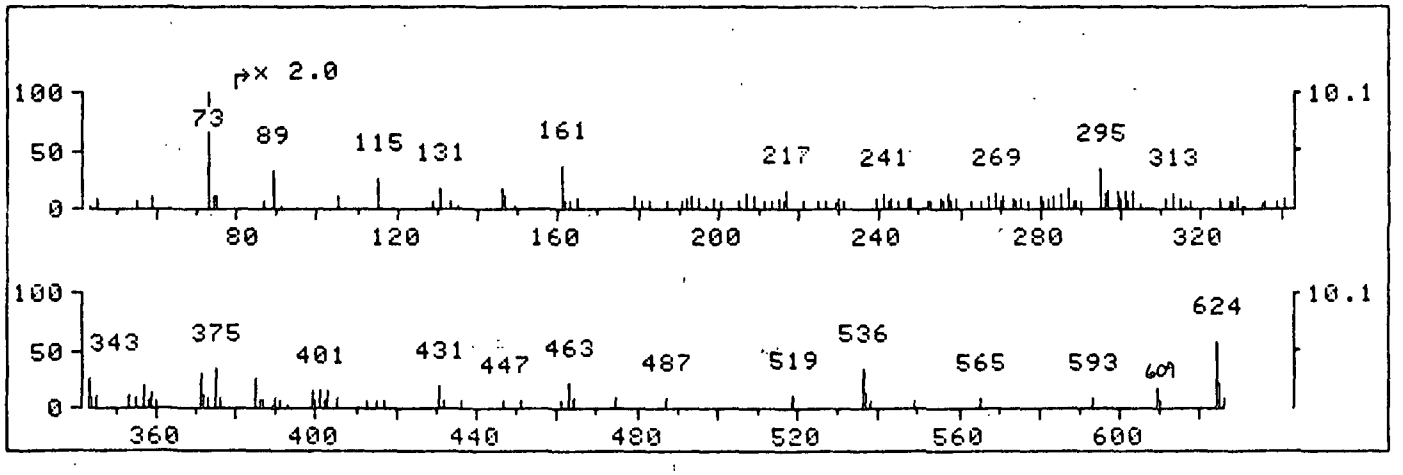

Figure 61. Mass spectrum and fragmentation pattern of the methylated/silylated derivative of XIX. The letters (A-D) refer to the pathways depicted in Fig. 60.

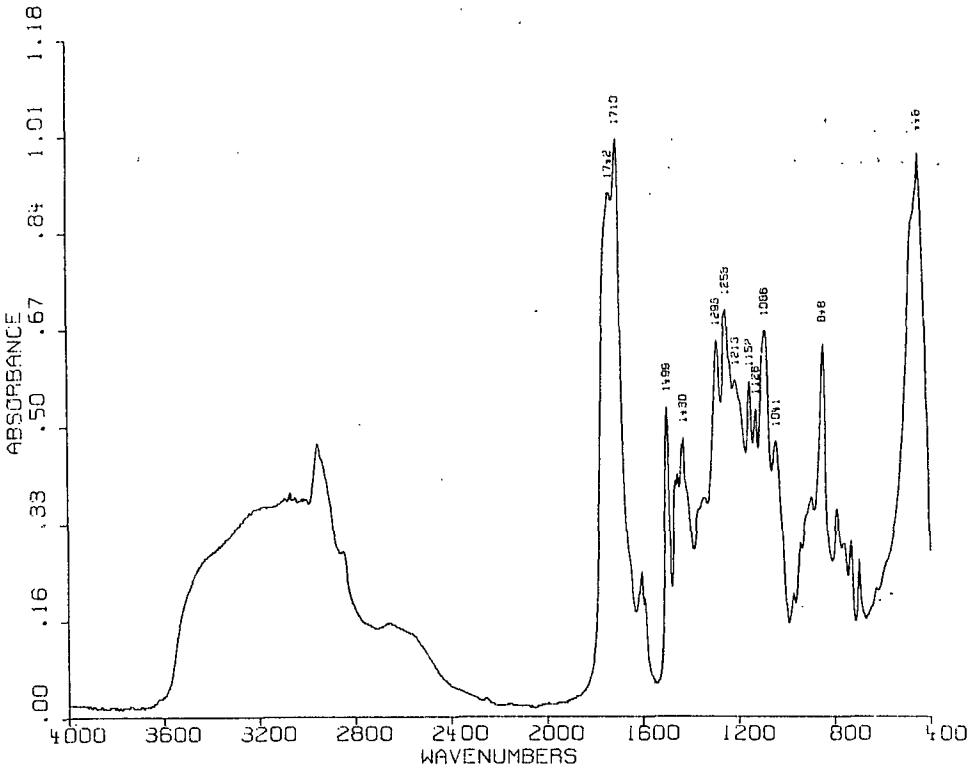

Figure 62. IR spectrum of TMS derivative of XIX isolated by prep-GLC.

UNIDENTIFIED PRODUCTS

The remaining products (IX, X, XII, XIII, and XV) could not be identified based on their mass spectra. Since they were present in such low concentrations, only mass spectral data of their TMS derivatives were obtainable, and their structures were not pursued. These unidentified products however only represented (in total) a maximum of ca. 8% of the reacted MBB in any one reaction (Table 12). Figures 66 and 67 show the mass spectra of the TMS derivatives of IX/X and XII/XIII, respectively. The only useful conclusion that can be drawn from a study of the spectra is that IX and X (TMS) appear to be isomers with a molecular weight of 522.

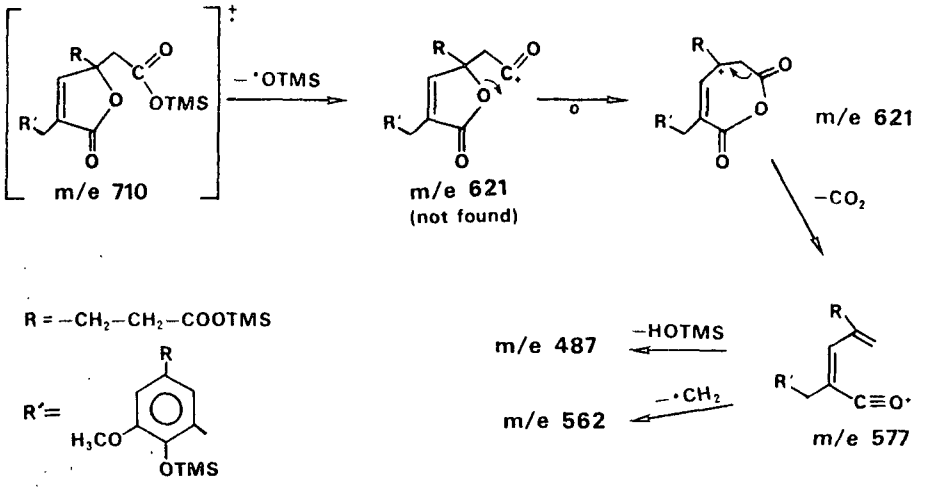

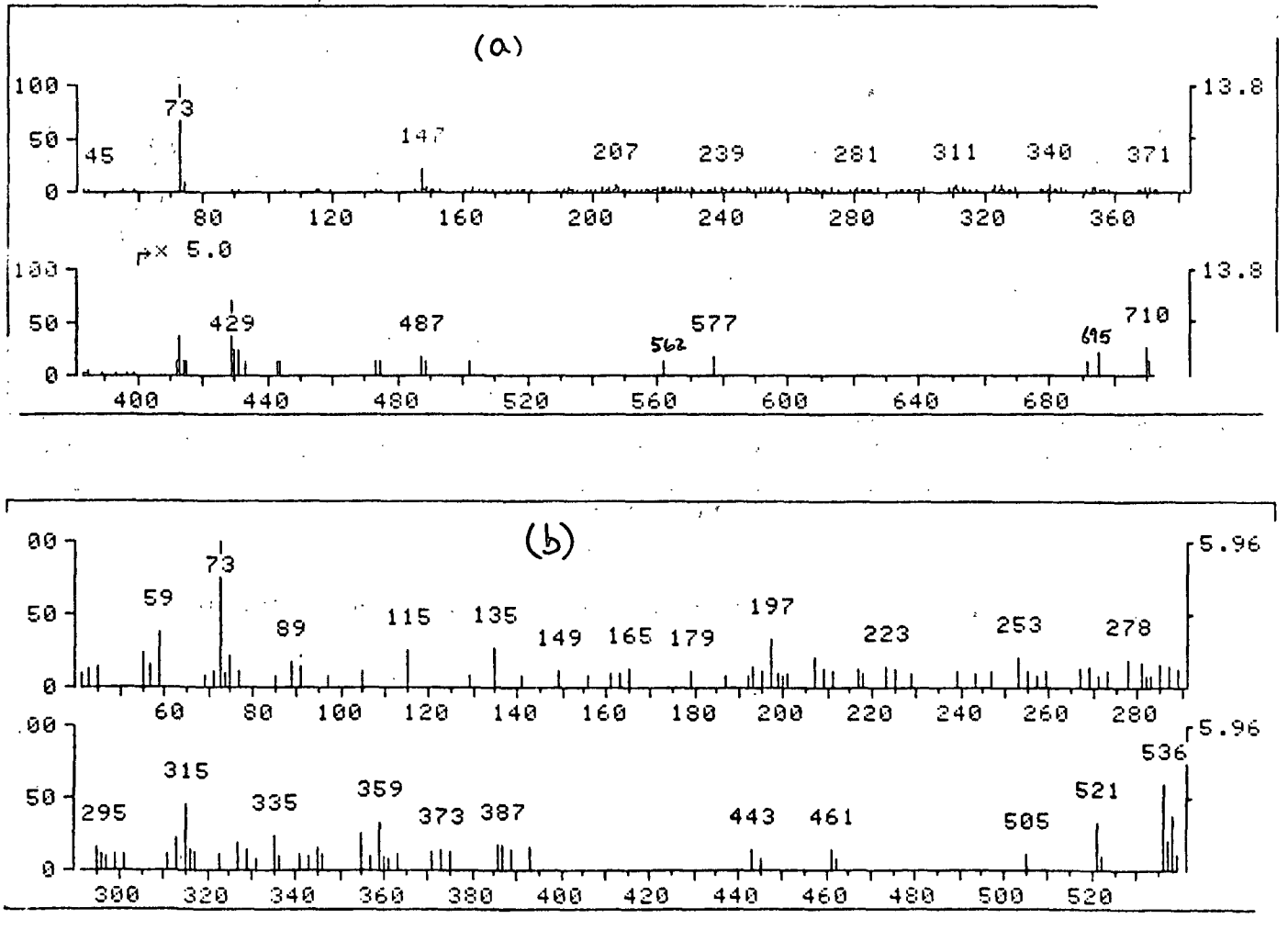

Figure 63. (a) Mass spectrum and fragmentation pattern of the TMS derivative of XX. (b) Mass spectrum of methylated/ silylated derivative of XX.

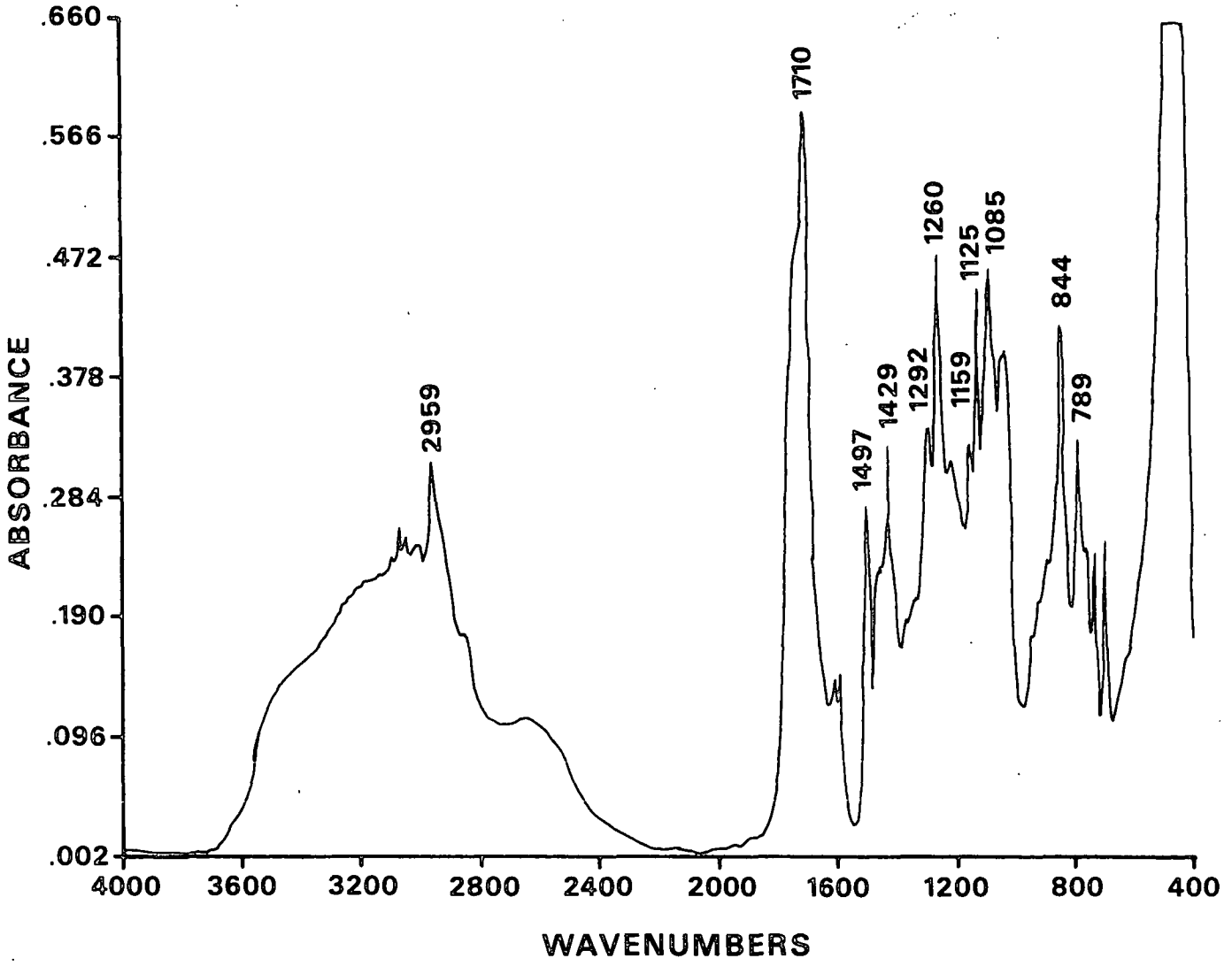

Figure 64. IR spectrum of TMS derivative of XX isolated by prep-GLC.

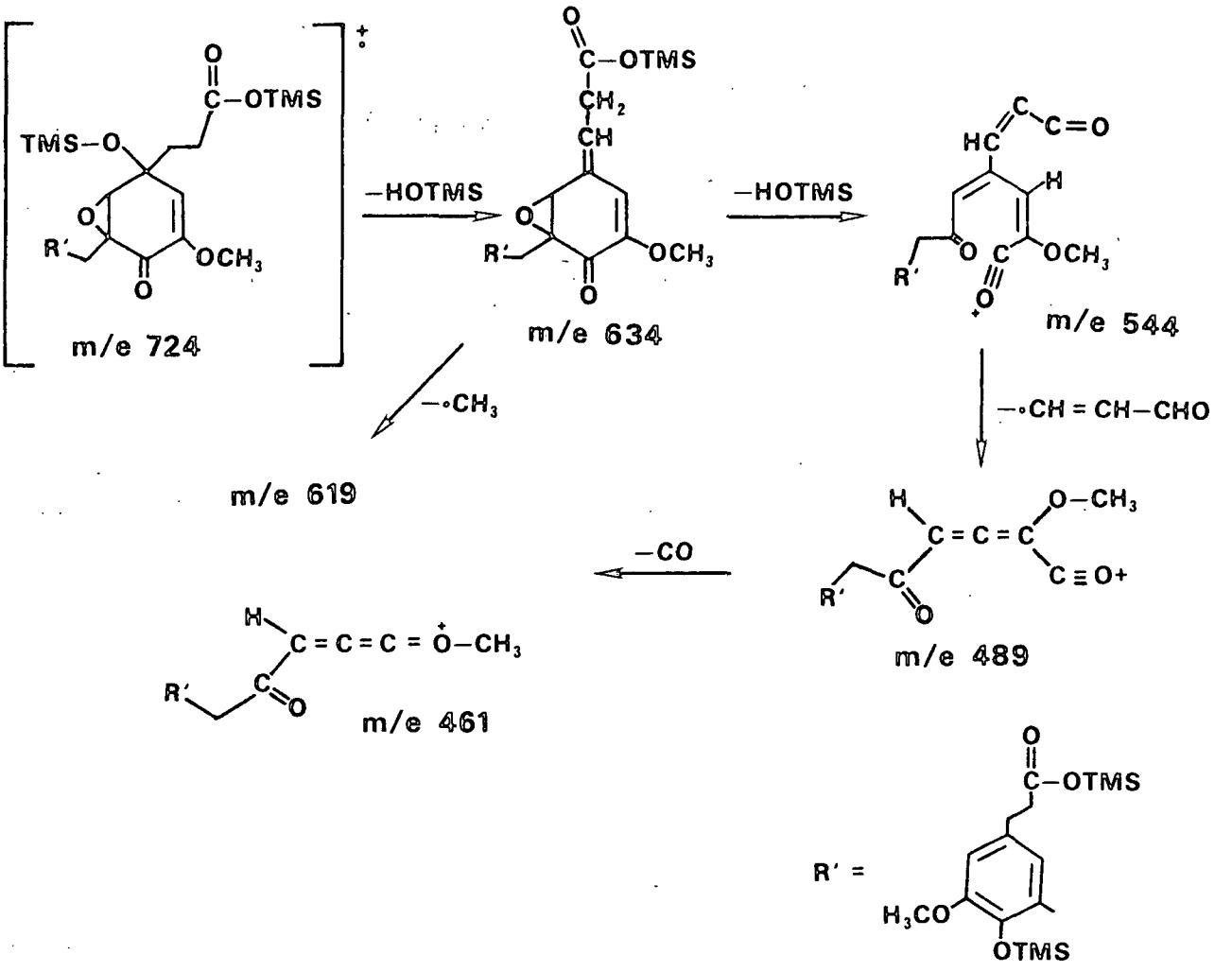

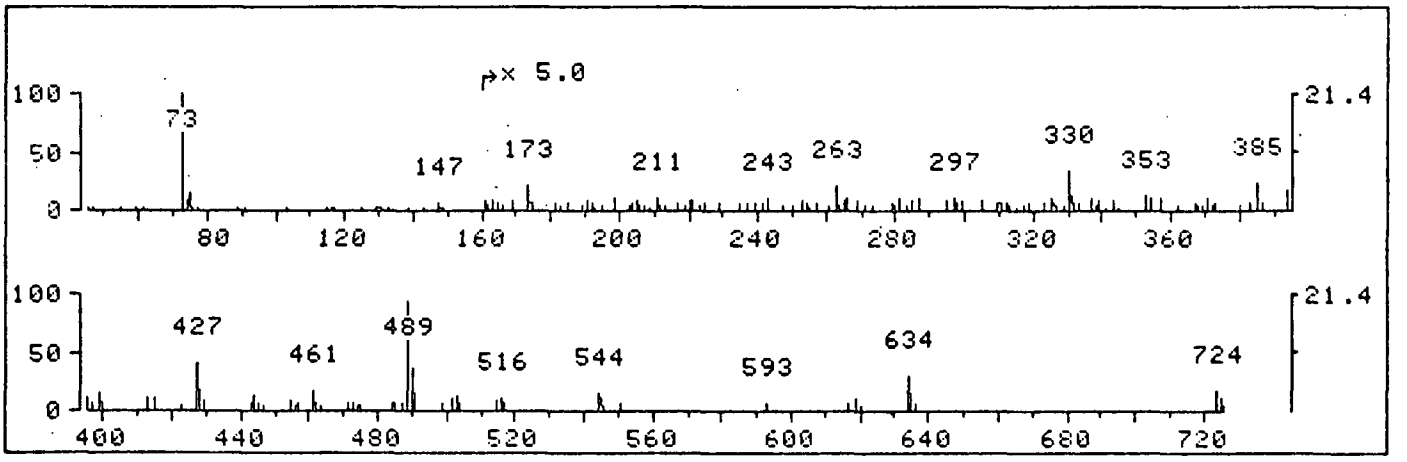

Figure 65. Mass spectrum and fragmentation pattern of the TMS derivative of XXI.

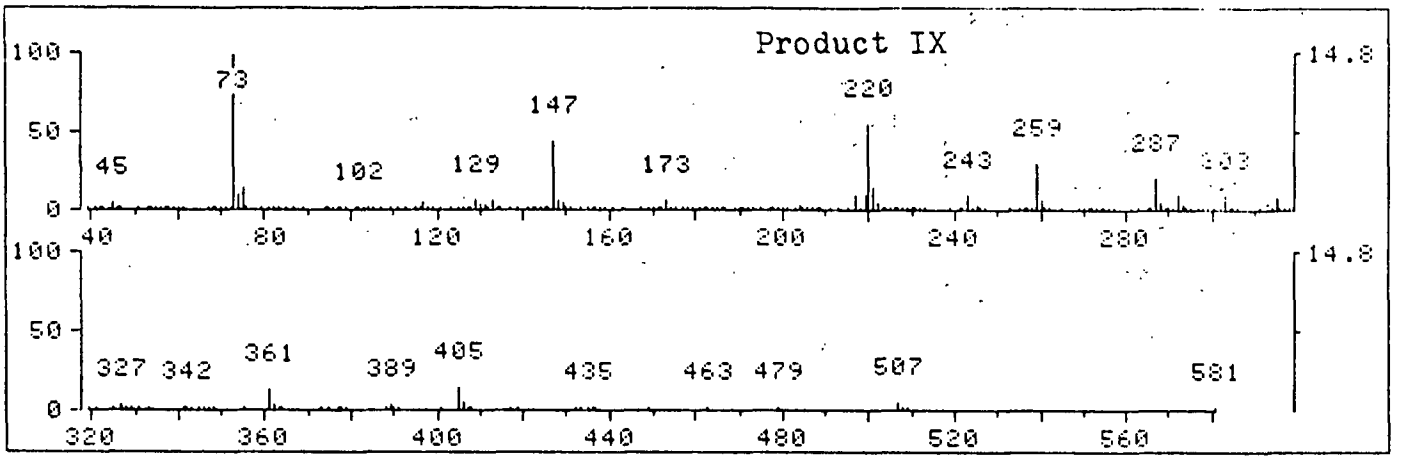

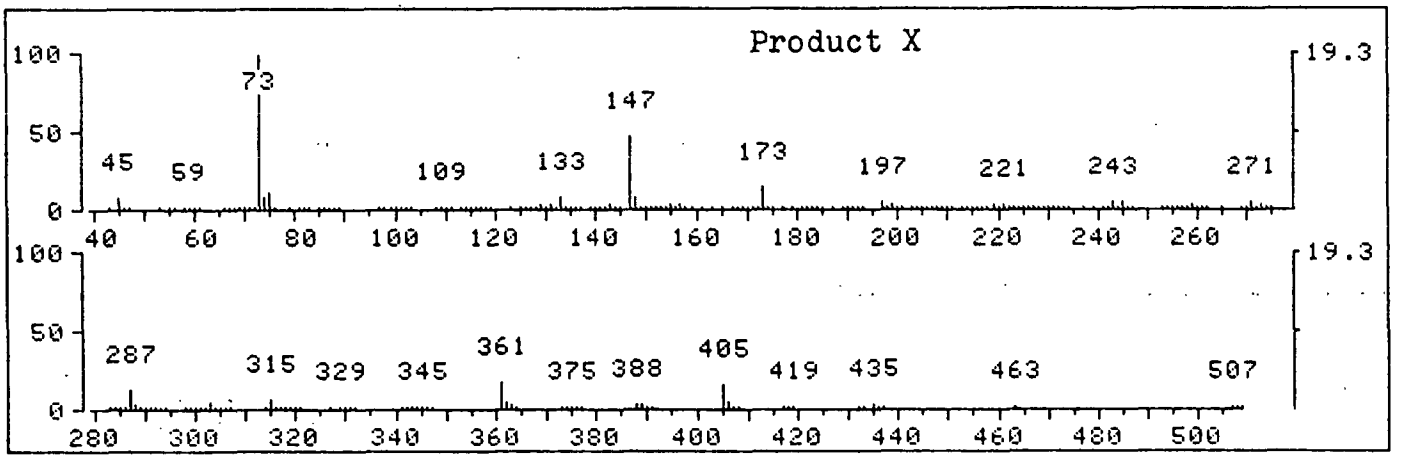

Figure 66. Mass spectra of the TMS derivatives of IX and X.

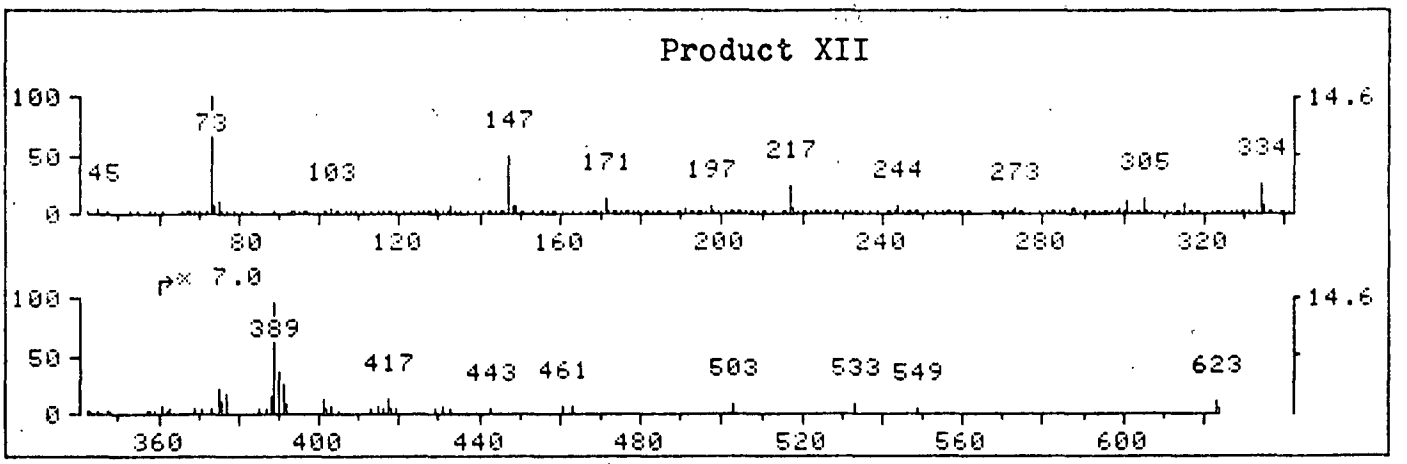

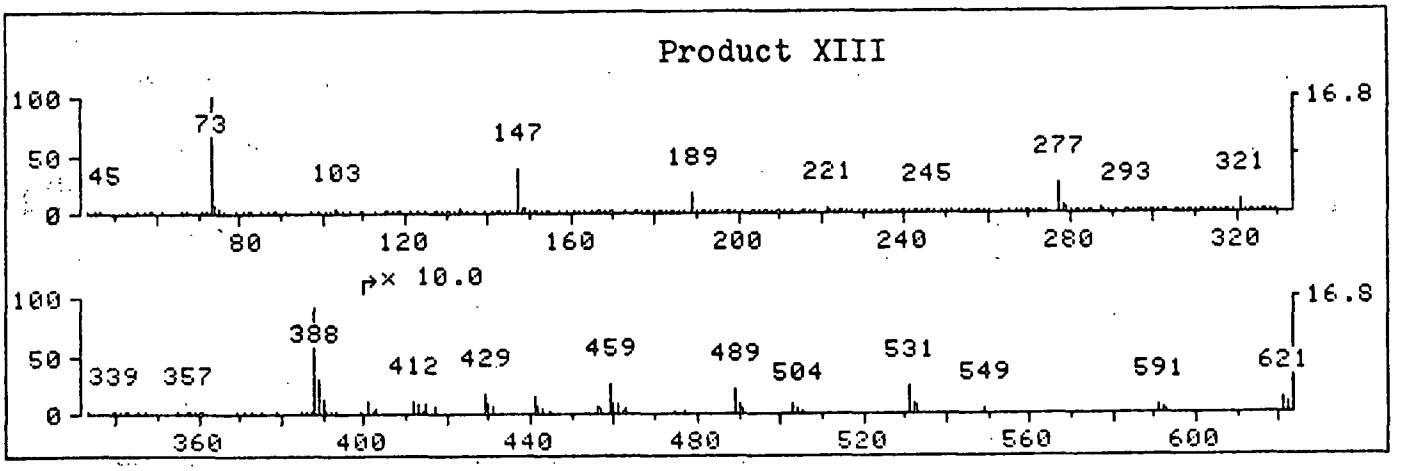

Figure 67. Mass spectra of the TMS derivatives of XII and XIII.

APPENDIX IX

GAS CHROMATOGRAPHIC-MASS SPECTRAL ANALYSIS

The operating conditions for the Hewlett-Packard 5985 GC/MS System are given in Table 33. The GLC conditions were previously described (conditions C, Appendix VII).

Table 33. Mass spectrometer operating conditions.

Jet separator temperature:	275°C
GC transfer line probe:	275°C
Ion source temperature:	200°C
Electron multiplier voltage:	1600-2200 V
Ionizing voltage:	70 eV
Vacuum:	3 x 10E-6 torr
Mass scan range:	33-900

The mass spectral data for the trimethylsilyl derivatives of the synthesized compounds are presented in Fig. 68-70. Figures 71-75 show the comparisons of the mass spectra of I-V with their respective references for the Wiley Library.

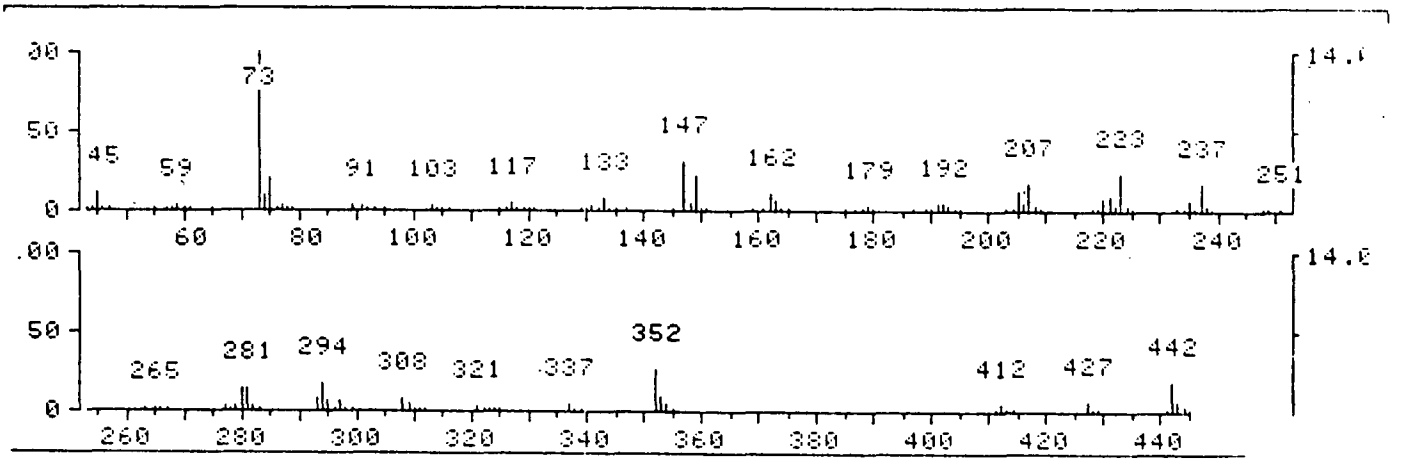

Figure 68. Mass spectrum of TMS derivative of 5-hydroxymethyl-hydroferulic acid (XI).

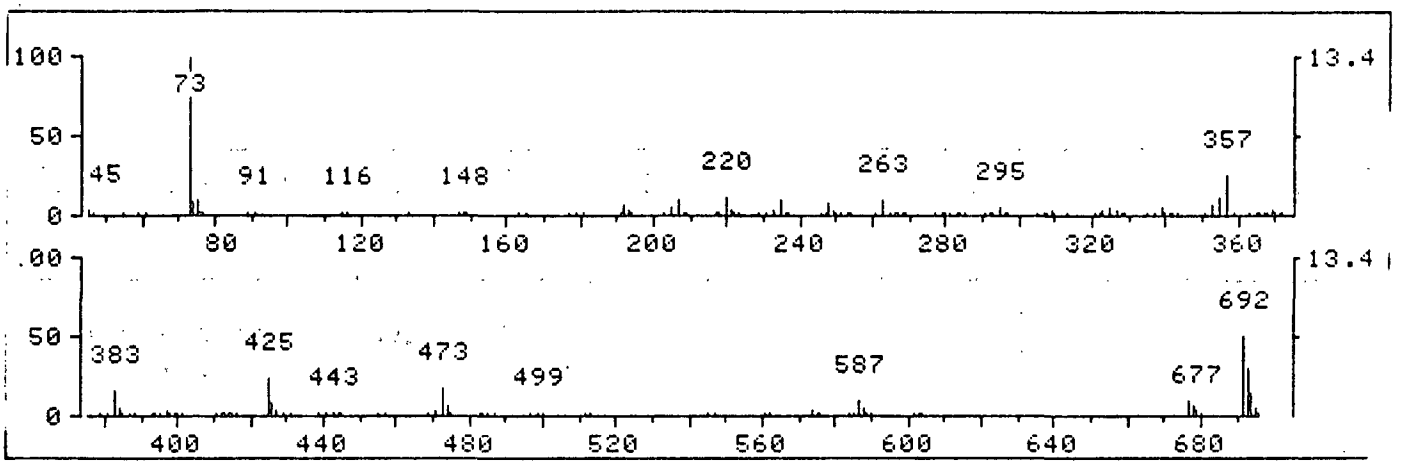

Figure 69. Mass spectrum of TMS derivative of MBB.

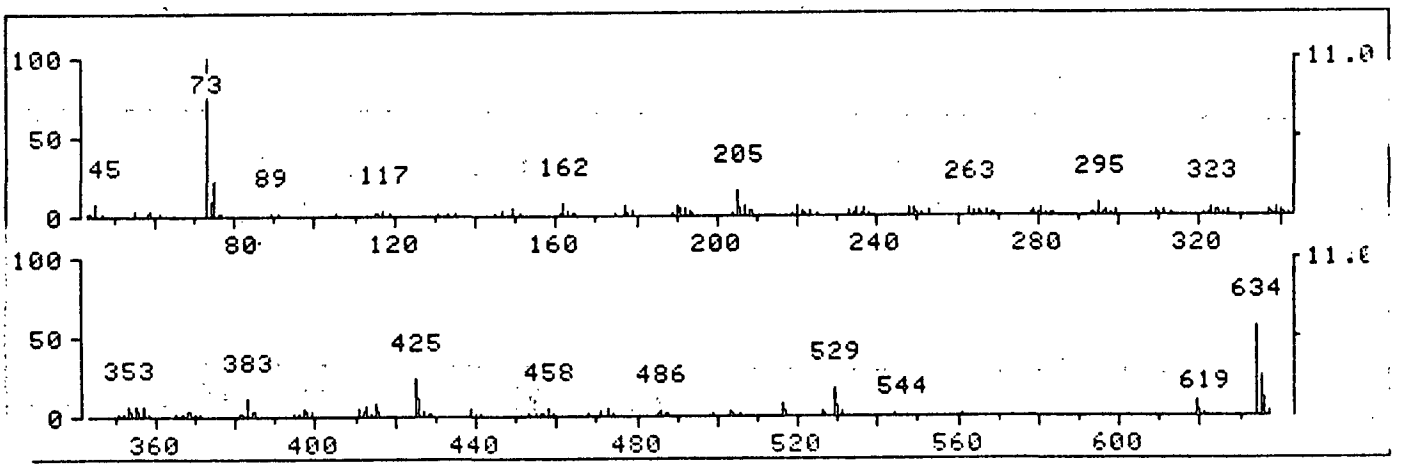

Figure 70. Mass spectrum of TMS derivative of the monomethyl ether of MBB.

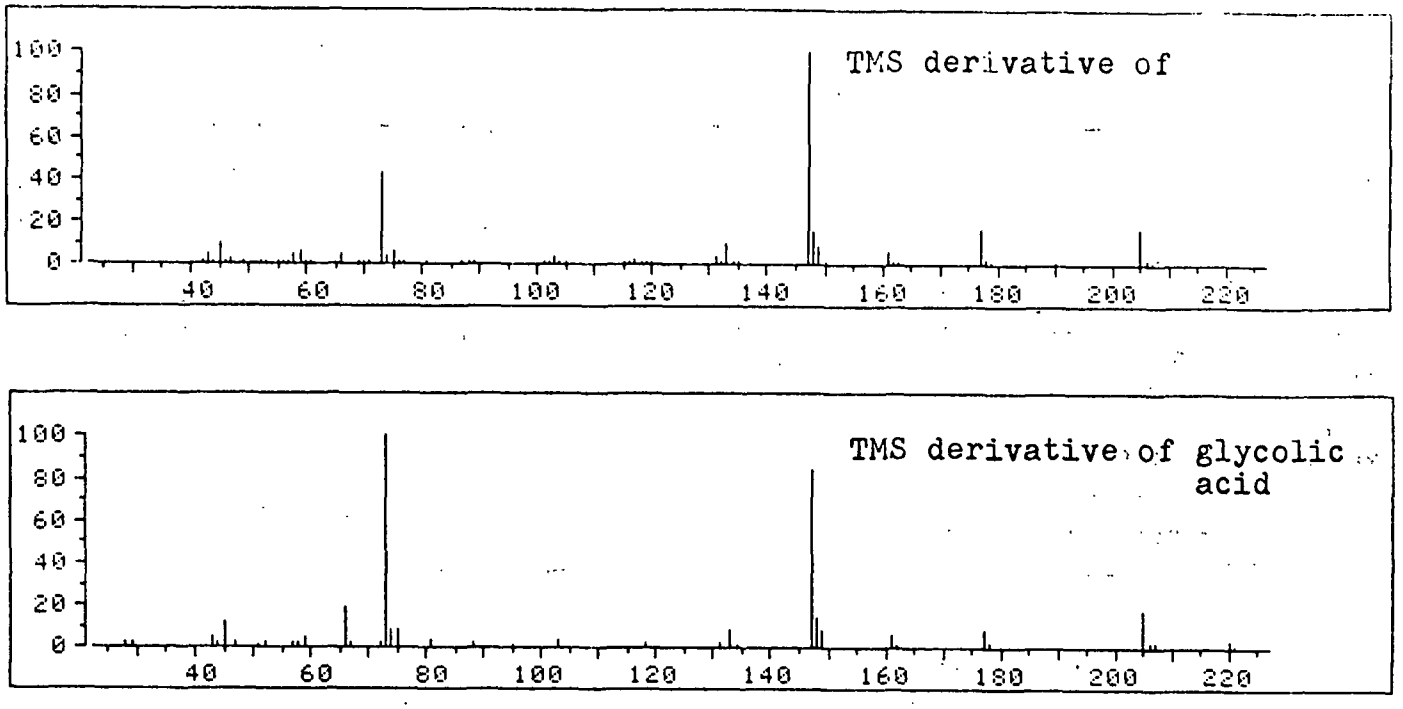

Figure 71. Comparison of mass spectra of TMS derivatives of I and glycolic acid.

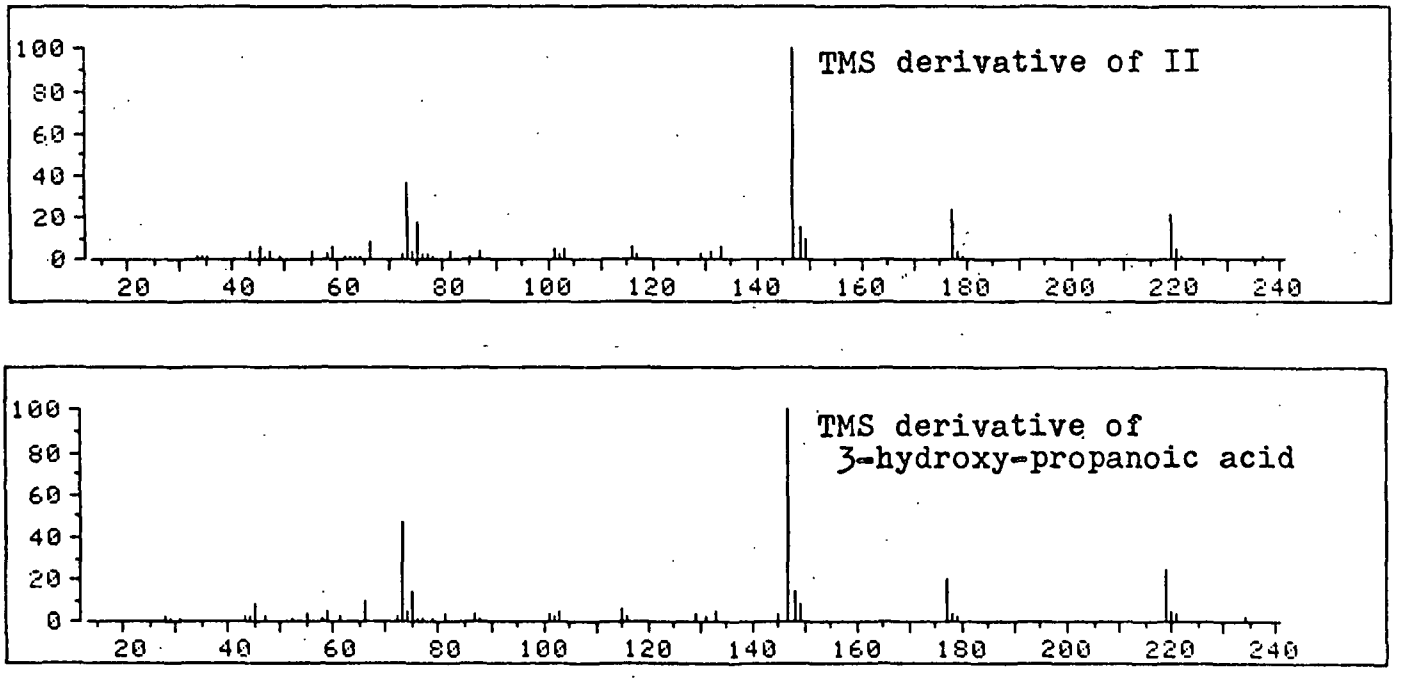

Figure 72. Comparison of mass spectra of TMS derivatives of II and 3-hydroxy-propanoic acid.

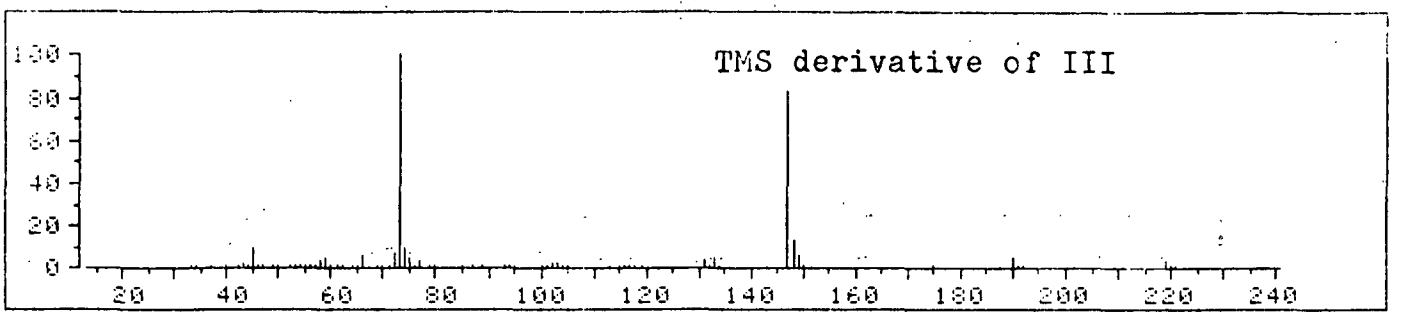

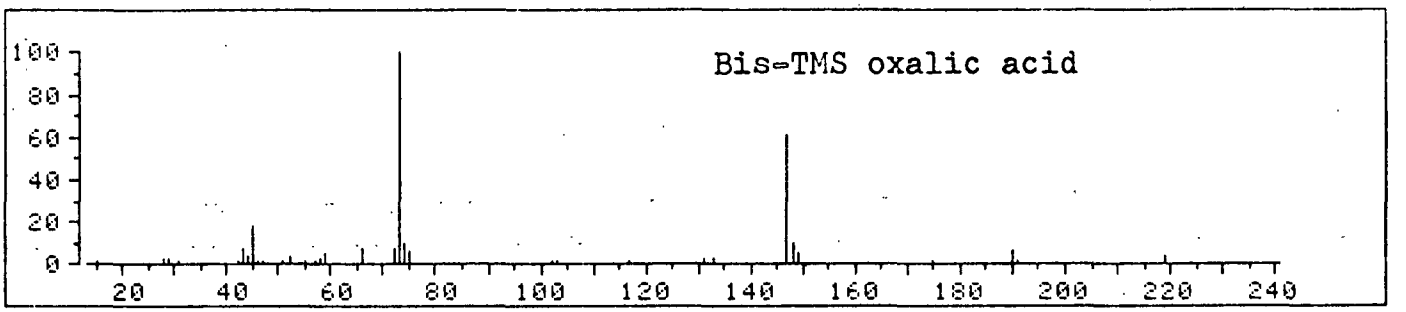

Figure 73. Comparison of mass spectra of TMS derivatives of III and oxalic acid.

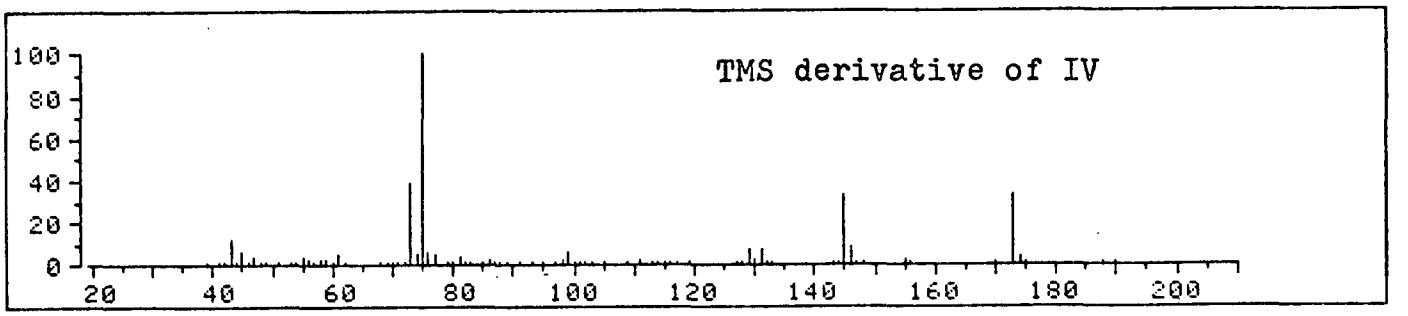

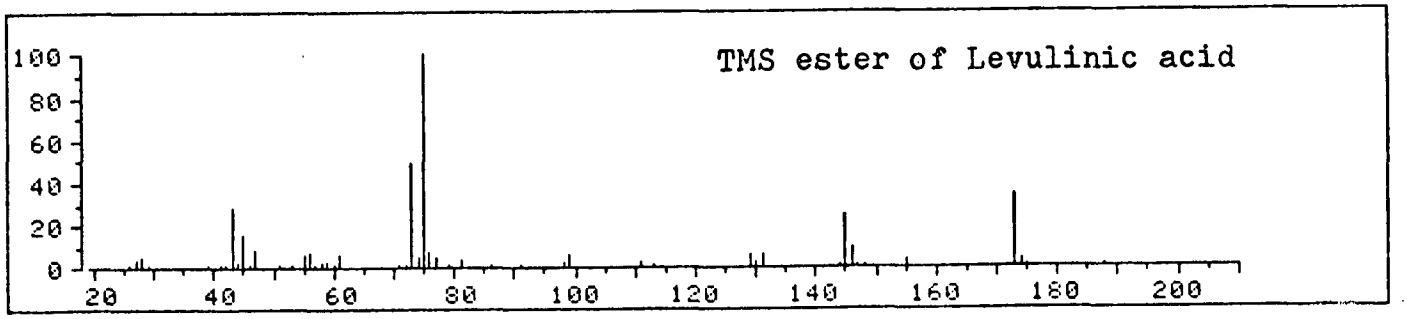

Figure 74. Comparison of mass spectra of TMS derivatives of IV and levulinic acid.

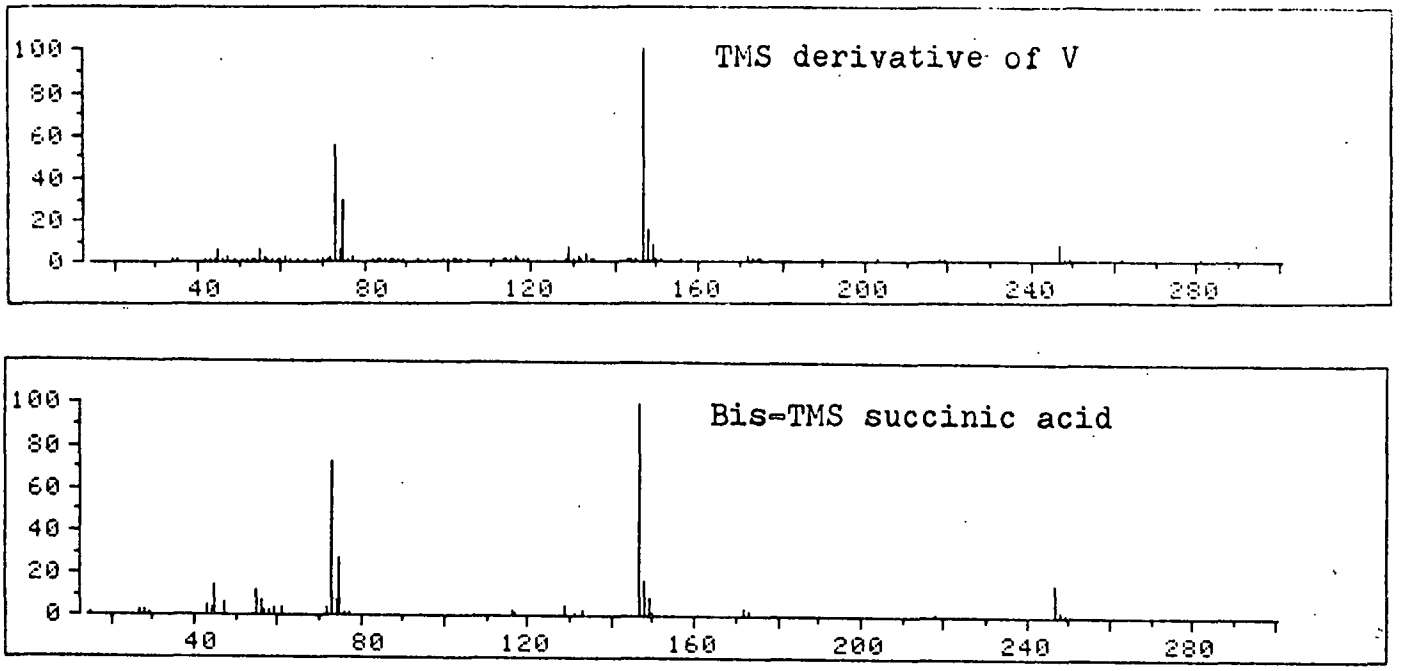

Figure 75. Comparison of mass spectra of TMS derivatives of V and succinic acid.

APPENDIX X

DETERMINATION OF PK_a's OF THE PHENOLIC HYDROXYLS OF MBB

The pK_a's of the phenolic hydroxyls of MBB were determined by UV spectroscopy. The method is given in detail by Albert and Serjeant (121) and is briefly discussed below.

The calculation for pK_1 is based on the following equations:

$$pK_1 = pH + \log [(A - A_1)/(A_o - A)] \quad (50)$$

where

A = absorbance of sample

A_1 = absorbance of monoanion

A_o = absorbance of unionized form

Rearrangement of Eq. (50) gives:

$$A = A_1 - (1/K_1)(A - A_o)[H+] \quad (51)$$

Similarly, pK_2 is calculated from:

$$pK_2 = pH + \log [(A - A_2)/(A_1 - A)] \quad (52)$$

where

A_2 = absorbance of di-anion

Rearrangement of Eq. (52) gives:

$$A = A_2 - (a/K_2)(A - A_1)[H+] \quad (53)$$

A regression analysis of the data in Table 34 using Eq. (50) gave values for A_1 (intercept) and pK_1 (slope). (The value for A_o was determined at pH 2.4 to be 0.027 at 296 nm.) In a similar manner pK_a was calculated from the data in Table 35 and Eq. (53) (with the value for A_1 obtained above).

Table 34. pH and absorbance (A) data for calculation of pK_1.

pH	A(296 nm)
8.69	0.161
8.80	0.203
9.13	0.263
9.30	0.926
9.56	0.336
9.74	0.362
9.96	0.378

NOTE: Samples contained 0.1 mM MBB in 0.01N boric acid with pH adjusted with KOH. Blanks prepared without MBB (25°C, μ = 0.01M, 1 cm cell).

Table 35. pH and absorbance (A) data for calculation of pK_2.

[NaOH], M	pH^c	A(296 nm)
0.5502	13.74	0.742
0.4122	13.62	0.711
0.2757	13.44	0.660
0.1374	13.14	0.571
0.0550	12.74	0.485

NOTE: pH^c = calculated pH measured by titration with standard acid. Samples contained 0.1 mM MBB with various amounts of NaOH and NaCl to give the pH value and μ = 1.26M (25°C, 1 cm cell).

The pK_a's determined by this method and their respective 95% confidence limits are: $pK_1 = 8.92 \pm 0.09$ and $pK_2 = 13.51 \pm 0.07$. This fairly wide difference between the two pK_a values is typical of o,o'-dihydroxydiphenylmethanes (122). It has been attributed to the formation of an intramolecular hydrogen bond upon ionization of the first hydroxyl.

The pK_a values were used to calculate the distribution of ionized MBB species as a function of pH. The results (Fig. 76) show that more than 90% of the MBB contains only one ionized hydroxyl over a wide pH range (pH 10-12.5).

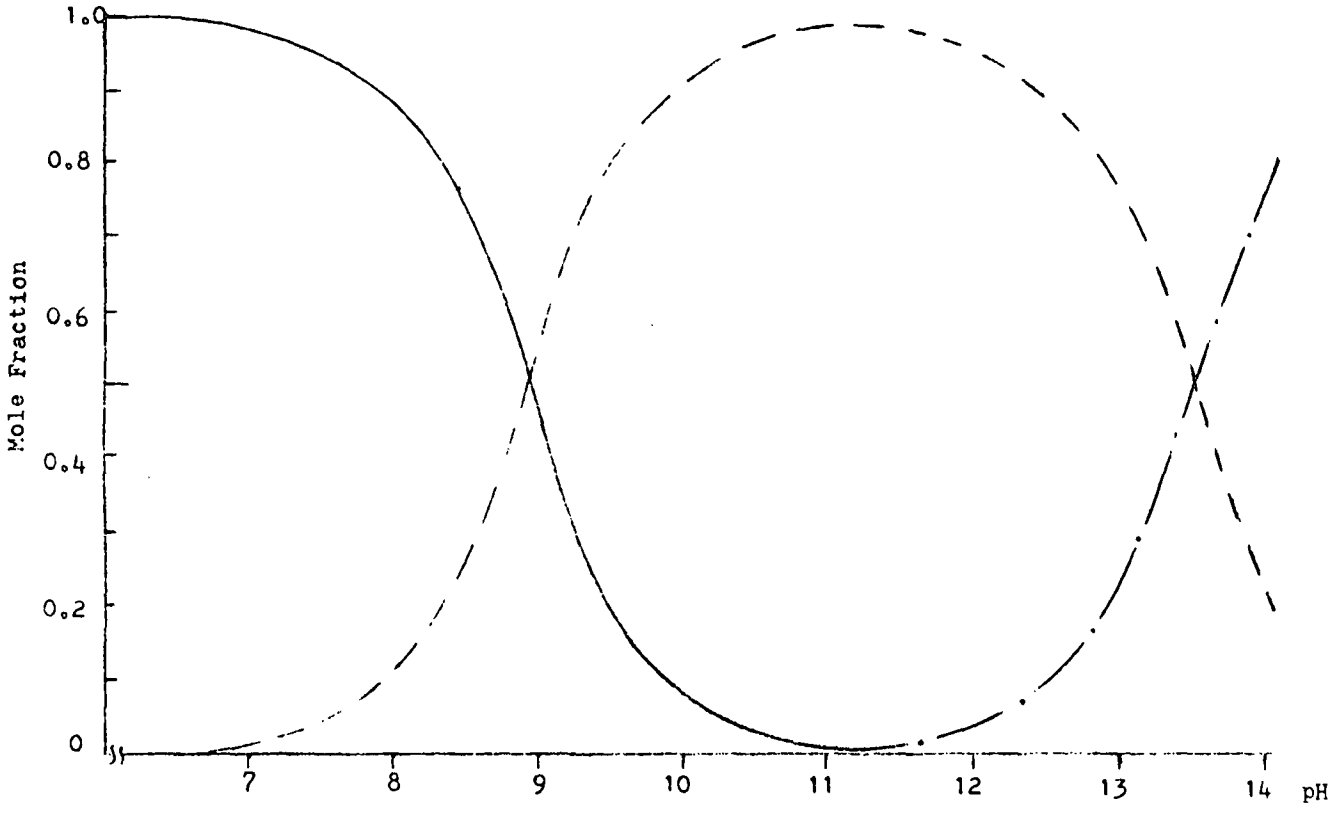

Figure 76. Calculated distribution of ionized MBB species as a function of pH (based on pK_1 = 8.92 and pK_2 = 13.51 for the phenolic hydroxyls at 25°C). The curves represent the three forms of MBB with respect to the state of ionization of the phenolic hydroxyls: undissociated (——), monoanion (- - - -), and di-anion (— · —).